A LASER STRAIN SEISMOMETER

VERHANDELINGEN DER KONINKLIJKE NEDERLANDSE
AKADEMIE VAN WETENSCHAPPEN, AFD. NATUURKUNDE
EERSTE REEKS - DEEL XXVI, No. 1

A LASER STRAIN SEISMOMETER

H. J. VAN VEEN

NORTH-HOLLAND PUBLISHING COMPANY
AMSTERDAM-LONDON - 1970

LIBRARY OF CONGRESS
CATALOGUE CARD NUMBER: 79–93054

AANGEBODEN MAART 1969
AANVAARD APRIL 1969
GEPUBLICEERD JANUARI 1970

CONTENTS

INTRODUCTION

Seismic signals cover a wide spectrum, extending from a fraction of a second to many hours and possibly to infinite periods (which would correspond to residual displacements). No single instrument to date is capable of covering this wide range of periods: a number of limited-bandwidth instruments is in use. These can be divided in two groups, *pendulum instruments*, which respond to ground accelerations and which form the great majority, and *strainmeters* or extensometers, which measure relative displacements.

This thesis describes the development of a novel seismic instrument of the strainmeter type. The instrument essentially consists of a gaseous optical maser or laser, with its end-mirrors fixed to the ground. Strains in the ground will cause a relative displacement of the mirrors, which in turn produces a frequency shift of the emitted radiation *). The instrument combines the favourable strainmeter response for long period waves with a modest size, comparable to that of a pendulum-instrument. Moreover, because of the remarkably narrow linewidth of the laser radiation the instrument should be sensitive over the entire seismic spectrum. This promising property, however, also results in a sensitivity for changes in environmental conditions other than seismic signals, and it is the suppression of these unwanted effects, that forms the major problem in the construction of a laser strain seismometer.

The contents of this thesis are divided into four major sections: In chapter I the gaseous optical maser is briefly described. The principle of operation of the laser strain seismometer (L.S.S.) and an estimate of its highest expected sensitivity is given. Some other instruments that measure strain are discussed.

Chapter II describes in detail the construction of the instrument and gives an account of the signal handling and electronics. The various sources of environmental and instrumental noise are discussed in chapter III; also the effect of nonlinearities in the laser itself is investigated here.

In the final chapter recordings obtained with the L.S.S. are presented and compared with records of the same events made by other instruments. Special emphasis is given to the recording of the magnitude $7\frac{1}{2}$ earthquake off Peru, occurring oct. 17, 1966.

---

*) This idea to use gas lasers for the detection of seismic strains was initially suggested by Prof. Leonard E. Alsop and Prof. George H. Sutton.

Chapter I

GASEOUS LASERS AND LINEAR STRAINMETERS, PRINCIPLES OF OPERATION

Lasers have become an established part of physics and some exellent introductions into this field are now available (e.g. Lengyel 1966, Thorp 1968). However, for the reader who is not familiar with the subject, we will start this chapter with some general remarks on laser physics for him to understand the particular application of lasers to seismology.

1.1. Principle of laser operation

In a system of atoms in thermal equilibrium, the relative population of any two levels is determined by Boltzmann's law. Consider two levels (1) and (2) with energies E_1 and E_2 with respect to the ground state. Then (see Fig. 1.1)

$$\frac{n_2}{n_1} = \frac{g_2}{g_1} \cdot e^{-(E_2-E_1)/kT} \tag{1.1}$$

where $n_{1,2}$ are the level populations and $g_{1,2}$ the statistical weights of the levels, k is Boltzmann's constant and T is the absolute temperature.

For an energy difference corresponding to an optical transition and at room temperature, this ratio is very small: substituting in eq. 1.1.

$$\frac{E_2-E_1}{h} = \nu = 2.6 \times 10^{14} \text{ Hz where } h = \text{Planck's constant,}$$

$$\frac{g_2}{g_1} \approx 1 \text{ and } T = 300° \text{ K gives} \frac{n_2}{n_1} \simeq 10^{-19}.$$

In the presence of external radiation of the frequency $\nu = \dfrac{E_2-E_1}{h}$, upward transitions in the system may occur through absorption of radiation and downward transitions with emission of radiation. This emission can happen in a random fashion and is then called *spontaneous* emission, or it can be induced by the external radiation. The latter process is called *stimulated* emission and yields radiation with the same frequency, phase, and direction as the stimulating external radiation. Since the absorption is proportional to $\dfrac{n_1}{g_1}$, and emission to $\dfrac{n_2}{g_2}$, normally in the optical region the absorption very strongly dominates, and radiation passing through the system is attenuated. If, however, one is able to bring the system out of thermodynamic equilibrium in a condition of population inversion:

such that $\frac{n_2}{g_2} > \frac{n_1}{g_1}$, then stimulated emission is enhanced over absorption and under certain conditions the point may be reached where coherent amplification of radiation or LASER-action takes place. (*L*ight *A*mplification by *S*timulated *E*mission of *R*adiation).

Rather than in amplification as such, the main use of stimulated emission in the optical region of the electromagnetic spectrum has been as the driving force of an oscillator, which is then called a laser lightsource or laser. Like any oscillator the laser oscillator is a noise amplifier, the noise now being spontaneous emission. The necessary feedback is obtained by enclosing the active medium between two mirrors. An important mirror configuration is the Fabry-Perot cavity consisting of two plane parallel mirrors normal to the line that connects their centers.

Spontaneous emission, emitted parallel to this line – the laser axis – is trapped within the cavity by repetitive reflexions at the mirror surfaces. If the amplification in the active medium is large enough to overcome the inevitable losses due to transmission of the mirrors, scattering and diffraction, the radiation energy builds up and the system starts to oscillate. Stimulated emission depletes the upper level, however, and the laser action may stop again or reach an equilibrium condition, depending on the pumping rate: that is, on the supply of upper state atoms. Also oscillations in other modes than the purely axial mode described, are

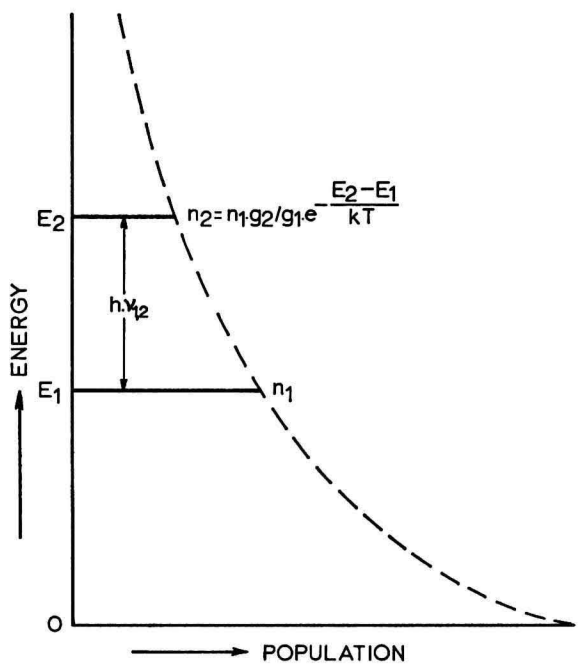

Fig. 1.1 Relative population of two levels in a system of atoms in thermal equilibrium.

possible. It should be clear that a laser light source is essentially different from any other source of light: the laser depends on population inversion and stimulated emission, whereas classical light sources all depend on spontaneous emission. On the other hand, a laser bears great resemblance in principle to a common radio-emitter since it also produces coherent radiation.

1.2. The Helium-Neon laser

Since the first ruby laser was built by Maiman in 1960, laseraction has been achieved at wavelengths extending from the ultraviolet to the far infrared, in such different media as crystalline solids, glasses, liquids, and gases. The first continuous gaslaser was realised by Javan et al. (1961), who used as active medium a mixture of helium and neon and obtained laser radiation in the near infrared at $\lambda = 1.15\ \mu$. It is this particular type of laser that was used in our experiments and therefore the following discussion will be restricted to the He-Ne gas laser. In this chapter its relevant properties will be described; constructional details will be given (mostly) in chapter II. The lasers used in the present experiment are of common design; they consist of a fused silica discharge-tube (of length 1 meter, bore 6 mm), containing the low pressure He-Ne mixture and sealed at both ends by optically flat windows. These windows are oriented at the Brewster angle, thus ensuring minimum losses for one direction of polarisation (Born & Wolf, p. 43). Mirrors that are highly reflective for $\lambda = 1.15\ \mu$ are placed at either end of the tube, normal to the tube axis.

Among the several interesting properties of the laser radiation, its frequency plays a crucial part in the present application. The different factors determining this frequency are described in the following three sections.

1.2.1. *The active medium*

The 1.15 μ laser line corresponds to a transition between the $2s_2$ and $2p_4$ levels (Paschen notation) in neon (Fig. 1.2). A gaseous discharge provides the pumping necessary to achieve population inversion by electron excitation. This pumping is made more effective by the presence of helium: neon groundstate atoms are excited to the $2s_2$ level by inelastic collisions with 2^3S He-metastables. (For information on different notations, see Allen & Jones 1967).

Only radiation that has a frequency within the width of the atomic line can gain intensity by stimulated emission. In a low pressure gas, the linewidth is determined primarily by doppler broadening caused by the thermally moving atoms. The fractional intensity gain $g(\nu)$ per single pass through a tube of length l, owing to stimulated emission is in this case a gaussian function of $(\nu - \nu_0)$, the frequency difference from the atmioc line-center ν_0.

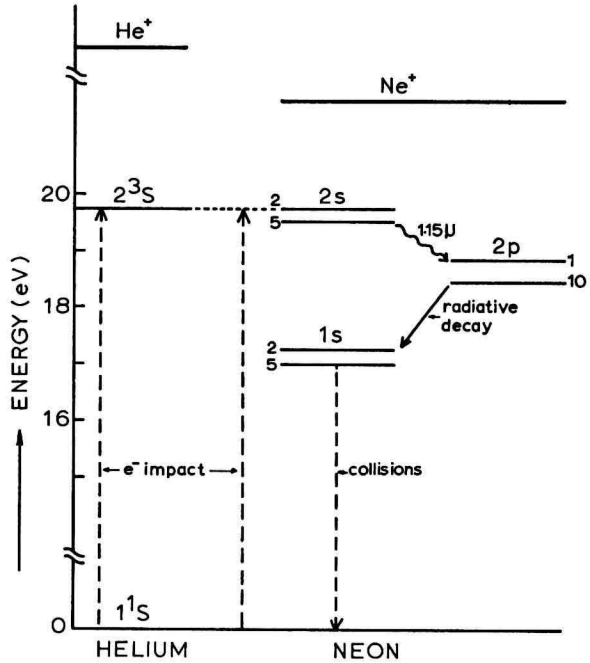

Fig. 1.2 Energy levels of He and Ne involved in the 1.15μ laser transition.

$$g(\nu) \equiv \frac{\Delta I}{I} \simeq g_0 \cdot e^{-\left(\frac{\nu-\nu_0}{0.6\Delta\nu_D}\right)^2} \cdot l. \tag{1.2}$$

where g_0 = gain at line center

$\Delta\nu_D$ = doppler width = full width at half maximum

One has

$$\Delta\nu_D = \sqrt{\frac{8\ kT ln\ 2}{M \cdot \lambda^2}} \tag{1.3}$$

where M is the atomic mass. Upon substitution of appropriate values: $T = 400°$ K, $\lambda = 1.15\ \mu$, eq. (1.3) yields $\Delta\nu_D = 800$ MHz.

The gain at line center depends on the degree of population inversion, the tube diameter, gas pressure etc. and amounts to several percents per meter for the 1.15 μ line under typical operating conditions.

1.2.2. *The resonator*

As a first intuitive approach one may visualize the laser field as consisting of plane light waves bouncing back and forth between the mirrors. For consecutive reinforcement to occur, it is necessary that the phase-shift after one round trip be a multiple of 2π.

For an evacuated cavity this resonance condition may be written simply as follows:

$$L = m \cdot \frac{\lambda}{2} \tag{1.4}$$

where m is an integer; for $\lambda = 1.15\ \mu$ and $L = 1$ meter: $m \simeq 10^6$. (1.4) is apparently satisfied for a series of equally spaced cavity resonances ν_c:

$$\nu_c = m \cdot \frac{c}{2L} \tag{1.5}$$

For a one meter cavity the resonance spacing $\frac{c}{2L} = 150$ MHz.

Because of the finite mirror dimensions, there are large diffraction-losses owing to spilling over of light at the mirror edges. Obviously plane waves do not represent a stable wave form or mode of oscillation for such a two-mirror system.

A great deal of work has been done in calculating the actual modes of these open resonators with plane parallel as well as several combinations of plane and curved mirrors (Fox, Li 1961; Boyd, Kogelnik 1962; review article: Kogelnik, Li 1966). It turned out that an infinite number of transverse electromagnetic (TEM) modes exists, which have different amplitude and phase distributions over a plane normal to the cavity axis. For circular mirrors these modes were designated TEM_{plq}, where p and l are transverse mode numbers which designate the number of radial and azimuthal nodal lines in the field distribution over a plane normal to the resonator axis. The third index, q, the longitudinal mode number, gives the number of field zeros between the mirrors; thus from (1.4) $q = m - 1$. As p and l increase, the mode pattern gets more complicated and also diffraction losses go up. The TEM_{ooq} or fundamental axial mode has an axially symmetric, approximately gaussian amplitude distribution and a nearly constant phase over most of the output area.

The bandwidth $\Delta\nu_c$ of any passive TEM resonance depends on the interferometer quality factor Q for that particular resonance.

This quality factor is defined as

$$Q = \frac{\nu_c}{\Delta\nu_c}, \tag{1.6}$$

and depends on the resonator losses. When these are small, as is the case with most gas laser cavities, the following expression may be derived (Birnbaum 1964, p. 75).

$$Q = \frac{2\pi L}{\lambda f} \tag{1.7}$$

Here f is the fractional loss per pass of the interferometer and is made up of transmission, scattering and diffraction losses, which typically add up to a few percents.

Substituting $L=1$ meter and $f=5$ % results in a value of $\sim 10^8$ for Q and in a cavity linewidth $\Delta\nu_c \simeq 2$ MHz.

The TEM_{ooq} mode which, according to its description given above, comes closest to the idea of plane waves, has diffraction losses lower than any other mode. This means, since transmission and scattering for the different modes remain approximately constant, that this mode will have the highest Q of all. Therefore in an active cavity when the pumping power is increased from zero, the fundamental axial mode will be the first to oscillate, provided the optics are of sufficient quality to allow the gain to surpass the loss anyway. We then say that the laser threshold – minimum pumping power for the axial mode – is reached.

1.2.3. *Laser radiation, frequency and bandwidth*

As was shown in the preceding section the empty resonator supports a series of axial modes ν_c, that are 150 MHz apart. Each axial mode is accompanied by a number of off-axis modes that are spaced much closer. Apparently several of these resonances fit under the gain curve, which from eq. (1.3) has a width $\Delta\nu_D = 800$ MHz. These resonances will actually oscillate for which the gain $g(\nu)$ surpasses the loss f, which depends on the type of mode. The reducing of $g(\nu)$ – that is: the pumping power – and/or the increasing of f can bring the situation down to the point where all non-axial modes and all but one of the axial mode oscillations are suppressed (Fig. 1.3). This "single mode" situation is assumed to apply in the rest of this chapter.

The actual oscillation frequency depends on both ν_c and the atomic line center frequency ν_0. If the interferometer resonance happens to be tuned exactly at atomic line center, then $\nu_c = \nu_0 = \nu$. Generally, however, ν_c will be different from ν_0. In this case the following expression for ν, derived by TOWNES (1961) holds to good approximation near threshold (BENNETT 1962)

$$\nu = \frac{(\nu_0 - \nu_c)\cdot\Delta\nu_c + \nu_c\cdot\Delta\nu_D}{\Delta\nu_D + \Delta\nu_c} \tag{1.8}$$

Since $\Delta\nu_c \ll \Delta\nu_D$, eq (1.8) may be simplified to

$$\nu = \nu_c + (\nu_0 - \nu_c)\cdot\frac{\Delta\nu_c}{\Delta\nu_D} \tag{1.9}$$

The oscillationfrequency has apparently somewhat shifted away from the cavity resonance towards atomic line center (Fig. 1.4). In the approximation given, this socalled mode-pulling is linear with cavity detuning $(\nu_0 - \nu_c)$. Non linear effects (BENNETT 1962, LAMB 1964) which are neglected

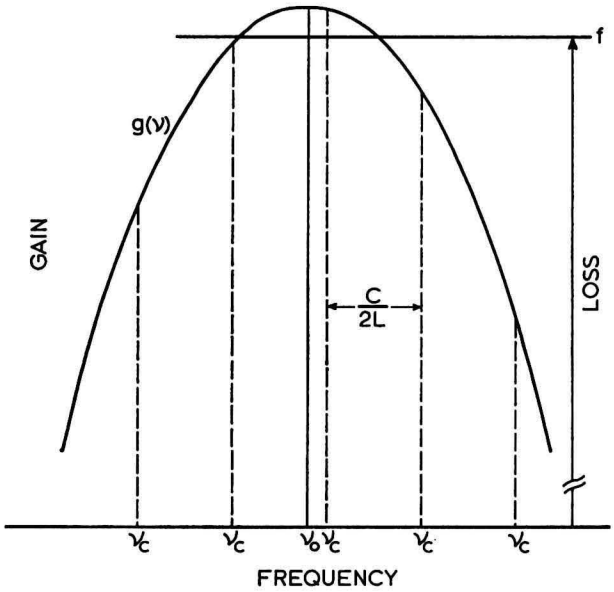

Fig. 1.3 Doppler broadened gain curve and cavity resonances spaced by c/2L Hz. The mode nearest to the line center is above threshold for oscillation.

here, are discussed in chapter III. Because of the effect of amplification in the active medium extreme line narrowing of the passive cavity resonance occurs. The resulting narrow laser linewidth $\Delta\nu$ has been estimated theoretically by several authors e.g. SCHAWLOW & TOWNES (1958), TOWNES (1961) to be:

$$\Delta\nu = \frac{h\nu}{2P}(\Delta\nu_c)^2 \tag{1.10}$$

where P = power in the mode.
Substitution of $P = 1\ mW$ and $\Delta\nu_c = 5$ MHz, results in a bandwidth $\Delta\nu \sim 2 \times 10^{-3}$ Hz for the 1.15 μ line.

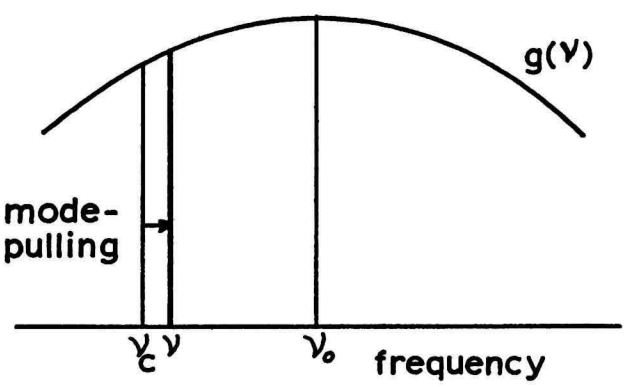

Fig. 1.4 The actual oscillation frequency ν is pulled away from the cavity resonance towards the atomic line center.

This exceedingly small value has little practical significance because of extraneous mechanical noise of for instance thermal or acoustical origin. Stability measurements by JASEJA et al. (1963, 1964), BALLIK (1964), and BOERSCH et al. (1967) yielded difference frequency fluctuations of some 20 Hz during a few seconds; and a constancy of 100 Hz over a 10 second period was obtained at times. Probably, with better environmental control, the bandwidth $\Delta\nu$ may be kept at some hundreds or thousands of cycles per second over periods of minutes, which means a stability $\frac{\Delta\nu}{\nu} \simeq 10^{-12}$ to 10^{-11}.

1.3. THE LASER AS A STRAIN MEASURING DEVICE

If mode pulling is ignored for the moment, then the laser oscillates at a cavity resonance: $\nu = \nu_c$ and consequently with eq. (1.5): $\nu = m \cdot \frac{c}{2L}$, which upon differentiating gives a simple relation between a change in cavity length and the corresponding laser frequency shift

$$\frac{d\nu}{\nu} = -\frac{dL}{L} \tag{1.11}$$

By mounting the laser mirrors on a rock surface, strains in the rock will cause the mirror distance L to vary (Fig. 1.5). This will change the laser frequency according to (1.11), which states that fractional changes in length and the corresponding fractional changes in frequency are equal and of opposite sign. Laser frequency ν and cavity length L are known: if the frequency shift $d\nu$ can be determined it is obvious that (1.11) represents an absolute measurement of displacement, or strain if one does not specify L.

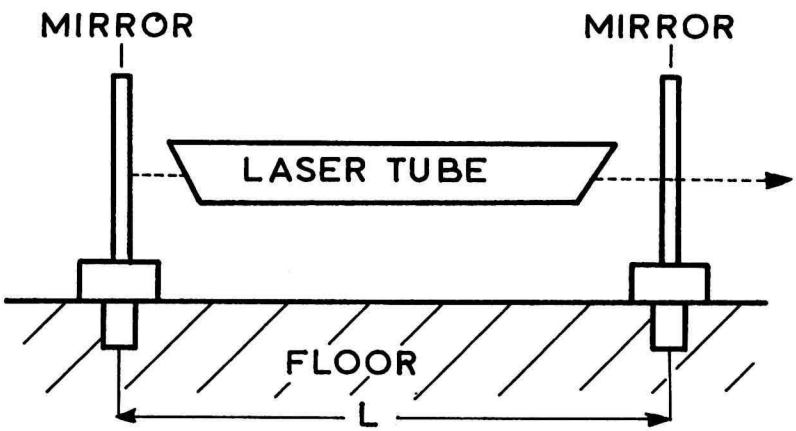

Fig. 1.5 Principle of the laser strain seismometer: strains in the floor will vary the mirror distance L and therefore the laser oscillation frequency.

The above result remains essentially the same if linear pulling is taken into account. From (1.9), the equivalent of (1.11) takes the form

$$\frac{d\nu}{\nu_c} = -\left(1 - \frac{\Delta\nu_c}{\Delta\nu_D}\right) \cdot \frac{dL}{L} \tag{1.12}$$

The factor in parentheses is a constant of the system and as was shown in sections 1.2.1. and 1.2.2., deviates approximately one percent from unity. ($\Delta\nu_c \ll \Delta\nu_D$).

1.3.1. *Dynamic range and sensitivity*

The main advantage of using a gaslaser for measuring earth strains is the high sensitivity and large dynamic range one may expect. Strains will change laser frequency; when these frequency changes become of the order of the axial mode spacing the laser will change to the next axial mode and the frequency no longer is a single valued function of the mirror separation. This puts an upper limit to the range of measurable strain. Since the axial mode spacing of a one meter long laser is approximately 150 MHz (sect. 1.2.2), frequency excursions should be limited to some tens of megacycles. Consequently from eq. (1.11), for a one meter long laser oscillating at 1.15 μ ($\nu = 2.6 \times 10^{14}$ Hz) this means an upper strain limit of about 10^{-7}.

More interesting of course is the smallest amount of strain that can be detected. This is determined by the laser radiation bandwidth. As was mentioned in section 1.2.3 a minimum linewidth $\Delta\nu$ of some hundreds to a few thousands of cycles per second seems to be a realisable figure. This would mean a least detectable strain of 10^{-12} or 10^{-11} which is approximately an order of magnitude more sensitive than are present day strainmeters.

1.3.2. *Detection technique*

To detect frequency changes ranging from several MHz down to some hundreds of Hz in an optical carrier wave, an extremely high resolving power of the order of the inverse strain is needed. The resolution of optical spectrometers and interferometers is at best some 10^5 and 10^7 respectively, which falls short of what is required by many orders of magnitude. Instead, a photomixing technique is being used (FORRESTER et al. 1961), similar to the heterodyning in a radio receiver. When the output beams of two independent single mode lasers are incident on the photosensitive surface of a photomultiplier tube or other suitable photodetector, the detector output will contain the difference- or beat frequency between the two optical frequencies. Necessary conditions are that the beams are (at least partly) polarized in the same direction, that they are lined up in such a way that their wave fronts coincide over the detector area and that the difference frequency is within the frequency response of the

detector. The beat frequency between two similar lasers is of the order of the axial mode spacing or less, and consequently the detector output can be handled by standard V.H.F. circuitry.

When we beat two lasers in the fashion just described, one of them – which would be called "the local oscillator" – may be stabilized to a constant frequency, and the other be left free-running, or alternatively both lasers may be free running. In the first alternative the difference frequency will change because of varying strains acting on one – the free-running – laser. In the other situation varying strains acting on both, effect the output.

The local oscillator arrangement, although it has the advantage of a somewhat simpler response pattern for longitudinal seismic waves (see section 1.3.3), has a serious disadvantage: It "sees" all environmental effects like temperature- and barometric pressure changes, whereas these effects disappear to first order if both lasers are free running, since they see the same environment which then cancels out in their difference frequency. For this reason the free running arrangement was chosen. The actual set-up, as given schematically in Fig. 1.6 consists of two laser cavities mounted at right angles to each other on a horizontal surface.

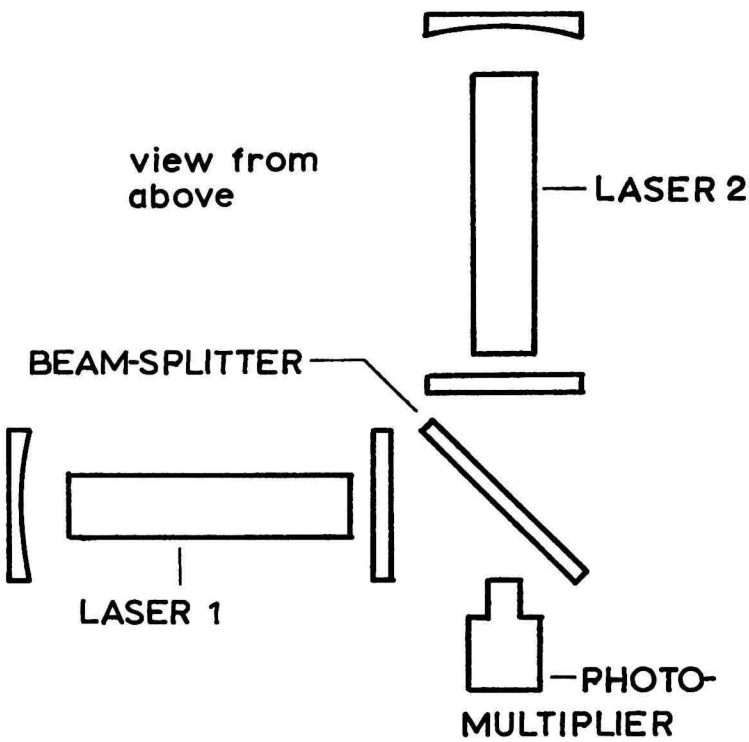

Fig. 1.6 Schematic of the actual laser strain seismometer set-up: Two laser cavities mounted at right angles on a horizontal rock surface. The varying difference frequency between the two laser frequencies is detected in the photomultiplier.

The two laser beams are superimposed by means of a 45-degree beam-splitting mirror; either output from this mirror is available for detection. For preliminary results see H. J. VAN VEEN et al. (1966).

1.3.3. *Directional response to seismic waves*

The laser strain seismometer (L.S.S.), as described in principle in the previous section, is sensitive to components of seismic waves that produce horizontal strains. This means that the instrument "sees" true and apparent surface waves. The latter are produced by incoming body waves and their speed depends on both speed and angle of incidence of the body wave.

The instrument's response is conveniently derived by subtracting the response for the separate lasers. These are linear strainmeters, the theory of which is well known thanks to the work of H. Benioff.

Given a plane surface wave $\xi = f\left(t - \frac{X}{V}\right)$ of wave length λ traveling with (apparent) speed V in a direction, making an angle α with the strain meter axis, one may derive the following expressions in which ξ denotes horizontal ground particle displacement and L is the strain meter length: For longitudinal surface waves:

$$\frac{dL}{L} = -\frac{\cos^2 \alpha}{V} \cdot \frac{d\xi}{dt} \tag{1.13}$$

and for transverse surface waves:

$$\frac{dL}{L} = -\frac{\sin 2\alpha}{2V} \cdot \frac{d\xi}{dt} \tag{1.14}$$

In the derivation it is assumed that the strain meter length is small compared with the wave-length of ξ. Equations (1.13) and (1.14) are represented in Figs. 1.7. and 1.8. Each of the two lasers has such a set of directivity patterns; corresponding patterns are equal but rotated over 90° in the horizontal. To find the overall response, corresponding patterns must be subtracted, resulting in the 4-leaf clover patterns of Fig. 1.9 for longitudinal waves and Fig. 1.10 for transverse waves. Apparently the responses for both types of waves have the same shape, the only difference being a rotation over 45°. The analytical derivation is simply as follows, for longitudinal waves:

$$\left.\begin{aligned} \frac{dL}{L} &= \left(\frac{dL}{L}\right)_1 - \left(\frac{dL}{L}\right)_2 = -\frac{1}{V} \cdot \frac{d\xi}{dt}(\cos^2 \alpha_1 - \cos^2 \alpha_2) = \\ &= -\frac{1}{V} \cdot \frac{d\xi}{dt} \cos^2 \alpha_1 - \cos^2 (\alpha_1 + 90°) = -\frac{\cos 2\alpha_1}{V} \cdot \frac{d\xi}{dt} \end{aligned}\right\} \tag{1.15}$$

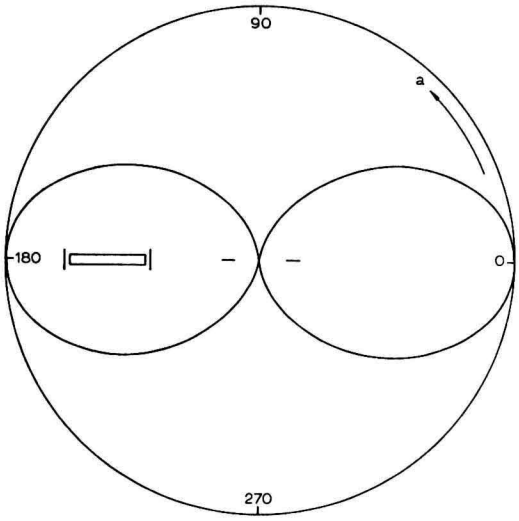

Fig. 1.7 $\frac{\Delta L}{L} = -\frac{\cos^2 \alpha}{V} \cdot \frac{d\xi}{dt}$

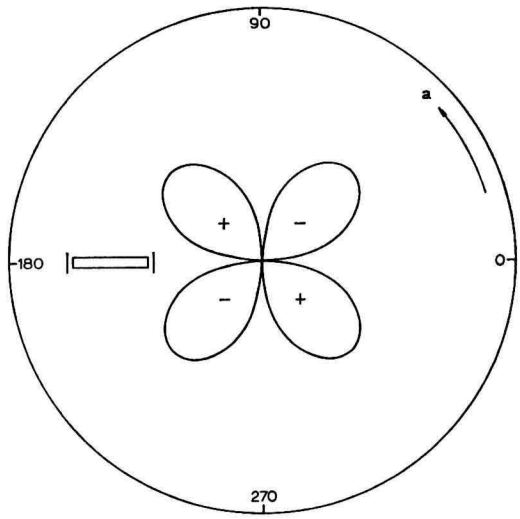

Fig. 1.8 $\frac{\Delta L}{L} = -\frac{\sin 2\alpha}{2V} \cdot \frac{d\xi}{dt}$

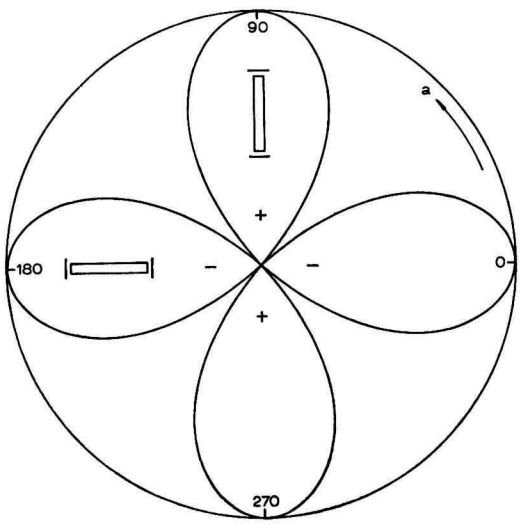

Fig. 1.9 $\frac{\Delta L}{L} = -\frac{\cos 2\alpha}{V} \cdot \frac{d\xi}{dt}$

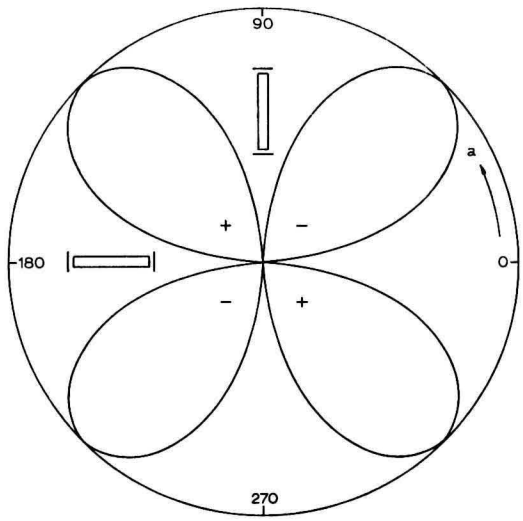

Fig. 1.10 $\frac{\Delta L}{L} = -\frac{\sin 2\alpha}{V} \cdot \frac{d\xi}{dt}$

Fig. 1.7

Directional response of Benioff linear strainmeter for longitudinal waves.

Fig. 1.8

Directional response of Benioff linear strainmeter for transverse waves.

Fig. 1.9

Directional response of laser strain seismometer foı longitudinal waves.

Fig. 1.10

Directional response of laser strain seismometer for transverse waves.

and similarly for transverse waves:

$$\left.\begin{aligned}\frac{dL}{L} &= \left(\frac{dL}{L}\right)_1 - \left(\frac{dL}{L}\right)_2 = -\frac{1}{2V}\cdot\frac{d\xi}{dt}(\sin 2\alpha_1 - \sin 2\alpha_2) = \\ &= -\frac{1}{2V}\cdot\frac{d\xi}{dt}(\sin 2\alpha_1 - \sin 2(\alpha_1 + 90°)) = -\frac{\sin 2\alpha_1}{V}\cdot\frac{d\xi}{dt}\end{aligned}\right\} \quad (1.16)$$

From Fig. 1.9 it is apparent that directions of maximum sensitivity for incoming longitudinal waves are the ones oriented parallel to one of the laser tubes; midway between these maxima are four azimuths that have zero response for longitudinal waves. A comparison of Figs. 1.9 and 1.10 shows that directions of maximum response for longitudinal waves have zero response for transverse waves and vice versa. Equations (1.13) to (1.16) show that both the simple linear strain meter and the L.S.S. have a response proportional to $\frac{d\xi}{dt}$. This socalled velocity transducer response is characterised by a 6 db per octave decrease in displacement sensitivity with increasing period.

1.4 Other strainmeters

The principle of measuring relative seismic motion between two neighbouring points, by means of some kind of yardstick as length standard was invented by John Milne (1888). The device failed because of lack of sensitivity. The first useful instrument of this type was built by H. Benioff, who also provided a theory (H. Benioff 1935). The principle of operation is as follows: Changes in the distance between two piers A and B are measured with a long rod or tube made from a material with a low coefficient of expansion like quartz. One end of the tube is fixed to pier A, the other end is free and extends to within a short distance from pier B. The tube is supported by thin wires, which prevent vertical movement, while the restriction of movement along the tube is negligible.

As seismic, tidal or secular strains effect the distance AB, the gap between the free end of the tube and B varies. Several types of transducers have been in use to pick up this signal. In the early versions an electromechanical transducer-galvanometer combination was employed; the response characteristic being determined by the damping and free period of the galvanometer. Later, because of growing interest in very long period phenomena, capacitor plate transducers were introduced (Benioff 1959, Major et al. 1964).

The principle advantage of strain meters over pendulum instruments is the superior long period performance; the mean reason for this is the lack of response to tilts and the slower decrease in displacement sensitivity with increasing period. For a strainmeter, the displacement sensitivity (section 1.3.3) is approximately inversely proportional to the period as

compared with an inverse proportionality to the period squared for pendulum instruments, i.e. when periods exceed the free period T_0 of the pendulum.

Less favourable properties of strainmeters, which severely restrict the number of possible installation sites, are: extreme sensitivity to temperature – and barometric pressure changes and to local strains produced within a distance, comparable to the strainmeter length. Also this length itself is cumbersome, instruments exist with lengths up to 60 meters, requiring a tunnel or minedrift for the installation.

Recently several authors have published modifications of the Benioff strainmeter. BLAYNEY and GILMAN (1965) maintained the essential Benioff design but achieved greater ease of installation mainly by modifying the tube supports; they also added a continuous interferometric calibration which is important for reliable secular strain measurements. VALI et al. (1965) abandoned the quartz tube and measured changes in the total distance AB interferometrically, using a He-Ne laser as a light source; changes in the refractive index of air caused by turbulence, however, forced them to use an evacuated tube over the full length AB, so that they ended up with the same kind of inconvenient construction. Recently Major installed several quartz strainmeters in shallow ditches at the surface; the huge effect of the daily temperature cycle was reduced by metal compensating joints between the sections of quartz tubing.

Of particular interest for the laser strain seismometer project is a set of quartz tube Benioff linear strainmeters (B.L.S.), located in the Ogdensburg Observatory of L.G.O.; see chapter II and for an extensive description: MAJOR et al. (1964). These instruments and the L.S.S. are all in the same location and, as was mentioned already, have the same period response. Therefore, if differences in directional response are taken into account, their recordings may be directly compared, several examples of which are given in chapter IV.

Chapter II

DESCRIPTION, INSTALLATION AND OPERATION OF THE LASER STRAIN SEISMOMETER

As is usual in an instrumental project the original design underwent many modifications in the course of time, and in view of the difference still existing between realisable and realised useful sensitivity, the version described here should not be considered as final.

This chapter describes construction, installation and running of the L.S.S.; the construction part being subdivided in sections on mechanical, electrical and electronic aspects.

2.1. Construction of the instrument

In this particular laser application, construction requirements for the instrument are rather uncommon: mirrors rigidly coupled to the floor and otherwise decoupled from each other. As a consequence no commercially available He-Ne lasers could be used; instead the set-up is assembled from components that were partly purchased (e.g. mirrors, coatings, laser tubes), partly designed and made in the laboratory (e.g. mirror holders, tube supports). In the following sections the more important parts of the system will be treated in some detail.

2.1.1. *Laser tubes and supports*

The laser tubes made from fused silica, were of well-known design as is shown in Fig. 2.1. Each tube was provided with antiparallel Brewster-windows, which were uncoated 1/20 wave flats, directly fused to the tube. The overall tube length of 985 mm was chosen as large as possible, to minimize the air gaps between Brewster windows and mirrors. Not all of this tube length was active however: the discharge ran through the smaller bore center section of the tube; the active tube length was there-

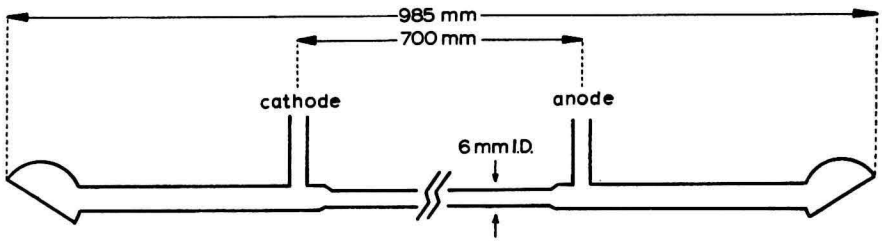

Fig. 2.1 The laser tubes were made from fused silica of approx. 1 mm wall thickness. For simplicity the tube is shown without its electrodes.

fore some 700 mm. Once in operation the tubes had to run continuously and in order to ensure an acceptable lifetime, great care had to be given to the cleaning process before the tubes were filled. This cleaning was done before the electrodes were attached and consisted of flushing subsequently with: a good grade detergent (e.g. alconox), deionised water, acetone, deionised water, reagent grade ethyl alcohol. The tube and especially its windows had to be spotlessly clean upon visual inspection. The electrodes sealed in pyrex bulbs were then attached to the tube. These bulbs were made quite large because they function as gas reservoirs. The complete tube was sealed to a vacuum system-filling station, pumped vacuum and baked overnight at 350° C. Usually tubes were filled two at a time; the same treatment ensuring roughly equal properties such as gain and lifetime. After activating the cathodes and cleaning anodes and getters by heating, the tubes were baked again, resulting in a final vacuum of 10^{-7} torr when the pumpvalve was closed.

The gas used for filling is a commercially available 9 : 1 mixture of naturally occurring helium and neon, with upper limits on impurities of a few parts per million.

The tube was made to lase while still attached to the filling station and the most efficient value for the He-Ne total pressure was determined by experiment, considering that:

1. for a long tube life the DC discharge current should be kept as low as possible to increase cathode lifetime and reduce gas clean-up.
2. the discharge should be electrically quiet, since a varying discharge current causes amplitude as well as frequency variations in the laser output radiation (see next chapter).
3. to counteract the effects of gas clean-up and diffusion, the tubes should be overfilled.

With He-Ne total pressure as a parameter, the discharge current noise was observed for various DC currents. In Fig. 2.2 the laser output (photomultiplier DC level) is plotted against discharge current for several gas pressures. Three different kinds of discharge behaviour can be distinguished and have been qualitatively indicated in Fig. 2.2. At $I = 20$ mA and pressures above 1 torr, the discharge was noisy with peak to peak noise amplitudes typically of 6 %, occasionally up to 25 % of the DC value as viewed on a DC to 50 MHz oscilloscope. As the discharge current was lowered, at some critical, pressure dependent value, the noise dropped out and oscillations started building up, having a frequency around 15 kHz. These increased in amplitude with decreasing current and finally caused extinction of the discharge. In between these two regions a noise- and oscillation-free discharge could be obtained with peak to peak current variations less than 0.1 %. This quiet region diminished with increasing pressure and was absent above 2.8 torr. At the selected filling pressure of 1.85 torr, the quiet current range extended from 4 to 9 mA. Over this range the laser output is nearly linear with discharge current and may

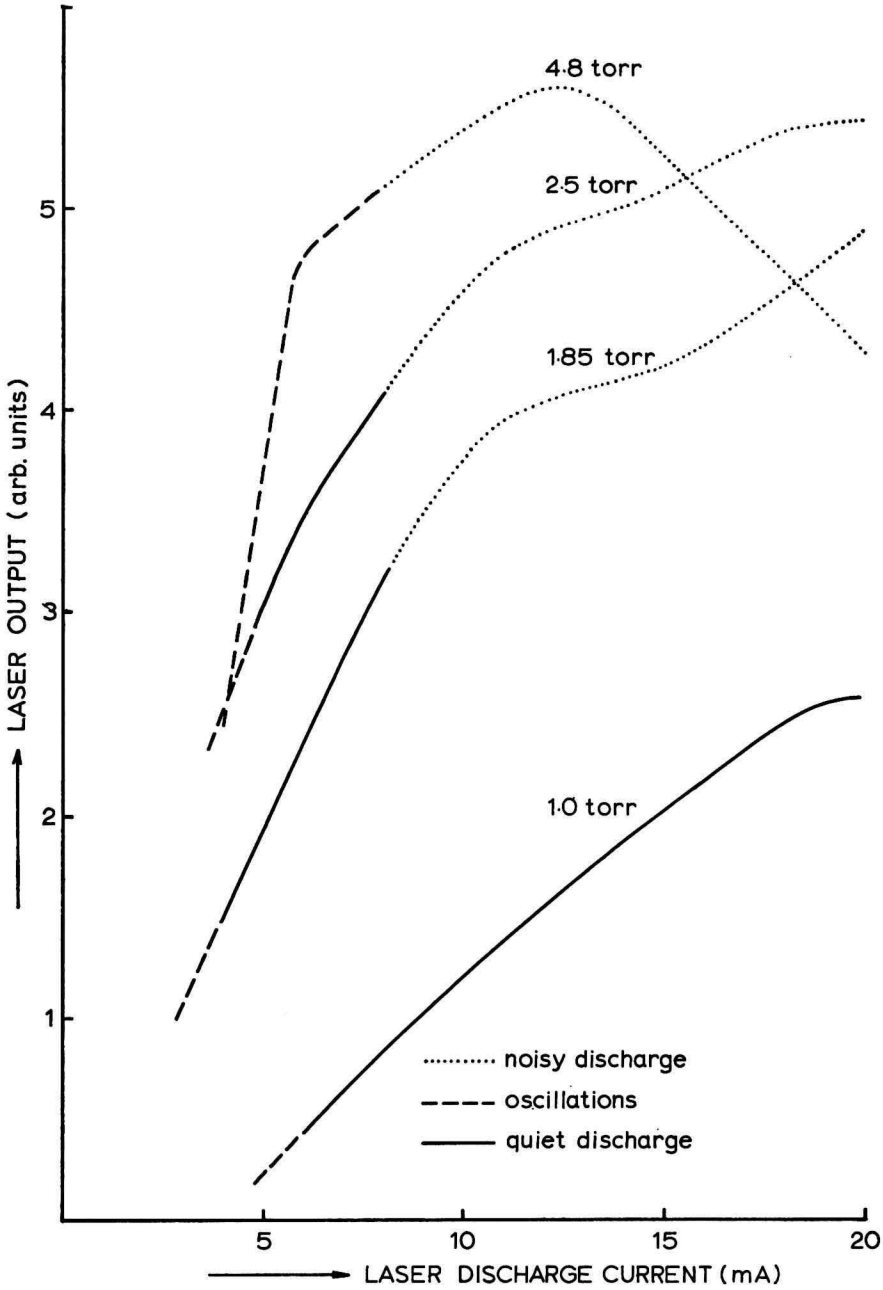

Fig. 2.2 Laser output power as a function of the DC discharge current, for different values of the He-Ne total pressure. The electrical condition of the discharge has been qualitatively indicated.

be varied by a factor of two. The tubes were then sealed off, the getters fired and the correct cathode filament current was determined with an optical pyrometer. Tubes thus prepared were running continuously for over five months, had then to be replaced because of cathode failure in one tube.

The used tubes were reconditioned in the laboratory by cleaning, sealing-on new electrodes and filling, in the way described above. At both ends of the laser tube a U-shaped aluminium block was cemented, its opening facing away from the electrodes. These blocks were clamped on a heavy support base as is shown in Fig. 2.3. This support could be adjusted sideways and vertically to accomodate for an uneven rock surface and tolerances in drilling the holes for mounting. By clamping the tube at the ends, transverse vibrations effecting the end windows which would change the optical cavity length and thus cause frequency shifts, were prevented.

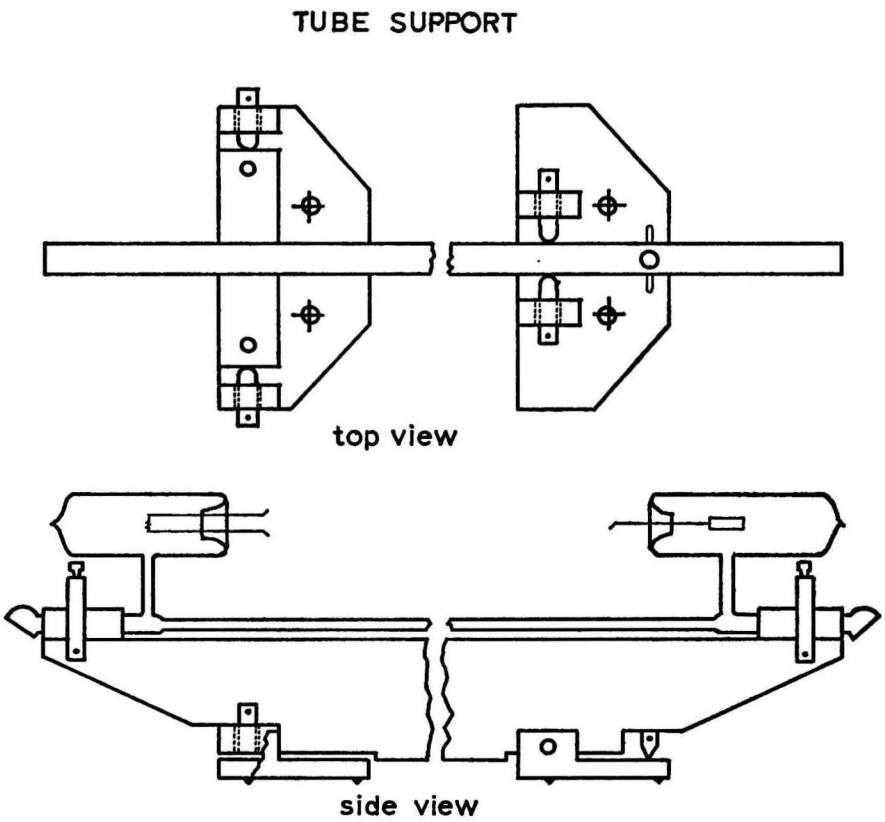

Fig. 2.3 Laser tube support. On the side view a laser tube is shown, clamped in position. The large vertical plate is 25 mm thick aluminium. This plate can be adjusted up and down or sideways to align the tube in the cavity.

2.1.2. *Mirrors*

In the first He-Ne lasers (JAVAN et al. 1962) flat mirrors were used. It was found, however, (BOYD & GORDON 1961) that spherical mirrors are far easier to align, but a disadvantage is that a smaller volume of discharge is active. In an evaluation of several combinations of flat and/or spherical mirrors as laser cavities by SINCLAIR (1964) the near hemispherical configuration turned out to be a favourable compromise between ease of alignment and active discharge volume. This configuration consists of one flat and one spherical mirror with a radius of curvature slightly larger than the mirror distance. An additional advantage of this configuration is the small output-beam diameter when the signal is taken off the flat mirror, provided the mirror to detector distance is kept small. The mirrors, flats and sphericals, the latter with 1 meter radius of curvature, are of fused silica with 1/20 wave surface figures. These substrata are coated for 99 % reflection at 1.15 μ with moisture resistant ("hard") multilayer dielectric coatings.

The mirror holders serve to couple the mirrors to the rock surface and allow for angular adjustments. As can be seen in Fig. 2.4, the stands, made of aluminium, basically consist of a rigid baseplate and a vertical plate holding the mirror, which can be adjusted with respect to the base. The mirror is clamped against three studs in the vertical plate. The baseplate is spring mounted on the rock surface and rests on three stainless-steel points. All mirror stands have fine manual angular adjustment screws, allowing for rotations of the mirror plane around two perpendicular axes, both normal to the laser axis. The minimum mirror rotation adjustment is 10^{-3} degrees. In addition, in each cavity, one mirror stand has a remotely controlled fine adjustment, consisting of a geared down

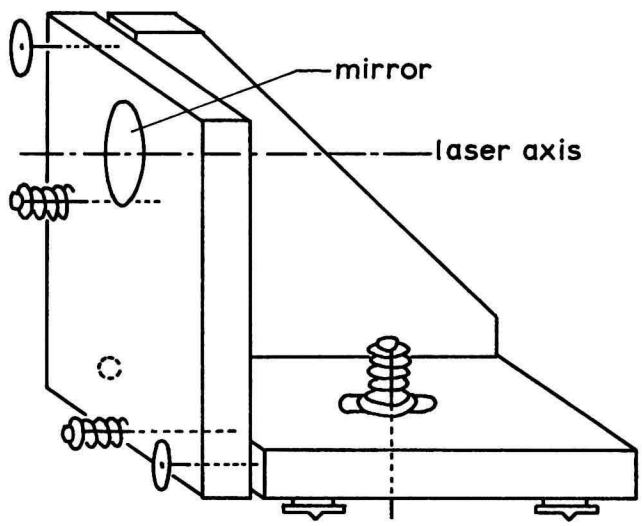

Fig. 2.4 Mirror holder; two to each laser cavity.

DC micromotor, which by wormgear drive rotates a threaded shaft. The lever construction which passes on the translation of this shaft to the plate holding the mirror, takes care of a further reduction of 25 : 1.

In this way it is possible to rotate the mirror in a controlled fashion over an angle as small as 2×10^{-3} arc seconds. This amount of rotation is too small to effect the cavity adjustment, but its influence on mirror position and therefore on cavity length is easily observed as a frequency shift in the laser output. Shifts as small as 0.3 MHz ($\Delta L \simeq 10^{-3}\ \mu$) can still conveniently be made by momentarily actuating the motor. These shifts can be made in either direction by reversing the polarity of the voltage that drives the motor. The cavity can be tuned through several longitudinal resonances, that is: over several times 150 MHz, without appreciable loss of alignment. To protect the laser optics from contamination, dustcover assemblies are fitted to each stand, enclosing the mirror and nearest Brewster window in a dust free environment. The covers are toy balloons cut in half, a punched hole fits snugly around the tube and the open end is sealed against the mirror stand, by means of a plexiglass ring and brass attachement-piece, as shown in Fig. 2.5.

To establish single-mode operation, the gain has to be lowered and/or the losses increased to near-threshold operation. One can realize a decrease in gain by decreasing the discharge current (with limits set by noise

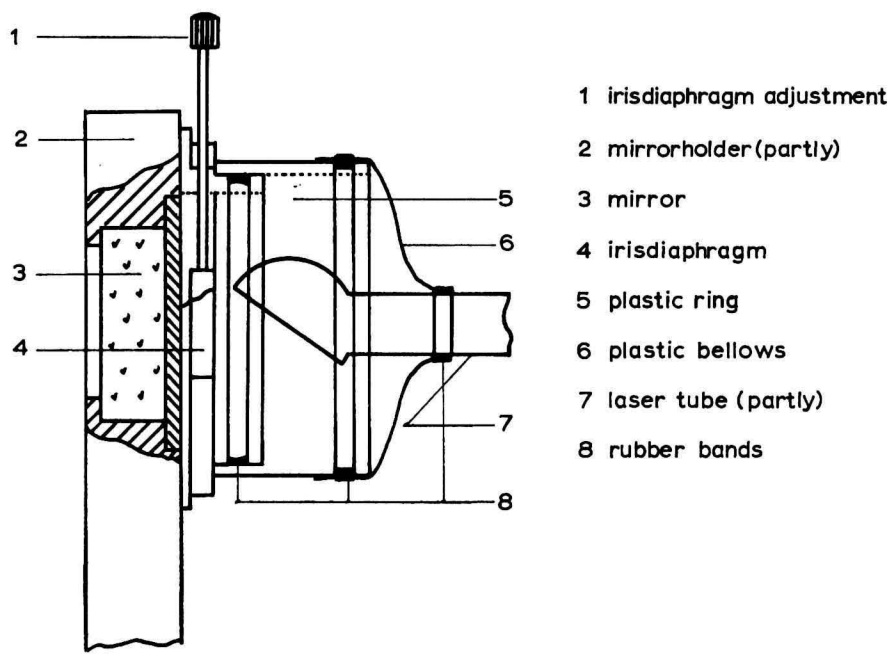

Fig. 2.5 Adjustable iris diaphragm. The ring and bellows form a flexible seal between mirror stand and discharge tube, protecting that part of the ray path which goes through air.

considerations as mentioned in the preceding section). The losses can be increased conveniently by inserting a diaphragm into the cavity (RIGROD 1963). By decreasing the aperture, diffraction losses go up and the number of simultaneously oscillating modes is reduced. To this end a commercially available iris diaphragm with maximum and minimum opening diameters 12 and 0.75 mm is mounted within the dustcover assembly, against the stand holding the spherical mirror. The diaphragm is modified to make possible continuous adjustments from the outside. Diffraction loss calculations for several mirror geometries and diaphragm openings have been given by T. LI (1965). Li gives powerloss versus Fresnel number N. From his graphs for the near hemispherical configuration:

N	$2a$ (mm)	loss (%)
4.0	5.6	3
2.0	4.0	7
1.0	2.8	18
0.5	2.0	35

where $N = \frac{a^2}{\lambda L}$

$2a$ = diaphragm opening diameter
L = mirror distance

From these figures, from the gain per meter of the 1.15 μ laser line as given by BENNETT (1965), and from the length of the active discharge column, it follows that the diaphragm opening can be made sufficiently small to stop laser action completely; a single axial mode is then obtained by not going quite that far (see the installation procedure in section 2.4.2).

The outputs from the two lasers which together form the essential part of the L.S.S. (see section 1.3.2), are made parallel and coincident with a beam splitting mirror placed at a 45° angle to both cavities (Fig. 1.6). This mirror is an optical flat similar to the ones used as cavity mirrors, and coated for equal reflexion and transmission of light of a wavelength $\lambda = 1.15\ \mu$ that comes in at a 45° angle. The beam-splitter is mounted in a stand fitted with two fine rotational adjustments similar to the ones described previously. Because of the Brewster window arrangement, the outputs of the two lasers are plane polarised. To ensure a maximum beat amplitude these planes of polarisation were made parallel (after the beam-splitter) by matching the position of the two laser tubes.

2.1.3. *Insulation and heater tape*

In order to shield the instrument from short-term temperature fluctuations, from air currents and falling rocks, the set-up was surrounded and covered by insulating material (Fig. 2.6). The two cavities and the beam-splitter were surrounded by a double-walled L-shaped box, made from 5 cm thick styrofoam plates, the outer and inner box were separated by a 10 cm thick layer of fiberglass wool. Similarly the cover consisted of a double layer of styrofoam and glass wool with in addition, a layer of heater tape. These tapes, sandwiched between sheets of aluminium foil form a heater blanket on top of the inner styrofoam cover and power

was supplied to them from a regulated line, using a variac for reduction. The purpose of the tape was to counteract air convection around the instrument caused by the laser discharge heat, by creating a stable air temperature distribution. The amount of power dissipated in the tapes was some 5 W total.

The empty space within the inner styrofoam box around the stands and tubes was filled with fiberglass wool, the purpose again: prevention or at least reduction of air convection.

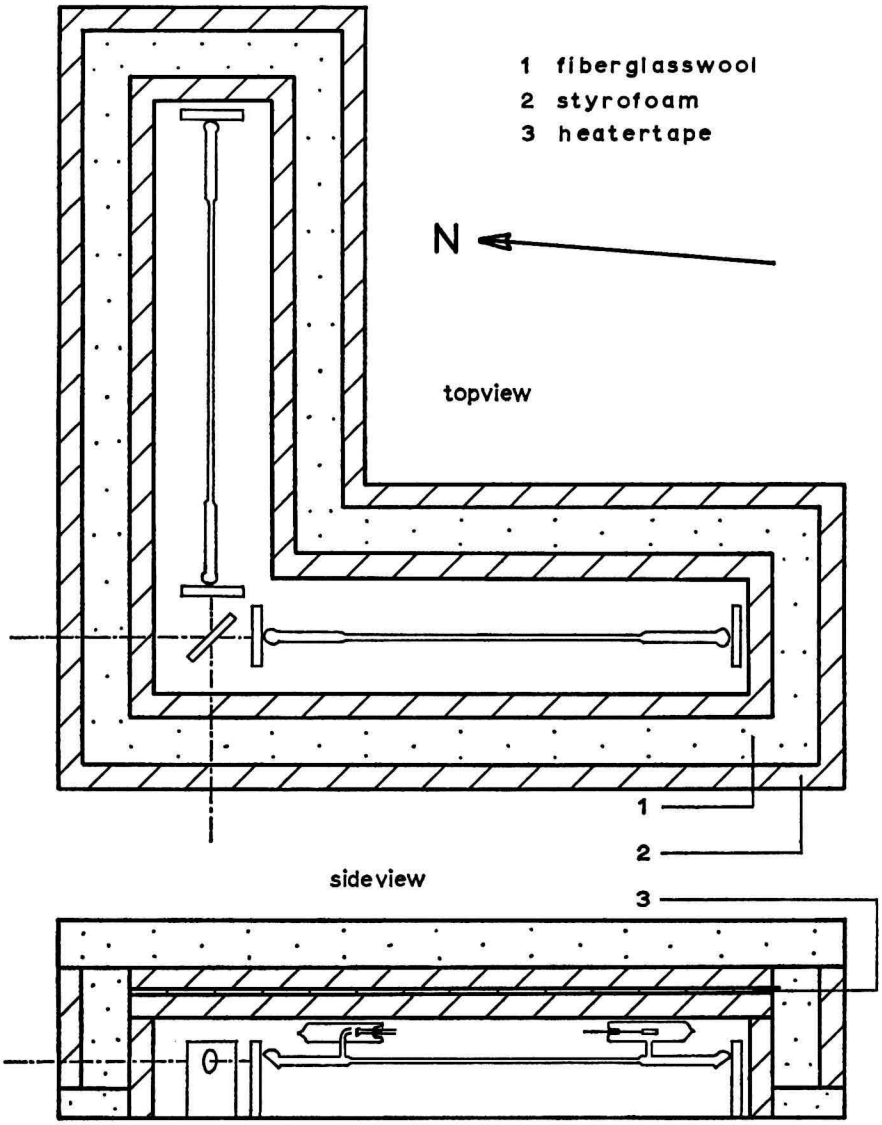

Fig. 2.6 The laser instrument was surrounded by several layers of insulating material.

Removal of the insulating cover once the tubes had been started, would change the thermal equilibrium situation and cause a pronounced drifting of the beat frequency. To avoid this each tube was fitted with a tesla coil which could be actuated by remote control to restart the tube in case the discharge stopped accidentally e.g. owing to a power line failure.

2.2. Discharge considerations

The He-Ne discharge providing the pumping energy for laser action may be either R.F. or D.C. excited. With R.F. excitation a noise free discharge is easily obtained (Bellisio et al. 1964); also, because the electrodes are external the tube is entirely without metal parts, therefore of simple design and easy to clean. However, with this kind of discharge, tube lifetime is restricted owing to loss of helium, which is driven out of the tube by the high potentials under the external electrodes (Lengyel 1966, Turner et al. 1964). D.C. discharges do not show this behaviour and furthermore allow better power regulation. Finally the use of an R.F. transmitter would be dangerous near mine blasting operations. D.C. operation requires internal electrodes; since cold cathodes will cause gas clean-up by sputtering, which will restrict tube life, a heated cathode was chosen, in spite of the added power consumption and complexity (see, however, Hochuli et al. 1967 and the suggestions in chapter III).

The cathodes used were directly heated 2.5 W oxide cathodes with 25 mA maximum rated discharge current and 950° C color temperature. Filament current was supplied by Harrison constant current power supplies.

The D.C. discharge current was provided by current-regulated high voltage supplies, one for each laser (Fig. 2.7). High voltage delivered to the regulator input was 4000 V, 12 mA. The sensing resistor R_1, and reference resistors R_2 and R_4 were General Radio precision resistors with temperature coefficients 0.001 % per °C, R_3 is a high quality potentiometer (0.002 % per °C). The stability of the reference voltage tube 5651 was listed as 0.1 %, and it is this figure that determined the regulator performance: the discharge current was stabilized to a figure between 0.07 and 0.2 %, depending on the setting of $R3$. The value of the discharge current could be changed continuously by varying $R3$, or in steps by changing the plug-in sensor $R1$. The laser tube with a 50 $k\Omega$ series resistor was connected to the regulator output. Regulator and other electronics were placed in a control room, 160 meters away from the laser tubes, and connections were arranged by coaxial cable. To prevent parasitic oscillations, the series resistor to anode connection had to be kept short.

2.3. Detection and signal handling

2.3.1. *Detection*

For detection of the beat frequency between the two lasers a square-law detector was used, as was mentioned in section 1.3.2. The choice of photo

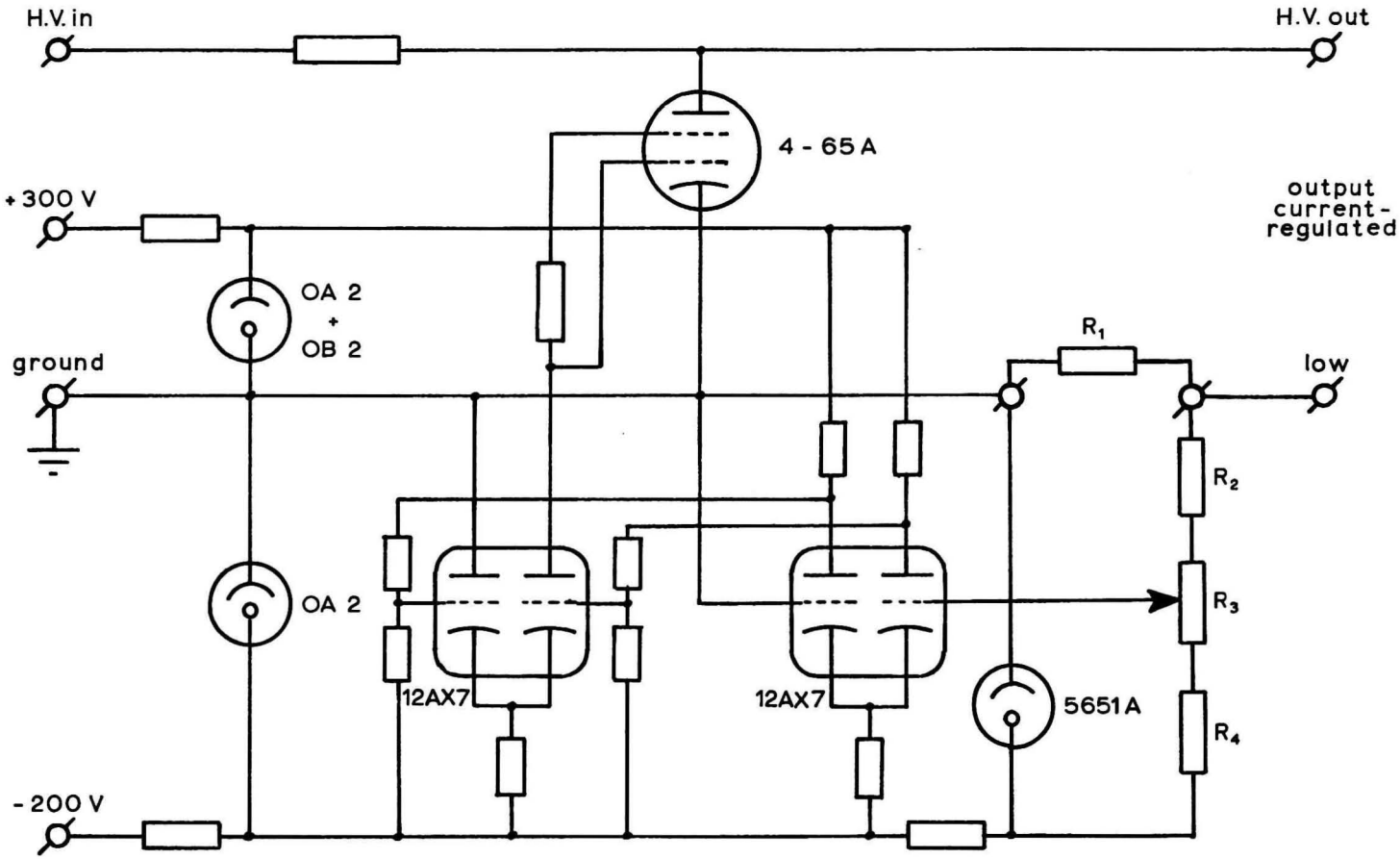

Fig. 2.7 Supply, providing constant current for the laser DC discharge.

detector depended on wavelength and power of the laser radiation and on the required signal bandwidth. With both lasers tuned to a single axial mode, the radiation power available for detection was quite low: 0.005 mW total. Because of expected beat frequency variations, the detector and amplifier bandwidth should be several tens of MHz. This combination of large bandwidth and low power pointed to the use of a photomultiplier tube because suitable solid state *IR* detectors were not available at the time.

The photomultiplier (P.M.) used, was a 7102 RCA 10-stage tube with a maximum rated anode current of 10 μA. The *S*-1 type cathode had a quantum efficiency $\eta \simeq 7 \times 10^{-5}$ for $\lambda = 1.15\ \mu$. Since η is very much larger for shorter wavelengths (up to $\eta \simeq 0.04$ for $\lambda = 0.7\ \mu$) it is very important to prevent such radiation from reaching the photo cathode; the use of an optical band-pass filter was therefore necessary. When Kodak 88A and Corning 7–57 infrared transmitting filters were used, still some 40 % of the PM anode current was due to non-coherent radiation, which increases PM shotnoise without contributing to the signal. It was possible to block this undesired radiation entirely with a Perkin-Elmer narrow band filter (80 % transmission at $\lambda = 1.15\ \mu$, halfwidth 0.02 μ) combined with a set of iris-diaphragms. The PM voltage divider arrangement and signal pick-off was standard circuitry. Both the VHF beat frequency and the PM anode current were recorded continuously, the latter to provide a check on laser- and P.M. performance. By adjusting the P.M. supply voltage, the anode current was set around 6 μA. Some 6 % of this was dark current, the rest was due to the radiation from both lasers, the contributions of which were not necessarily equal due to tube differences and beam-splitter asymmetry. Assuming that, upon reaching the photomultiplier, the laser outputs consist of plane waves with nearly the same frequencies ω_1 and ω_2: $E_1 = A_1 e^{i\omega_1 t}$ and $E_2 = A_2 e^{i\omega_2 t}$, the photo current, which is proportional to light intensity i.e. to electric field amplitude squared, is given by the following expression (see e.g. Alkemade en Bolwijn, 1966):

$$\left.\begin{aligned} i(t) &= \frac{\eta e}{2h\nu}|E_1+E_2|^2 = \frac{\eta e}{2h\nu}[A_1^2+A_2^2+2A_1A_2\cos(\omega_1-\omega_2)t] = \\ &= \frac{\eta e}{h\nu}[P_1+P_2+2\sqrt{P_1P_2}\cdot\cos(\omega_1-\omega_2)t] \end{aligned}\right\} \quad (2.1)$$

with: η = quantum efficiency

e = electron charge

$P_{1,2} = \dfrac{A_{1,2}^2}{2}$ = radiation power.

The first two terms in the right-hand side of equation 2.1 are the DC photo currents due to the two lasers separately $i_{1,2} = \dfrac{\eta e}{h\nu} P_{1,2}$, the time-

dependent term is the beat signal:

$$i_{(\omega_1-\omega_2)} = 2\frac{\eta e}{h\nu}\sqrt{P_1 P_2} \cdot \cos(\omega_1-\omega_2)t$$

The beat amplitude may be expressed in terms of the DC photocurrents

$$i_1 \text{ and } i_2\text{: } i_{(\omega_1-\omega_2)\max} = 2\sqrt{i_1 \cdot i_2} \tag{2.2}$$

The transition from photocurrent i to anode current I simply follows from multiplying by the P.M. current-amplification: $I = G.i$. Equation 2.2 in terms of anode currents remains unchanged:

$$I_{(\omega_1-\omega_2)\max} = 2\sqrt{I_1 \cdot I_2}.$$

This expression gives an upper limit for the beat amplitude since differences in polarisation or angle of incidence of the two beams or incomplete superposition, will reduce $I_{(\omega_1-\omega_2)\max}$ without effecting I_1 or I_2. The difference frequency signal at the VHF P.M.-output was typically a few hundred μV across 50 ohm and at best 90 % of the optimum value from equation 2.2.

2.3.2. *Electronics and recording equipment*

The signal available at the P.M. VHF output is a sine wave with frequency varying between 0 and 150 MHz and several hundred μV peak to peak amplitude. The handling of this signal was for the most part done with standard electronic equipment, indicated on the block diagram given in Fig. 2.8. Everything outside the dashed line was located

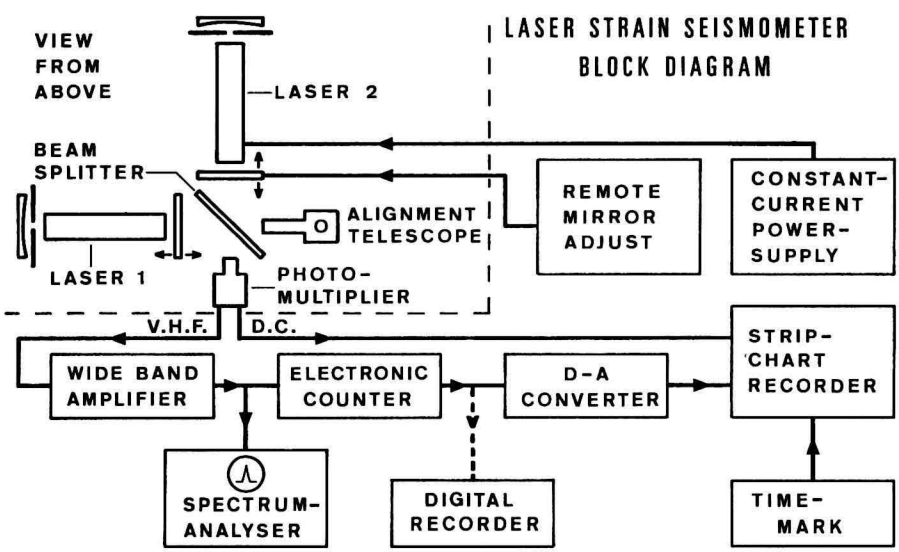

Fig. 2.8 Block diagram of the laser strain seismometer. Everything outside the dashed line is approximately 160 m removed from the lasers.

in a control room some 160 meters away from the lasers. The signal handling was as follows: The VHF P.M. signal was amplified by a factor 10^4, using two 40 dB Hewlett Packard 461 A amplifiers, the first one situated near the laser instrument, the second one in the control room connected by 160 meters of 50 ohm coaxial cable. The signal was then counted by a Hewlett Packard 50 MHz electronic counter, set at a few seconds sampling time. Although in routine operation one would prefer to keep the signal in digital form, in this experimental situation it was advantageous to convert the digital counter output into an analog voltage, which was displayed on several recorders running at different speeds. With this set-up it was possible to count laser beat-frequency reliably within the frequency band 2–40 MHz. The counter reliability was easily verified by monitoring the signal on a spectrum analyser.

Because of the limited dynamic range of analog recorders it was impossible to display more than three digits at a time. Usually these three were chosen such as to make full scale recorder deflection equal to 10 MHz frequency variation. See e.g. Fig. 4.6. The signal was recorded on a Varian G-10 recorder running at 4 inches per hour, the same speed as have the Benioff quartztube strainmeter tidal outputs. This record served mainly for observation of longterm stability and tides. Parallel to this tidal output ran a two-channel Brush recorder, usually at 0.5 mm/sec. with on one channel: beat frequency, on the other: photomultiplier anode current or any variable whose effect on the signal is of interest, such as e.g. air temperature, barometric pressure, rectified line voltage etc. Besides, a helicorder was sometimes used in combination with high pass filtering. Hour or minute marks were obtained in the usual way from time switches in an electronic chronometer. The spectrum analyser (Singer Metrics SPA 4) appeared to be an indispensable tool all along, giving information on frequency, amplitude, quality of the signal, on the number of simultaneously oscillating modes, on counter reliability. Beat frequency bandwidth measurements were limited to the spectrum analyser's maximum resolution of 10 kHz.

2.4. Installation and operation of L.S.S.

With the exception of initial preparations and some instrument-modification trials, carried out at the laboratory, the experiments and recordings were performed in an underground seismic observatory.

2.4.1. *The Ogdensburg observatory*

The observatory (41° 05′ 15″N; 74° 35′ 45″W) is situated in Ogdensburg N.J. at a depth of 560 meters in an inactive part of the Sterling hill mine, owned by the New Jersey Zinc Company. The mine-drifts housing the observatory are driven in the precambrian Franklin formation, a competent calcite marble. This station has been extensively described by M. W. Major et al. (1964). The present description will therefore be brief, and

mainly limited to some recent changes. As can be seen on the map given in Fig. 2.9, the observatory's entrance and only exit to the surface is from the west. This entrance can be closed by a set of two ships doors, seated on rubber and mounted in airtight concrete bulkheads. The space behind these doors is divided in two sections: a recording and an instrument section, separated by another set of pressure doors. Part of the recording section is a darkroom for photographic registration, the remainder is operating room with ink recorders, clocks, test equipment, machineshop etc. The instrument section contains amongst other things the World-Wide Standardized Seismograph Network instruments, other long- and short period pendulums, three horizontal and one vertical quartz tube strainmeters and several experimental set-ups. By closing the airtight doors

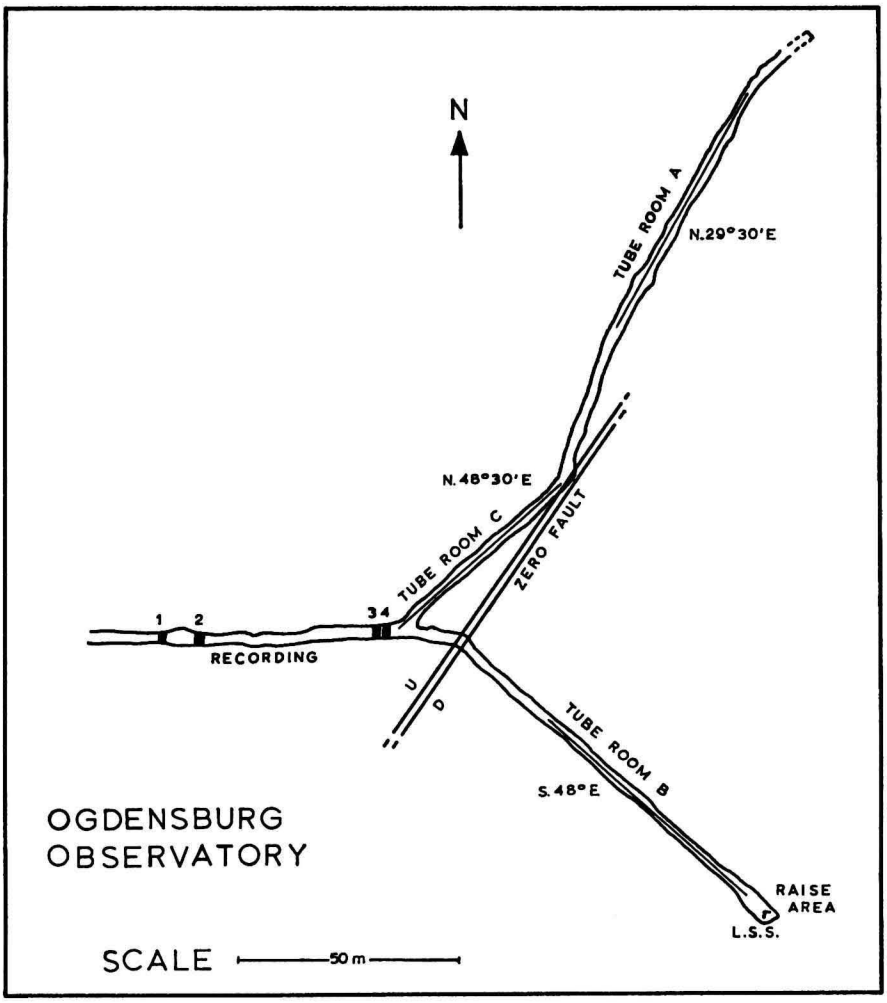

Fig. 2.9 Map of the Ogdensburg underground observatory. The laser instrument was located in the raise area.

the instruments are sealed against short-period air pressure and temperature variations, occurring in the operating room, mainly owing to ventilation with compressed air and to changes in power consumption. In Fig. 2.10 simultaneous records of microbarographs in operating- and instrument room illustrate the effect of the pressure seal. The seal is obviously not tight, it rather acts as a low pass filter. The leak caused by water drain from the observatory to the drift west of the entrance was sealed with a solenoidvalve and sump pump. This helped to increase the leak time-constant from 45 minutes to the present value of 2 hours. Especially for tidal observations it will be advantageous to increase this time-constant to at least 12 hours. An improved construction of the concrete bulkheads is planned for this purpose.

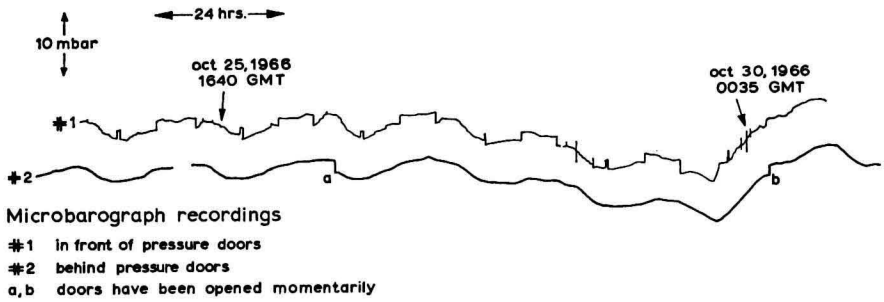

Fig. 2.10 Variations in the barometric pressure during one week. Record nr. 2 shows the effect of the pressure doors which close off the instrument section.

2.4.2. *Installation procedures and routine operation.*

During the period that the records shown in chapter IV were made, the instrument was situated in the raise area at the end of tuberoom B (see Fig. 2.9). The floor of the raise area consists of a layer of concrete poured on the rock; at the site of the lasers, this layer is 0.5 meter thick. The mirror holders were fastened to the floor with 25 mm long lead expansion anchors, put into the concrete along lines that run roughly NS and EW. By means of an alignment telescope, the mirror holders were then positioned in such a way that their centers all line up along the telescope axis. With the telescope as an autocollimator, the mirrors were then adjusted to a position normal to this axis within 0.1 minute of arc. The beam-splitter of course took care of the 90° difference between the two cavities. A check on the orientation, using mine surveyer marks gave the following cavity directions:

azimuth	cavity 1	84°	± 30′
	cavity 2	174° 30′	± 30′

These orientations together with directional sensitivity patterns for longitudinal and transverse apparent waves are given in Fig. 2.11. It can be seen that the instrument has maximum sensitivity for longitudinal

waves coming in from azimuths N 84° E, N 174° E, N 264° E and N 354° E and for transverse waves coming in from azimuths N 39° E, N 129° E, N 219° E and N 309° E. Now laser tubes and diaphragms were put in position and centered by telescope. Any dust that might have settled on mirrors and Brewster windows was blown off with low pressure dry nitrogen and the dust-cover assemblies were put into place. At this point the tubes were started and the current set within the quiet range, as discussed in section 2.1.1. Laser action was observed with an infra red image converter. Some mirroradjustment was usually necessary to maximize the laser outputs. The near-field pattern as observed in the I.R. converter was a bright, roughly circular, pattern with spatial variations in intensity: apparently a combination of different modes was oscillating simultaneously. By slowly decreasing the diaphragm aperture, the mode pattern became simpler, losing intensity at the same time. Finally the pattern assumed an axially symmetric, approximately gaussian intensity distribution, as is characteristic for TEM_{ooq} modes. Both lasers were adjusted in this fashion while at the same time mirrors, diaphragms and

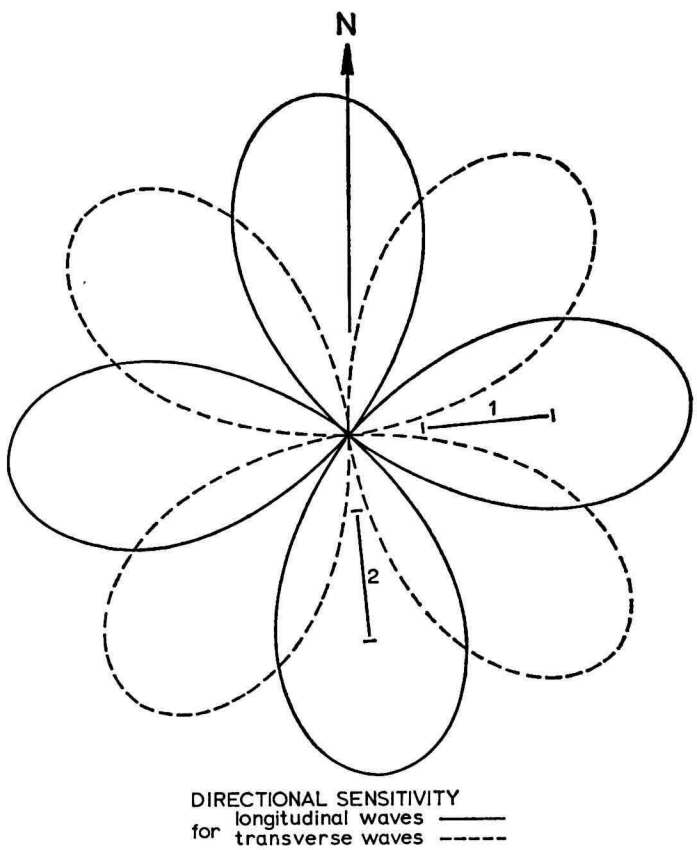

Fig. 2.11 Directional sensitivity pattern of the laser strain instrument for longitudinal and transverse waves.

beam-splitter were readjusted if necessary to keep both outputs parallel and coincident.

By now the P.M. output would produce beatsignals, which then served as a sensitive indicator for further fine adjustments. While the spectrum analyser was monitored, the cavities were tuned back and forth several times over their axial mode spacing and the iris diaphragms were reduced until the selfbeats at 150 MHz were absent during most of the time. By closing the diaphragm openings to 2.5 or 3 mm diameter, the single mode-double mode ratio – defined as the ratio of the lengths of time the laser oscillates in a single axial mode and in two axial modes respectively, when the cavity length is being changed at a constant rate – was set roughly between 2 : 1 and 3 : 1. A "vernier" adjustment was later possible by slightly changing the discharge current. The P.M. high voltage was adjusted for a total photocurrent around 6 μA (see section 2.3.1). At this point the insulation cover and heater tapes were installed and the instrument was allowed to reach thermal equilibrium, which took several days. Both tubes were then tuned near atomic linecenter and were off-set with respect to each other to produce a beat-frequency within the counting range: say 10 MHz. This difference frequency was then recorded continuously as described in section 2.3.2.

Because of seismic signals, tides and drift the beat-frequency will change with time. Because the lasers were free-running, drifts acting equally on both cancel out: the signal was only effected by drift differences. However, as both cavities drift away from linecenter, the beat amplitude will decrease and finally two axial modes will appear in one or both tubes, resulting in a reduced signal to noise ratio and faulty counter operation.

Usually the drift rate was such as to cause a need for resetting once every 2 or 3 days. This was done conveniently by actuating the mirror-stand motors for a few seconds. To cancel out the effect of heating up of the mirror-stands during this adjustment, the motors were always run simultaneously: in opposite directions to change beat frequency, in the same direction to change beat amplitude. On the average the motors should be actuated equally long in both directions, otherwise cavity alignment will eventually be affected.

Chapter III

NOISE; INSTRUMENTAL AND ENVIRONMENTAL EFFECTS ON L.S.S. PERFORMANCE

In this chapter an account is given of the influence that several noise sources, nonlinearities and measuring errors have on instrument performance. An estimate of the useful sensitivity is given and the chapter ends with some suggestions for further improvement. As was explained in chapter I, the LSS is essentially described by the equation

$$\frac{d\nu}{\nu} = -\frac{dL}{L} \tag{3.1}$$

Apparently seismic strain is found by measuring laser frequency shift. Now, besides these seismic and tidal signals, the laser frequency may be changed by a number of other effects, both caused by the instrument itself and by the environment.

3.1. Instrumental effects

Before evaluating the noise caused by the instrument the validity itself of equation (3.1) should be questioned since it is the result of two simplifications:

1. By ignoring the effect of the active medium the laser frequency was assumed to coincide with a cavity resonance.
2. The effective distance over which strain is measured was taken equal to the mirror separation.

These points are treated in the next two sections.

3.1.1. *The active medium, mode pulling and pushing*

To account for the effect of the amplifying medium on oscillation frequency a linear mode-pulling term was introduced in chapter I, resulting in equation (1.12). To check whether this linear approximation is justified, non-linear effects will now be evaluated that follow from a more general description based on Lamb's theory (Lamb 1964). With his notation the single mode oscillation frequency may be written as follows:

$$\nu = \Omega + A + B \tag{3.2}$$

with

$$A \equiv \tfrac{1}{2}(\nu/Q)\eta Z_r(\Omega-\omega)/Z_i(0) \tag{3.3}$$

$$B \equiv \tfrac{1}{2}(\nu/Q)\{\eta Z_i(\Omega-\omega)/Z_i(0)-1\}\cdot\gamma_{ab}(\Omega-\omega)/(2\gamma_{ab}^2+(\Omega-\omega)^2) \tag{3.4}$$

where ν = oscillation frequency
Ω = cavity resonance frequency
ω = atomic line-center frequency
} in circular frequencies
Q = interferometer quality (see equation 1.6)
γ_{ab} = natural linewidth
Ku = Doppler linewidth parameter related to the full Doppler linewidth $\Delta\nu_D$ by:

$$\frac{Ku}{2\pi} = 0.6\Delta\nu_D$$

η = relative excitation above threshold, defined as $\eta \equiv N/N_T$, where N is the excitation density: the excess density of active atoms in the absence of oscillation; N_T is the excitation density needed to reach the oscillation threshold when the cavity is tuned at atomic line-center $\Omega=\omega$.

Z_r and Z_i are the real and imaginary parts of a complex function

$$Z(\zeta) = 2i \int_{-\infty}^{i\zeta} \exp[-(t^2+\zeta^2)]dt \tag{3.5}$$

with

$$\zeta = x+iy$$

$$x = \frac{\Omega-\omega}{Ku}\,;\; y = \frac{\gamma_{ab}}{Ku}.$$

Tabulated values of this function $Z(\zeta)$ can be found in the literature (FADDEYEVA and TERENT'EV 1961). In equation (3.2), A and B describe modepulling and -pushing respectively, both terms are non linear functions of cavity detuning and especially the latter is power dependent.

Near threshold of oscillation $B \ll A$ and if also $x \ll 1$ and $y \ll 1$, the pulling term becomes approximately linear and reduces to equation (1.9):

$$A \simeq \nu-\Omega \simeq (\omega-\Omega)\frac{\Delta\nu_C}{\Delta\nu_D} \tag{3.6}$$

we rewrite (3.3) and (3.4) somewhat:

$$\frac{A}{\nu/Q} = \tfrac{1}{2}\eta Z_r(x,y)/Z_i(0,y) \tag{3.7}$$

$$\frac{B}{\nu/Q} = \tfrac{1}{2}\{\eta Z_i(x,y)/Z_i(0,y)-1\}\cdot\frac{y\cdot x}{2y^2+x^2}. \tag{3.8}$$

The relative excitation η, expressed in terms of Z is:

$$\eta = Z_i(0, y)/Z_i\left(\left(\frac{\Omega-\omega}{Ku}\right)_T, y\right) \tag{3.9}$$

or

$$\eta \simeq e^{\left[\left(\frac{\Omega-\omega}{Ku}\right)_T\right]^2} \text{ if } y \ll 1 \text{ as is usually the case.} \tag{3.10}$$

The threshold detuning $(\Omega-\omega)_T$ in a particular experimental situation, may be found directly by observing the frequency value at which a certain beatnote drops out on the spectrum analyser, while beating two lasers, one of which is being detuned to the left and right of the line-center.

It may also be derived from the behaviour of the self beat of one laser that is being detuned: one may write

$$\left(\frac{\Omega-\omega}{2\pi}\right)_T = \tfrac{1}{2} \cdot \frac{r+2}{r+1} \cdot \frac{c}{2L},$$

where r is the single mode/double mode ratio, defined in section 2.4.2.

From our measurements, the threshold detuning was found to be

$$\left(\frac{\Omega-\omega}{2\pi}\right)_T = 100 \pm 5 \text{ MHz}.$$

Substitution of this value in eq. 3.9, together with suitable values for atomic- and Doppler linewidth parameters y and Ku, and use of the tables of Faddeyeva and Terent'ev results in a relative excitation $\eta = 1.04$ for $y = 0.1$ and $\frac{Ku}{2\pi} = 480$ MHz (Bennett 1965, Bolwijn 1967). Next from 3.7 and 3.8, pulling and pushing is calculated as a function of cavity detuning and plotted in Fig. 3.1. In this figure negative values for $\frac{\nu-\Omega}{\nu/Q}$ of course represent frequency pulling, positive values represent pushing. Apparently at this low excitation level the pushing effect is small compared with pulling, while the latter comes fairly close to being linear. In Fig. 3.2 the non-linear behaviour is magnified by plotting total frequency shift minus linear pulling. The curves of Fig. 3.1 and 3.2 apply to both lasers, each of them oscillating near its own unknown cavity resonance frequency: a point somewhere on the horizontal axis of Fig. 3.1 or 3.2. The difference frequency not corrected for mode pulling and pushing is then represented by the distance between those two points along the horizontal axis.

Obviously, linear mode pulling is independent of the individual laser frequencies and is proportional to the beat frequency. This is not true for the non-linear pulling and pushing: Taking a fixed beat frequency, the non-linear frequency deviations as found from Fig. 3.2 clearly depend on the setting of the individual cavities. The deviation apparently is

highest, when the derivative of the curve of Fig. 3.2 is maximum, i.e. when the lasers are offset to opposite sides of atomic line-center, and lowest when this derivative is minimum, that is, when the lasers are offset to opposite sides of a point (denoted by P in Fig. 3.2) some 60 MHz away from atomic line-center. Also from Fig. 3.1 it is clear that the non-linear effects tend to decrease the linear pulling. In order to evaluate the magnitude of these effects it follows from eq. 3.7 and 3.8 that the value

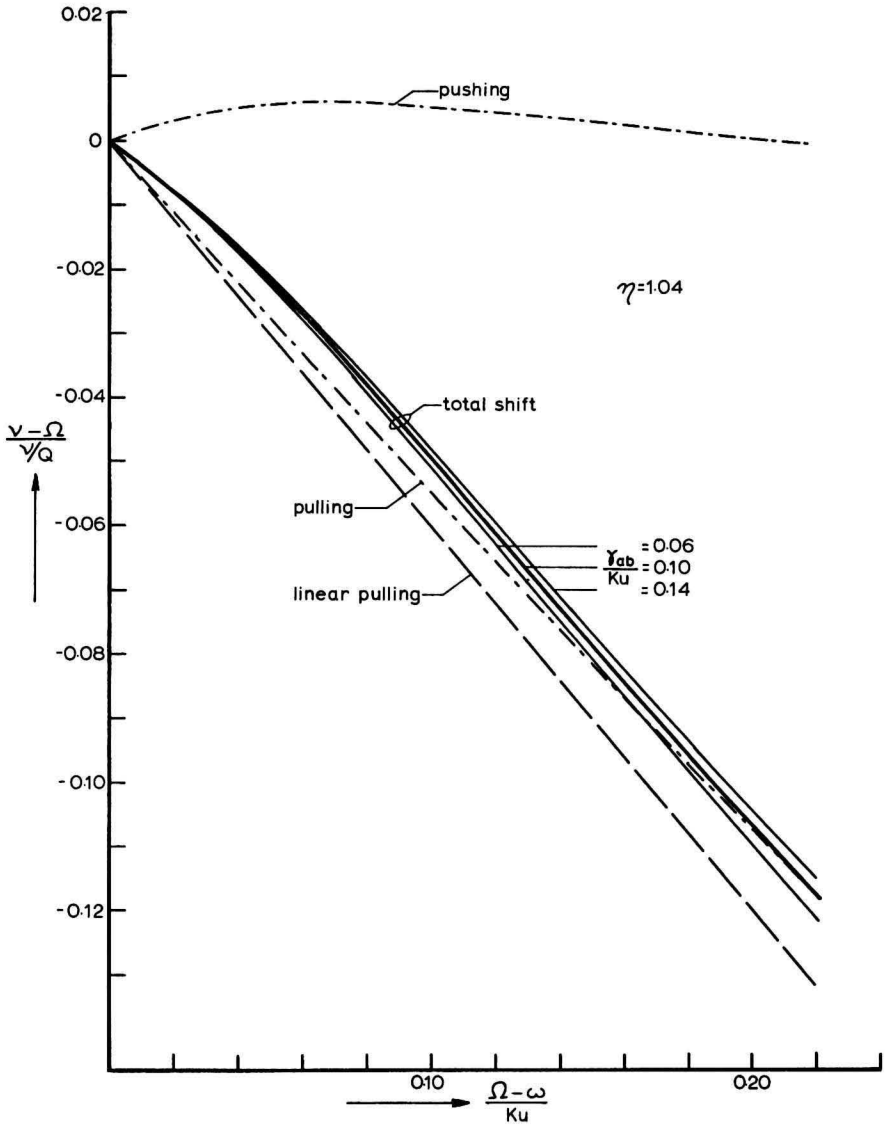

Fig. 3.1 The shift of the oscillation frequency ν from the cavity resonance frequency Ω as a function of the frequency difference between the cavity resonance Ω and the atomic line center ω, for different values of the natural linewidth parameter γ_{ab}/Ku.

of ν/Q must be known. Using eq. 1.6 and realising that, in Lambs notation, ν is expressed in circular frequency, one finds

$$\frac{\nu}{Q} = 2\pi\Delta\nu_C. \tag{3.11}$$

An estimate of the active cavity width is obtained as follows: When one of the lasers oscillates in two axial modes, its selfbeat-frequency is,

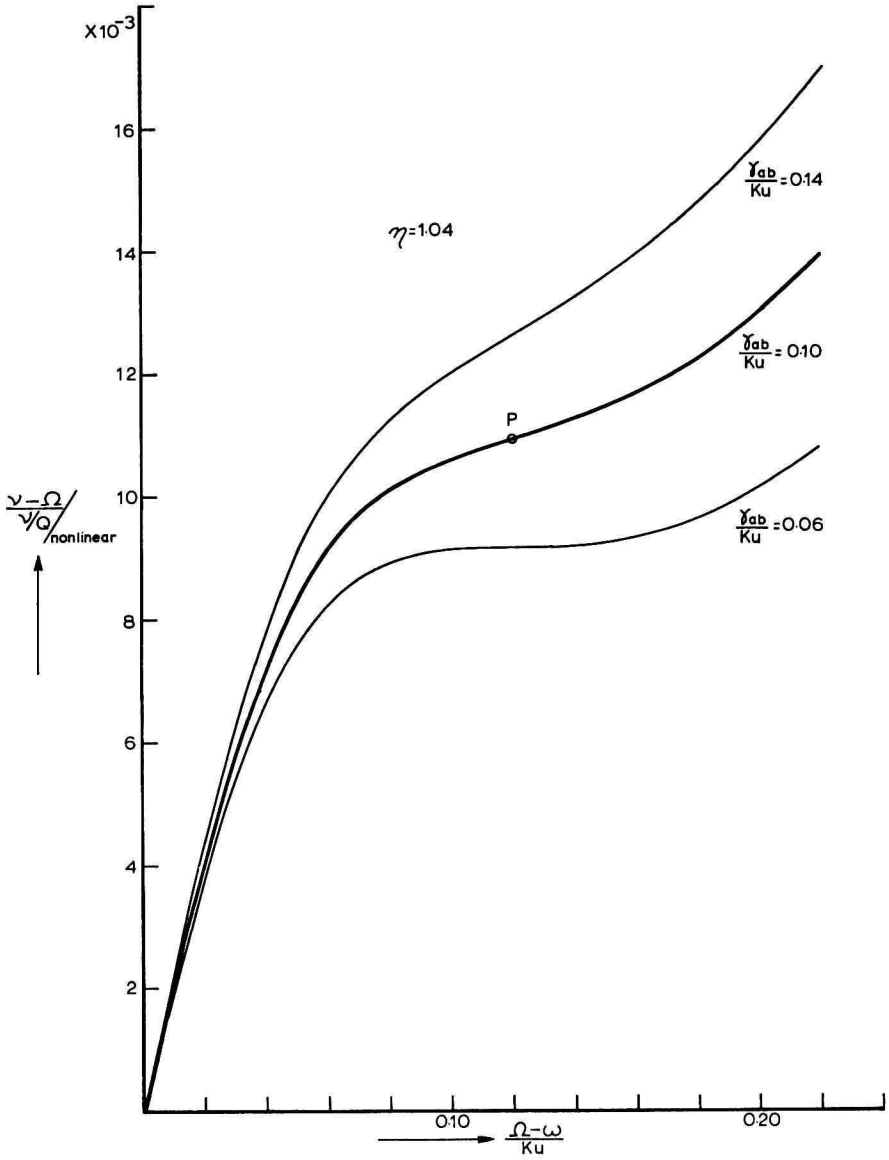

Fig. 3.2 The non-linear part of the oscillation frequency shift of Fig. 3.1, obtained by subtracting the effect of linear pulling. The γ-scale is 10 times larger than in Fig. 3.1.

from measurement, approximately 148.5 MHz. From the known mirror distance L, the difference between cavity resonances is easily found:

$$\frac{c}{2L} = 150.20 \text{ MHz}.$$

If we substitute these values in eq. 3.6 and thus assume that pulling on the two modes is linear and independent, and take the Dopplerwidth $\Delta\nu_D = 800$ MHz, we obtain an active cavity width $\Delta\nu_C \simeq 9$ MHz. With equation 1.7, this value for $\Delta\nu_C$ leads to a cavity loss $f = 19$ %. As a check this loss figure is determined independently in two other ways, apparently with consistent results:

1. Since mirror transmission losses amount to 1 %, the loss must be due almost entirely to diffraction at the iris diaphragm. The diaphragm-openings actually used were some $2\frac{1}{2}$ to 3 mm in diameter; according to the table in section 2.12, based on Li's calculations, the associated diffraction loss is found to be between 25 % and 16 %.
2. If we operate close above threshold, gain and loss are approximately equal. Gain figures for the 1.15 μ line and for similar tube parameters are listed as 12 % per meter by BENNETT (1965) and 13.8 % per meter by BALLIK (1964). Since the active discharge length is 70 cm the gain per roundtrip is 1.4 times the above figures, or 17 % and 19 % respectively.

Substituting $\Delta\nu_C$, in equation 3.11 and using the value obtained for ν/Q in combination with Fig. 3.1, one finds that strains calculated with eq. 3.1 are too low by roughly 1 % owing to linear pulling. The additional correction for non linear shifts is equal to the product of the uncorrected beatfrequency times the derivative of the curve of Fig. 3.2 taken at the appropriate position along the x-axis. Depending on this position (i.e. the amount of detuning of the two lasers), the non linear correction is found to vary between 0.4 % and 0.04 %, which being of opposite sign, has to be subtracted from the linear correction.

Taken together, the total shift due to the presence of the active medium causes the measured beat frequency to be too low by an amount varying between 0.6 % and 1 %, depending on the (unknown) tuning of the cavities.

3.1.2. *Cavity length and effective mirror stand separation*

The mirror distance L has so far been identified with the distance, across which the strain is measured. The latter, which will be called L', is the distance between the mirror stands or more precisely: between their effective points of contact with the ground. From Fig. 2.4 it is obvious that L' is smaller than L. Since each stand rests on three different points, the effective point of contact is located somewhere in between, and its choice somewhat arbitrarily leads to a value $L' = 930$ mm $\pm$ 50 mm.

Because of this difference between L and L', equation 3.1 should read:

$$\frac{d\nu}{\nu} = -\frac{dL'}{L}. \tag{3.12}$$

By substitution of $L = a \cdot L'$ with $a = 1.08 \pm 0.05$ in eq. 3.12, the actual strain is

$$\frac{dL'}{L'} = -a \cdot \frac{d\nu}{\nu}. \tag{3.13}$$

Apparently, according to 3.13, the actual strain is 8 % ± 5 % higher than is indicated by the measured relative frequencyshift. It seems reasonable to expect that this error can be reduced to 1 % or 2 % by a more careful mirror stand design.

A possible source of instrumental noise related to the mirror separation which was not observed but which may become important as the effects of other sources of instability are being reduced, may be the fluctuations in the position of the average mirror surface as seen by the wavefront.

1. Partly these fluctuations will arise from movements of small particles for instance molecules of the coating material over the mirror, thus changing the topography of the mirror surface on an atomic scale.

Since molecular dimensions are of the order of 1 Å, the effect of these movements will be vastly reduced by the averaging done by the wavefront, which extends over thousands of Ångstroms. However, a stability of 10^{-12} implies for a 1 meter long cavity, that the position of the averaged mirror surface be constant to within 0.01 Å.

Apparently this is no problem for short periods of time since stabilities of 10^{-13} during several seconds have been reported (JASEJA et al. (1964), BOERSCH et al. (1967)). Whether the above mentioned fluctuations will be a limiting factor in the ultimately realisable stability over longer periods is not known. The long term instabilities of the LSS that were observed, can be explained as caused by slow variations of several environmental parameters, all of which can be considerably reduced as is explained in the following sections.

2. A second source of fluctuations are the thermal vibrations of the mirror holders and theoretically also of the rock sample on which the instrument is mounted.

The fractional change in frequency caused by the fundamental mode thermal vibrations is given by

$$\frac{d\nu}{\nu} = \sqrt{\frac{2kT}{E.V.}}$$

where k = Boltzmann's constant

$$\left.\begin{array}{l} T = \text{absolute temperature} \\ E = \text{modulus of elasticity} \\ V = \text{volume} \end{array}\right\} \text{ of vibrating body}$$

Substituting appropriate values
$E(\text{aluminum}) = 6.6 \times 10^9$ kg/m^2, $V(\text{mirrormount}) \simeq 380$ cm^3 results in $\frac{d\nu}{\nu} \simeq 6 \times 10^{-14}$ for the mirrormount.

For the rock sample this figure will be considerably smaller, because of the much larger volume of material.

3.1.3. *Discharge current variations*

Variations in discharge current effect the laser frequency in three ways:

1. The accompanying change in heat dissipation will cause thermal variations of the instrument's dimensions, thereby changing the cavity length.
2. Since the index of refraction of air depends on temperature, the optical cavity length will change when the temperature of the air between windows and mirrors changes.
3. Changes in current effect the tube gain (Fig. 2.2), which causes a variation of frequency because of power dependent mode pulling and pushing.

The first effect was evaluated as follows: At some point during the experiment the discharge current in one laser was adjusted from 7.85 *mA* to 7.65 *mA*. This caused the beatfrequency to drift for over a day, the record showing a roughly exponential behaviour with a time-constant $\tau \approx 7$ hours and around 160 MHz total frequency shift.

It follows from this observation that a 1 % change in discharge current will cause a frequency shift of some 60 MHz. As was mentioned in section 2.2, the discharge current in each laser is stabilized independently to 0.2 % or better, which means that current variations with periods $T > \tau$ may cause at the worst frequency variations up to 24 MHz, equivalent with variations in strain of 8×10^{-8}. Fortunately, the 7 hours time constant, which is caused by the instrument's thermal mass, acts as a low-pass filter such that faster current variations are attenuated by a factor T/τ. If e.g. $T = 4$ min. then an apparent strainsignal $\frac{\Delta\nu}{\nu} = 8 \times 10^{-10}$ is produced.

The second effect, the influence of changes in refractive index of the air in the gaps between windows and mirrors, is of course included in the experimentally observed frequency shift due to a current variation, that was mentioned above.

However, since the time constant involved is probably considerably less – several minutes instead of several hours –, the effect may be more prominent for short period current variations. Therefore a separate evaluation is given: the dependence of the refractive index of air on temperature and pressure is as follows (Am. Inst. of Physics handbook 6–96):

$$(n_{T,p} - 1) = (n_{15,760} - 1) \cdot \frac{p}{760} \cdot \frac{1 + 15\alpha}{1 + T\alpha} \cdot \frac{1 + \beta_T \cdot p}{1 + \beta_{15} \cdot 760} \tag{3.14}$$

with $n_{15,760} - 1 = 2.74 \times 10^{-4}$ for $\lambda = 1.15\ \mu$.

T = temperature in °C.
p = pressure in Torr
$\alpha = 0.003661$
$\beta_T = (1.049 - 0.0157\ T)10^{-6}$

In this equation the last factor may be ignored since its effect, when compared with the remaining expression is 1000 and 300 times smaller for pressure- and temperature changes respectively:

$$(n_{T,p} - 1) = (n_{15,760} - 1) \cdot \frac{p}{760} \cdot \frac{1 + 15\alpha}{1 + T\alpha} \tag{3.15}$$

Differentiating with respect to T and substituting $p = 760$ torr and $T = 15°$ C yields:

$$\frac{\Delta n}{\Delta T} \simeq 0.94 \times 10^{-6} \cdot /°\text{C}.$$

The change in cavity length due to a change in n of course depends on the length l of the airgaps:

$$\Delta L = \Delta n \cdot l$$

Now from 3.1, neglecting the minus sign:

$$\Delta \nu = \frac{\nu \cdot \Delta n \cdot l \cdot}{L} \tag{3.16}$$

$$\frac{\Delta \nu}{\Delta T} = \nu \cdot \frac{l}{L} \cdot \frac{\Delta n}{\Delta T}.$$

Substitution of $l = 28$ mm and of appropriate values for the other variables, results in

$$\frac{\Delta \nu}{\Delta T} = 6.5 \text{ MHz}/°\text{C} \tag{3.17}$$

The temperature variation in the airgaps is not known from measurement. One may, however, evaluate its effect as follows:

Suppose the temperature in the airgaps is 10° C higher than the environmental temperature of the instrument. This difference will be caused by the powerdissipation of the discharge.

Discharge current variations with periods of at least several minutes will change the airgap temperature and consequently cause beat frequency variations.

The experimentally observed beatfrequency noise usually has periods of several minutes and peak to peak amplitudes (see Fig. 3.4) of some 50 kHz. From eq. 3.17 this figure corresponds with a variation in airgap temperature of $T \simeq 0.008°$ C. This value of T, in turn points to a variation

of 0.08 % in the power dissipation of the discharge, which means discharge current changes of 0.04 %. These may indeed be expected from variations of the reference voltage, which can produce current changes up to 0.2 % (see section 2.2). Improvement of the discharge current stability therefore seems of considerable importance to reduce the long period noise level. For short period current variations (periods typically less than 1 minute) the same reasoning will hold but the effects will be attenuated because the instrument's thermal mass will act as a low pass filter.

The third effect is apparent from equations 3.2–3.4, in which the relative excitation depends on discharge current: $\eta(I)$. The variation of η with current was experimentally determined by observing the change in threshold detuning, following a change in current. By means of the approximate expression 3.10, the dependence of η on current was found to be

$$\frac{\Delta\eta}{\Delta I} \approx 0.02/mA.$$

Considering that the DC discharge current $I \simeq 6\ mA$, that the current stability is 0.2 %, and that the relative excitation η is 1.04, one may expect variations in η of 0.0002 due to changes in I. According to eq. 3.7, modepulling is directly proportional to η, while from eq. 3.8 it follows that since $Z_i(x, y)/Z_i(0, y) \leqslant 1$, modepushing is approximately proportional to $(\eta - 1)$. A change in η of 0.0002 owing to current variations means a change in $(\eta - 1)$ of 0.5 %. The uncertainty in the beat frequency due to modepushing was found to be 0.4 % in section 3.1.1. The effect of a 0.5 % variation in $(\eta - 1)$ therefore amounts to an additional 0.002 %, uncertainty which may obviously be ignored. The same is true for the effect of $\Delta\eta$ on modepulling which is even smaller.

3.1.4. *Air convection around the instrument*

When the LSS is installed in a normal laboratory environment without any protective cover, the noise level and drift rate will be so high as to drown any (tele)seismic signals: fluctuations of several MHz over a few minutes are superimposed on a drift, which in a non airconditioned room may be several tens to more than 150 MHz per hour, depending on weather conditions. The fluctuations can be substantially decreased by installing protective covers around the ends of the tubes (no. 6 in Fig. 2.5), thus reducing air convection between Brewster windows and mirrors. In addition a styrofoam box, (Fig. 2.6) covering the entire instrument, will filter out fast temperature changes and reduce acoustical noise due to for instance running equipment and talking people. Of course the drift due to slow temperature changes remains the same. The combined effect of both types of shielding is apparent in Fig. 3.3 which shows two record samples of 1 hour duration and 50 MHz full scale recorder deflection. The samples were taken on different days, which explains the difference

in thermal drift rate. The short-term improvement is considerable: frequency variations are reduced by a factor of 6 to less than 0.5 MHz peak to peak. Fig. 3.3.2. illustrates quite clearly the limited frequency range acceptable to the counter. Apparently the meaningful counting range extends from 2 to 40 MHz .This subject is dealt with in section 3.1.6.

By moving the LSS to the underground observatory, the drift caused by the daily temperature changes disappears and a record such as presented in Fig. 3.4.1 is the result. The records of Fig. 3.3.2 and Fig. 3.4.1 have roughly the same short-period noise level although this is somewhat hard to see because of the differences in paper speed and sensitivity, which are a factor 8 and 40 respectively. The noise in record 3.4.1 has periods of predominantly around 1 minute, and to check whether this was still caused by air convection, we filled the empty space around the instrument within the boxcover with pieces of styrofoam. This turned out to improve the noise level as is apparent from record 3.4.2. Also the noise-period decreased, caused perhaps by the smaller size of possible

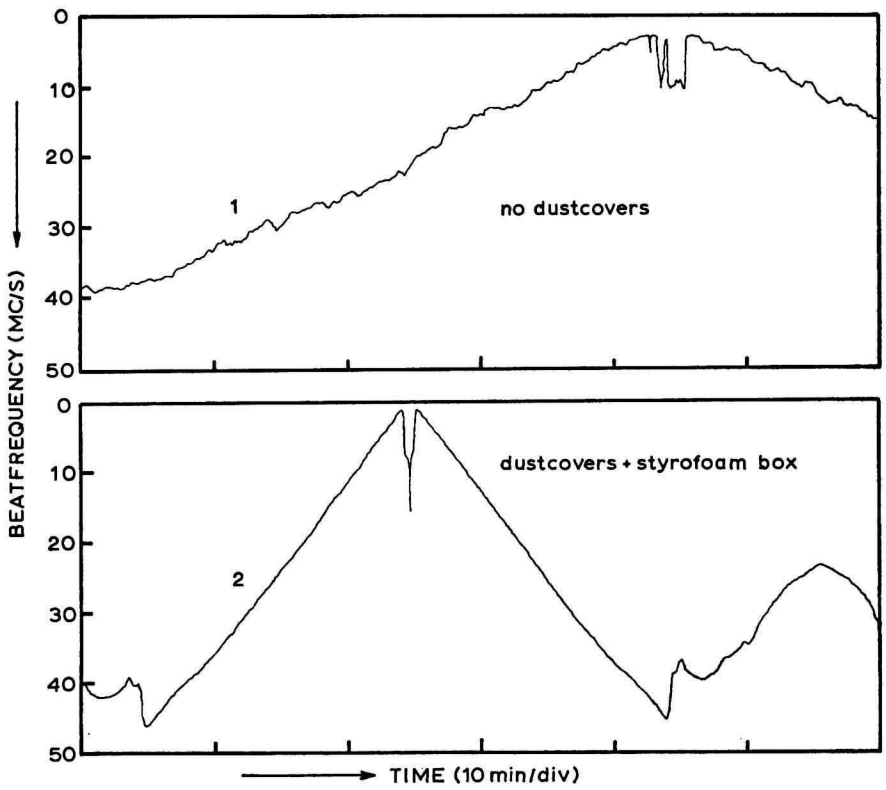

Fig. 3.3 An early recording of one hour duration of the laser strain seismometer output. The instrument was then operating in a normal laboratory environment. Shielding of the instrument improves the short period noise level. The records were taken on different days, which explains the difference in thermal drift. The electronics were such that beat-frequencies in the range 2–40 MHz were reliably counted.

convection cells. To further improve on instrument noise a stable air temperature distribution around the laser tubes was created by adding a top layer of heater tape, as is described in section 2.1.3. The resulting improvement is demonstrated by the third test record in Fig. 3.4. Initially a 12 mm wide ribbon type heater tape was used, this was subsequently replaced by a 60 mm one, thus creating a much more even temperature distribution. This modification plus some other improvements – notably the removal of nearly all electronic equipment from the vicinity of the instrument – again resulted in a lower noise level as is shown by the recordsamples 3.4.4 and 3.4.5. These records were taken during a microseism storm and on a fairly quiet day respectively, which explains the difference in 5–6 second-period noise. The 100–300 second noise level is approximately the same in both records and has amplitudes around 20 kHz which amounts to 8×10^{-11} strain.

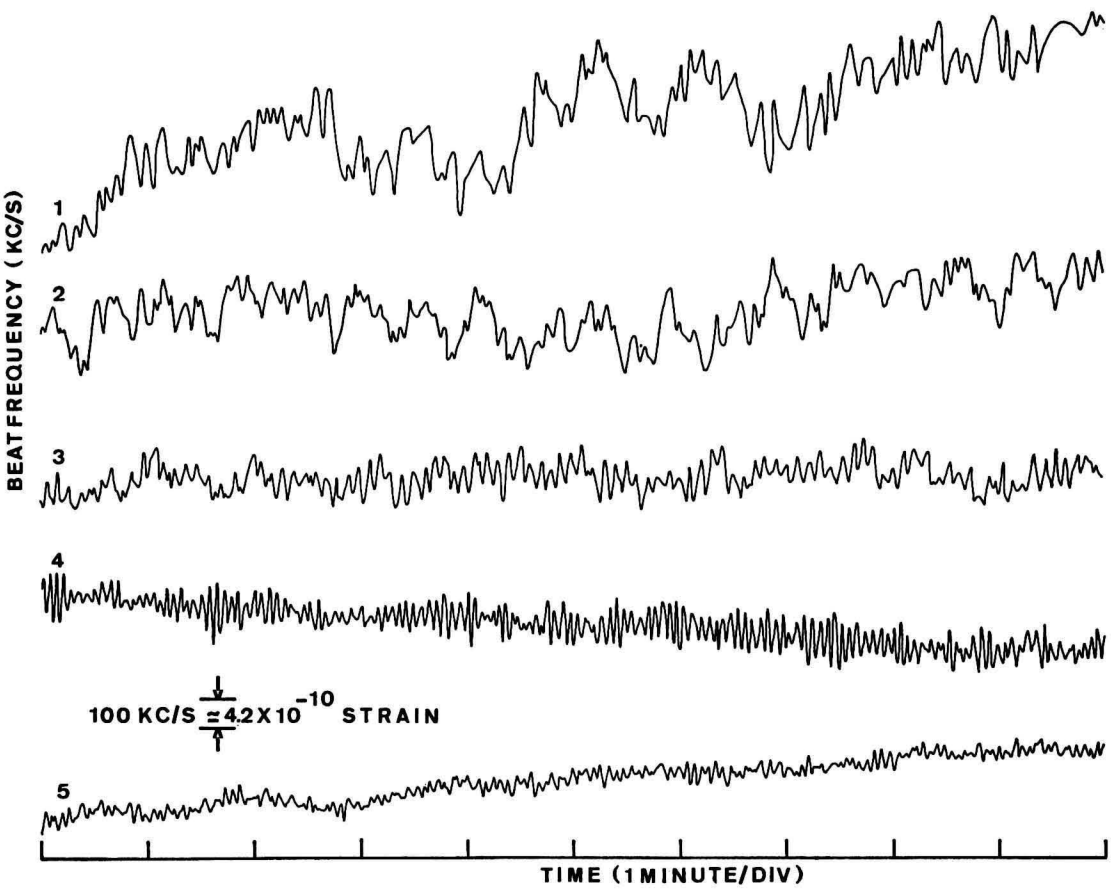

Fig. 3.4 10 Minute record samples to illustrate the noise level reduction in successive stages of the instrument's development.

3.1.5. *Heat from motor drives*

As was mentioned in section 2.4.2 the heat, produced when running the mirror-stand motors will also cause the beat frequency to change. No permanent offset is produced, however, and the effect is noticable only when the cavities are tuned over several tens of MHz. By running both motors simultaneously, the effect is removed because the thermal expansion taking place in both cavities is equal and cancels out in the difference frequency.

3.1.6. *Photomultiplier- and amplifier noise*

The noise made by photomultiplier and amplifier will bring about fluctuations in signal amplitude, not frequency. It is therefore of interest only in so far as it will interfere with frequency counting. With the iris diaphragms adjusted as described in section 2.4.2 for a single mode/double mode ratio of $2\frac{1}{3}$: 1, the fraction of the output power of the two lasers, hitting the photomultiplier cathode was measured to be 1.8 and 3.3 μ W $\pm$ 30 %. With this power coming in, the P.M. dark current amounted to some 6 % of the photo current. In order to maximize the ratio of signal to the noise of the first amplifier, the P.M. high voltage is adjusted for a photo current as high as is compatible with the tube's maximum ratings. In this way the amplifier noise voltage is less than 10 % of the signal. When we monitored the signal on a wideband 50 MHz oscilloscope, the best possible overall signal to noise ratio that could be obtained was $S/N \approx 3$.

According to ALKEMADE and BOLWIJN (1966), the S/N to be expected due to shotnoise in the P.M. cathode is given by

$$S/N = \sqrt{\frac{\eta}{h\nu B} \cdot \frac{P_1 \cdot P_2}{P_1 + P_2}} \qquad (3.18)\,*$$

where B = amplifier bandwidth

$P_{1,2}$ = power from laser 1,2 hitting the photo cathode.

Substitution in equation 3.18 of appropriate values:

$$\eta = 8.4 \times 10^{-5},$$

$P_1 = 1.8\,\mu W$, $P_2 = 3.3\,\mu W$, $B = 50$ MHz, and increasing the value of $(P_1 + P_2)$ by 6 % so as to take care of the dark current, will result in a signal to noise ratio $S/N = 3.3 \pm 0.7$. The error is caused by estimated uncertainties of 30 % in P and η. Comparing the observed S/N with what is to be expected from shot noise alone, there does not appear to be any other appreciable noise source such as excess noise from laser or discharge.

---

*) The square root, which is absent in the reference, is added to get S/N expressed in voltage.

With this $S/N \simeq 3$ it has been possible to count frequencies reliably up to 40 MHz, as is illustrated quite clearly in Fig. 3.2.2: with time increasing from left to right the beat frequency was drifting downwards from above 50 MHz and was not being counted correctly. As the frequency decreased the counter started picking up and the signal was counted properly from around 40 MHz downwards. As the signal approached zero frequency, the counter, because of the low cutoff frequency of the P.M. output circuit, started acting erratic on higher frequency noise. The result was a reliable counting range extending from 2–40 MHz. Since the beat drifted through zero and up again, this range was displayed twice in Fig. 3.3.2.

If a laser drifts too far from atomic line-center, another axial mode starts to oscillate and thus part of the emitted laser radiation will not contribute to the signal while it does supply shot noise. The S/N ratio then goes down, which reduces the counting range. The same thing happens when the two beams are not completely parallel and/or coincident. This could be observed during the installation: while the system was poorly aligned a signal to noise ratio $S/N \simeq 1.5$ was observed; the counting range then was reduced to some 25 MHz.

3.2. Environmental noise

Disturbing effects caused by the environment are of both natural and human origin.

Meteorological changes do not penetrate to the depth at which the observatory is located. The one exception of course is barometric pressure, its direct and indirect effects on the LSS are described in the next two sections.

The noise of human origin is caused mainly by mining operations and is described in section 3.2.3.

3.2.1. *Barometric pressure changes*

Comparing the records from two barographs, one located in the recording room of the observatory and one at the surface, it is obvious that, disregarding a constant pressure difference due to the difference in altitude, the two records are very similar. Apparently the air pressure in the observatory closely follows the normal barometric pressure changes. In addition short period changes or jumps take place, caused by forced ventilation of the recording room with compressed air and by the mine's ventilation system itself, which is turned on and off twice a day, each time causing pressure steps of some 2 mbar. (see Fig. 2.10). As was mentioned in section 2.4.1, these short period pressure variations do not penetrate into the instrument section owing to the presence of two pressure doors which act as a low-pass filter with a time constant of roughly two hours (Fig. 2.10).

To evaluate the influence of barometric pressure changes on beat frequency its effect must of course be separated from that of other noise sources. Since the pressure effect is almost instantaneous when compared with e.g. thermal variations, this is easy to realize: Usually a pressure step of a few mbar is caused just by opening the air-tight doors to the instrument section (Fig. 2.10). A larger pressure change may be created using the mine's compressed air system in combination with timely opening and closing of air-tight doors. In this way a 20 mbar step in pressure was obtained. Both methods gave the same frequency-pressure relation:

$$\frac{\Delta\nu}{\Delta p} = 0.3 \pm 10\% \text{ MHz/mbar} \simeq 1 : 10^9 \text{ strain/mbar}.$$

The reason why the LSS should be sensitive to barometric pressure changes is that part of the optical path between the mirrors goes through air. The refractive index of air depends on pressure (equation 3.15) and therefore the optical cavity length changes with pressure. This is true for both cavities, however, and the effect should cancel in the difference frequency if only the air-gaps would have exactly the same length. Because of a difference in length of several mm between the laser tubes that were used at that time the residual pressure effect of 0.3 MHz/mbar is quite large. From this figure the actual airgap difference is easily found; differentiating eq. (3.15) with respect to pressure:

$$\frac{\Delta n}{\Delta p} = 0.36 \times 10^{-6}/\text{torr} = 0.27 \times 10^{-6}/\text{mbar}.$$

The change in optical cavity length, caused by a change Δn in refractive index is $\Delta L = \Delta n \cdot l$, where l is the length difference between the airgaps in cavities I and II. By means of the basic relation (3.1), the ratio $\frac{l}{L}$ is found to be:

$$\frac{l}{L} = \frac{1}{\nu} \cdot \frac{\Delta\nu}{\Delta p} \cdot \left(\frac{\Delta n}{\Delta p}\right)^{-1}. \tag{3.19}$$

Substituting appropriate values gives $l = 4.3$ mm. This pressure effect may be reduced by a factor ten if tubes of equal length are used and if more care is taken during the lining out procedure to reduce air-gap differences.

3.2.2. *Ambient temperature changes*

The mine temperature at the 1850′ level is some 17° C constant throughout the year. In the recording section of the observatory the temperature is approximately 8° C higher due to the power dissipation of light bulbs and instruments. Variations in this temperature of around 1° C occur as

a result of ventilation with compressed air and changes in power dissipation.

Because of the changes in barometric pressure and the air leak of the pressure doors, some of this relatively warm air may be pushed into the instrument section, where the temperature again is around 17° C. This effect is clearly demonstrated by momentarily opening the second set of pressure doors. If the air pressure on the recording room side is lower, no heat transport into the instrument room takes place, only equalisation of pressure, resulting in a stepwise change of the beat frequency as described in the previous section. If on the other hand the pressure in the recordingroom is higher, then not only will the laser signal show a shift owing to the pressure step, it will also start drifting because of the changing air temperature. The initial drift rate of the laser signal was observed to be roughly 0.5 MHz/hour for a pressure change of 1 mbar.

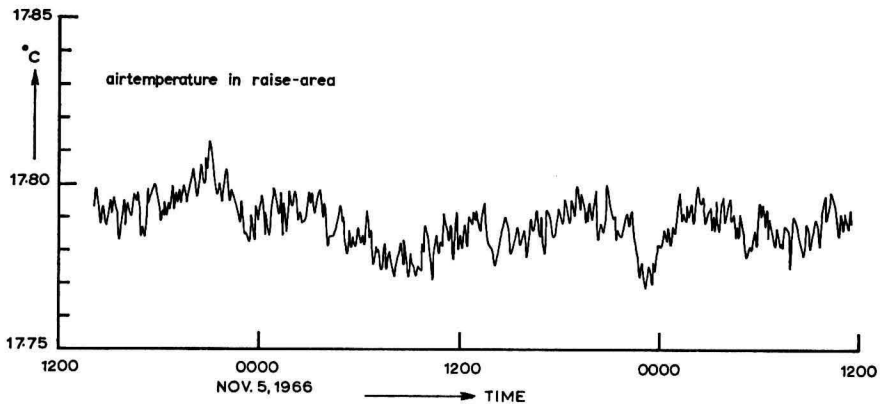

Fig. 3.5 Typical record sample of air temperature variations near the laser instrument.

Since no sensitive thermometer was available at the time, the actual change in air temperature was not known. In a later stage a Dymec quartz thermometer became available *) and for one week a continuous record of air temperature was made (see Figs. 3.5 and 3.6). The long-term zero drift of this instrument is listed as better than ± 0.01° C per month. The thermometer sensor probe loosely packed in insulating material, was placed on the floor of the raise area at a distance of about one meter from the LSS. The short-term temperature fluctuations shown in Fig. 3.5 are of no importance since they result from local air convection caused by the LSS and by the thermometer electronics. Temperature changes of some 0.02° C occur within several hours and the maximum change in temperature over the week is some 0.05° C. These figures are questionable,

*) Courtesy of Hewlett Packard Company.

however, and they can serve as an upper limit only, since on account of the limited time available no provision was made to exclude the effect of the heat dissipated by the thermometer electronics. This effect is believed to be responsible for the temperature variations with a few hour period, which appear in Fig. 3.6. In Fig. 3.6 the temperature record (the air convection fluctuations have been filtered out) is plotted together with air pressure and beat frequency. No temperature increase following a rise in barometric pressure is observed, although a fairly large pressure variation took place; the effect is apparently masked by changes in local probe temperature, which shows – in a somewhat suspicious coincidence – a rise in temperature on nov 3 following a barometric pressure decrease.

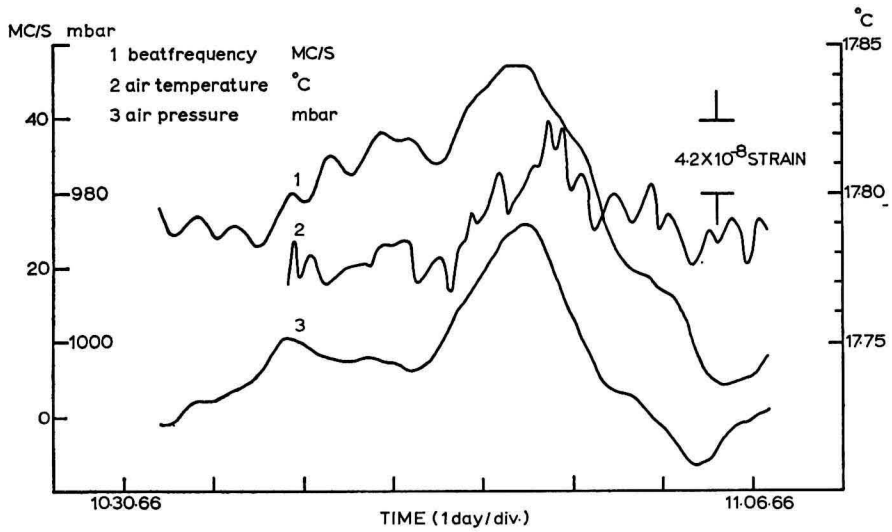

Fig. 3.6 Continuous recording over a period of one week of the laser strain seismometer signal, showing semidiurnal tides of some 10^{-8} strain peak to peak. The curves labeled 2 and 3 are recordings of air temperature and pressure around the instrument.

3.2.3. *Other effects caused by the environment*

As was described by MAJOR et al. (1964), because of its depth beneath the surface the observatory is well shielded from meteorological effects with the one exception of barometric pressure variations. The few remaining environmental factors influencing the LSS are therefore of human origin:

The electric power used in the observatory was obtained from the mine's power system. An AC regulator was used to suppress the large line fluctuations. Because of the long thermal time constant of the LSS, the instrument will be disturbed for many hours after linepower is restored following a temporary power shut-down. Although these shut-downs fortunately

occurred very infrequently, a more reliable operation of the LSS would be achieved if the discharge current supplies were battery-powered. Two more effects arizing from mining operations need to be mentioned:

Drilling produces high frequency noise with periods of less than 0.1 sec. The laser beat frequency is of course F.M. modulated by this noise, as is obvious when the signal is monitored on a spectrum analyser. Since these high frequencies are uninteresting, they are averaged out by selecting a sufficiently long counter gate-time; a gate-time of one second is sufficient to completely suppress drilling noise.

The second mining effect is due to blasting operations. Unlike drilling, which is of no importance, blasting is sometimes bothersome because some of the more violent explosions may permanently offset the signal to a frequency outside the counting range. This necessitates frequency-resetting which is not immediately possible if the explosion takes place at a time when the station is unattended. A device which in this case automatically resets the LSS would increase the instrument's reliability.

3.3. Evaluation of present useful sensitivity

In chapter I it has been mentioned that the inherent spectral purity of He-Ne gas lasers should make it possible to detect extremely small strains of the order of 10^{-11} to 10^{-12}. This of course requires, over the period range of interest, adequate suppression of – or shielding against – the different sources of noise described earlier in this chapter.

When evaluating the useful sensitivity that has been reached up to date it is convenient to make a distinction between 'seismic' and 'tidal' periods, that is between periods of the order of minutes and periods of the order of hours.

3.3.1. *Long-term stability*

The long-term stability may be inferred from Fig. 3.6 which shows the variation of the beat frequency for one week. The record begins after the instrument was allowed some time to recover from a modification that had upset its thermal equilibrium and the recording period ends forcefully because of a line power shut-down. In the second half of the week the barometric pressure changes more than 30 mbar; in the same time the beat frequency shows a pronounced drift of 1 MHz/hour which is roughly five times higher than the 5 MHz/day drift figure for the first days of the record. According to section 3.2.1, the beat frequency varies with barometric pressure with 0.3 MHz/mbar. This is not enough to explain the beat frequency variation mentioned above, which amounts to roughly 1 MHz/mbar. It seems likely, however, that part of the remaining drift is caused by ambient temperature changes and thus indirectly by the change in barometric pressure (section 3.2.2); part also must be due to a slow change in the discharge currents (section 3.1.3). The thermometer recording does not give much evidence one way or the

other since for reasons explained in 3.2.2, it is masked by its own influence on local temperature.

In conclusion, the present long-term stability may be listed as follows:

When no large barometric pressure variations take place, slow changes and drift amount to some 5 MHz $\approx 2 \times 10^{-8}$ strain/day; this is ten times less stable than are the Ogdensburg quartz tube strainmeters. The above figure may increase to 10^{-7} strain/day on days when large pressure variations occur.

3.3.2. *Short period noiselevel*

The short-term or 'seismic' stability is determined mainly by noise of 2 to 5 minutes period. As can be seen on the record samples 4 and 5 of Fig. 3.4, after averaging out the microseisms, peak to peak amplitudes are usually less than 40 kHz or 1.6×10^{-10} strain. Noise on the Ogdensburg quartz tube seismic outputs has about the same predominant periods and peak to peak amplitudes equivalent with some 9×10^{-11} strain. For seismic periods the LSS apparently approaches the quartz tube strainmeters already to within a factor of two.

The noise source that is believed to be mainly responsible is short-term discharge current variations. These effect the optical cavity length as explained under point 2 of section 3.1.3. Another possible noise source may be residual air convection around the instrument.

3.3.3. *Suggestions for further improvement*

As has been mentioned at the beginning of chapter II, this thesis describes an intermediate stage in the instrument's development. The preceding list of noise sources rather obviously suggests several measures that may be taken to improve both short-term noise level, long-term stability, as well as reliability of operation.

Short-term improvements are expected from:

1. A better discharge current regulation. In the present situation, according to the specifications of the voltage reference tube 5651 A, discharge current jumps of 0.2 % may occur arising from instantaneous voltage fluctuations across that tube.

2. A different construction of the dust-cover assembly (see Fig. 2.5) between mirrors and Brewster windows. This can be redesigned in such a way that the radial diameter of the air-gaps is reduced from several cm to a few mm. This would result in a decrease of both amplitude and period of air convection within the optical path.

Long-term stability is expected to improve by:

1. Sealing off barometric pressure variations by a better construction of the concrete bulkheads in which the pressure doors are mounted.

2. Better discharge current regulation. The present regulator stability is 0.2 % while chopper-stabilised constant-current supplies can go down to 0.001 %.
3. Using invar instead of aluminium for the construction of mirror mounts. Since the expansion coefficients are $9 \times 10^{-7}/°$ C and $2.4 \times 10^{-5}/°$ C respectively, thermal expansion of the cavity will be reduced more than 25 times.

In conclusion, several possible alterations to improve the instruments reliability, ruggedness or ease of handling, are suggested:

1. The addition of a self-resetting feature, to keep the beat frequency within the linear counting range (see also 3.2.3).
2. Battery operation of the discharge current supplies, to prevent the long warm-up time after a line power break-down (see also 3.2.3).
3. The use of cold instead of heated cathodes. Power dissipation is reduced, the need of a stabilised filament current supply is eliminated and the laser tube is simpler and more rugged. According to HOCHULI et al. (1967) the restriction of tube lifetime caused by sputtering can be overcome by using aluminium cathodes with the right surface treatment.
4. The use of shorter tubes and cavities. Reducing the cavity length to 50 cm for instance is attractive for several reasons: the axial mode separation increases to $\frac{c}{2L} = 300$ MHz. Keeping the relative excitation at the present value $\eta = 1.04$ by keeping threshold detuning at $(\Omega - \omega)_T = 100$ MHz, means that the lasers are always in single mode or not lasing at all. This has the advantage of a better S/N ratio and thus an increased linear counting range, because no extra P.M. shot-noise can be generated by a second axial mode. Also, it becomes simpler to make an automatic resetting device since the amount of cavity detuning is indicated by the drop in DC laser output level.

An additional advantage is the possibility of a trade-off between increased signal power i.e. increased linear counting range and increased mode pulling and pushing effects. This is possible because η may rise to $\eta = 1.09$ before a second mode can possibly appear. Other important advantages of shorter lasers are: power dissipation is decreased; less high voltage is required for the discharge, which facilitates current stabiliser design; laser tubes are less fragile; the instrument becomes more portable and evacuation of the entire instrument becomes feasible if this would seem necessary at a later stage.

In view of what was mentioned in section 3.1.2 about the uncertainty of L, it is of course necessary to scale down the mirror holders by the same factor.

The agreement between the LSS recordings and simultaneous records of the quartz tube strainmeters (see chapter IV) proves that a priori fears (VALI 1968) of local strain differences disturbing the overall strain pattern are unjustified and gives confidence to try the size reduction mentioned above. Should, however, fluctuations of the average mirror surfaces, as were mentioned in section 3.1.2 become the limiting factor in the further reduction of long-term instabilities, then the use of shorter laser cavities would be undesirable since the noise caused by mirror fluctuations will be inversely proportional to the distance between the mirrors.

In conclusion, for a further improvement of useful sensitivity both long-term and short-term, the necessity may be stressed here of simultaneously recording the changes in several instrumental and ambient parameters together with the actual LSS signal. Parameters that seem to be worth monitoring, would be: air pressure, air temperature in instrument-room, temperature at different places underneath the LSS cover, rock temperature underneath the instrument, heater tapecurrent, DC discharge currents and DC laser outputs.

Chapter IV

RECORDINGS

When a new type long-period seismic instrument is to be developed in a limited amount of time, a conflict of interests arises: On the one hand it is preferable to allow the instrument to operate undisturbed for long periods of time, while on the other it is desirable to improve operation by making modifications which, of course, create disturbances.

The emphasis has been mainly on the latter which shows up in a positive way, for instance in Fig. 3.4. The negative aspect results in the limited duration (one week) of the tidal record of section 4.1 and also in the drift apparent on some of the seismograms of section 4.2. The final section of this chapter gives an account of the LSS response to free oscillations.

4.1. Tidal observations

The tidal recordings of the three BLS-instruments and the corresponding LSS tidal recording cannot be compared as such since the first three each give strain along a certain azimuthal direction, while the latter gives the difference between strains along two perpendicular azimuthal directions. With carthesian coordinate axes x and y, which are parallel to the lasers, the horizontal strain e_i in an arbitrary direction δ_i, can be expressed in terms of e_{xx}, e_{yy} and e_{xy} as follows:

$$e_i = e_{xx} \cos^2 \delta_i + e_{yy} \sin^2 \delta_i + e_{xy} \sin \delta_i \cdot \cos \delta_i. \tag{4.1}$$

Since BLS records for three different directions δ_i are available (see Fig. 4.1), eq. 4.1 gives three linear equations for e_{xx}, e_{yy} and e_{xy}. Consequently an LSS tidal recording can be calculated from the three BLS recordings, using $e_{LSS} = e_{xx} - e_{yy}$.

BLS-recorder displacements Δ_i are converted into strains as follows:

$$e_i = \frac{\Delta_i}{L_i \cdot A_i}$$

where Δ_i – recorder displacement
L_i – quartz tube length
} in mm
A_i – amplification: recorder-displacement/tube-displacement

The necessary orientation, length, and calibration figures are given in table 4.1. BLS 1, BLS 2 and BLS 3 stand for the horizontal Benioff linear

strainmeters oriented in the direction N 29° 30′ E, N 48° 30′ E and S 48° E respectively.

Solving equations (4.1) results in

$$e_{LSS} = \frac{D_1 - D_2}{D}$$

with

$$\left.\begin{aligned} D &= \begin{vmatrix} \cos^2\delta_1 & \sin^2\delta_1 & \sin\delta_1\cos\delta_1 \\ \cos^2\delta_2 & \sin^2\delta_2 & \sin\delta_2\cos\delta_2 \\ \cos^2\delta_3 & \sin^2\delta_3 & \sin\delta_3\cos\delta_3 \end{vmatrix} \\ D_1 &= \begin{vmatrix} e_1 & \sin^2\delta_1 & \sin\delta_1\cos\delta_1 \\ e_2 & \sin^2\delta_2 & \sin\delta_2\cos\delta_2 \\ e_3 & \sin^2\delta_3 & \sin\delta_3\cos\delta_3 \end{vmatrix} \\ D_2 &= \begin{vmatrix} \cos^2\delta_1 & e_1 & \sin\delta_1\cos\delta_1 \\ \cos^2\delta_2 & e_2 & \sin\delta_2\cos\delta_2 \\ \cos^2\delta_3 & e_3 & \sin\delta_3\cos\delta_3 \end{vmatrix} \end{aligned}\right\} \tag{4.3}$$

Substitution of the appropriate values from table 4.1 results in

$$e_{LSS} = 7.74\times10^{-10}\times3.082\Delta_1 - 8.85\times10^{-10}\times3.064\Delta_2 - 4.64\times10^{-10}\times0.018\Delta_3 =$$
$$23.86\times10^{-10}\Delta_1 - 27.12\times10^{-10}\Delta_2 - 0.08\times10^{-10}\Delta_3.$$

Clearly the LSS calculated strain is equal to roughly three times the difference between the strains recorded by the BLS 1 and 2 instruments, after weighing these with the appropriate calibration factors. The BLS 3

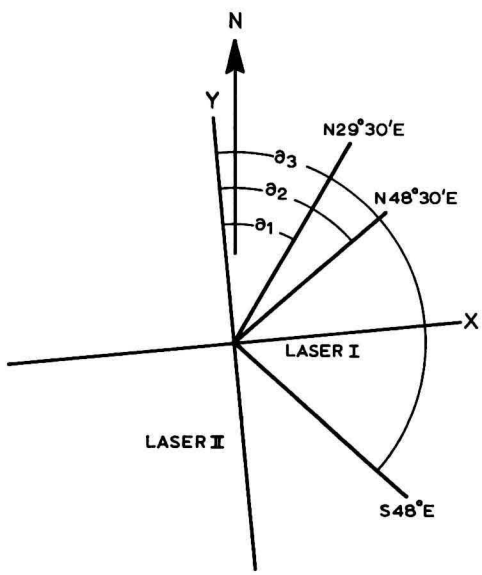

Fig. 4.1 Orientation of the three horizontal Benioff linear strainmeters and of the laser strain seismometer. All instruments are in the Ogdensburg underground observatory.

TABLE 4.1

BLS	orientation	orientation with respect to LSS	tube length L (mm)	tube displacement (mm)	recorder displacement (mm)	amplification A	e_i/Δ_i $(LA)^{-1}$
			← calibration →				
1	N 29°30′ E	35°	609.6×10^{2}	21.2×10^{-4}	45	2.12×10^{4}	7.74×10^{-10}
2	N 48°30′ E	54°	518.2×10^{2}	14.2×10^{-4}	31	2.18×10^{4}	8.85×10^{-10}
3	S 48° E	137°30′	609.6×10^{2}	12.7×10^{-4}	45	3.54×10^{4}	4.64×10^{-10}

Orientation and calibration figures for the three horizontal Benioff linear strainmeters from Ogdensburg.

recording has very little influence. From (4.3) it can be easily verified that the coefficient of Δ_3 will completely vanish when $\delta_1 = \pi/2 - \delta_2$. This appears to be nearly so (see table 4.1), explaining the negligable influence of the BLS 3 data in the calculated LSS recording.

In Fig. 4.2 the tidal records of the laser- and the three quartztube instruments during the period oct 30–nov 5, 1966 are plotted; all are corrected for calibration differences to the same vertical scale: 1 division corresponds to a strain of 10^{-8}. Also plotted are two calculated $(e_{xx} - e_{yy})$-curves; curve 5, using the calibration figures as given in table 4.1, curve 6, using a 25 % higher value of $\frac{e_i}{\Delta_i}$ for the N 48° 30′ E quartz tube instrument.

Although the LSS record is considerably affected by very long period noise, it is obvious that its general shape agrees quite well with the calculated curves: a succession of semidiurnal peaks and troughs of roughly equal amplitude; whereas the three BLS-instruments show a mixture of semidiurnal and diurnal tides. The calculated amplitudes of curve 5, however, are significantly higher than those observed (curve 4). From (4.3) it is clear that the calculated e_{LSS} depends strongly upon the BLS calibration figures. This is illustrated by curve 6, which shows a much closer resemblance to the LSS record both in the times of successive peaks and troughs and in amplitude, and which has been obtained by taking a 25 % higher calibration figure for the N 48° 30′ E instrument. From a comparison of different earthquake phases on LSS and BLS records (see section 4.2) it seems that the N 48° 30′ E recorded strain amplitudes are indeed too small by some 20 or 25 percent.

4.2. Seismic observations

In the following sections several earthquake records made by the LSS in the period july-november 1966 are shown and compared with BLS records of the same events. Emphasis will be on comparing the calibration of the different instruments. In table 4.2 the events are listed; origin-times, epicentral coordinates, depth and surface wave magnitudes are as given by the USCGS. Distance and azimuth from Ogdensburg have

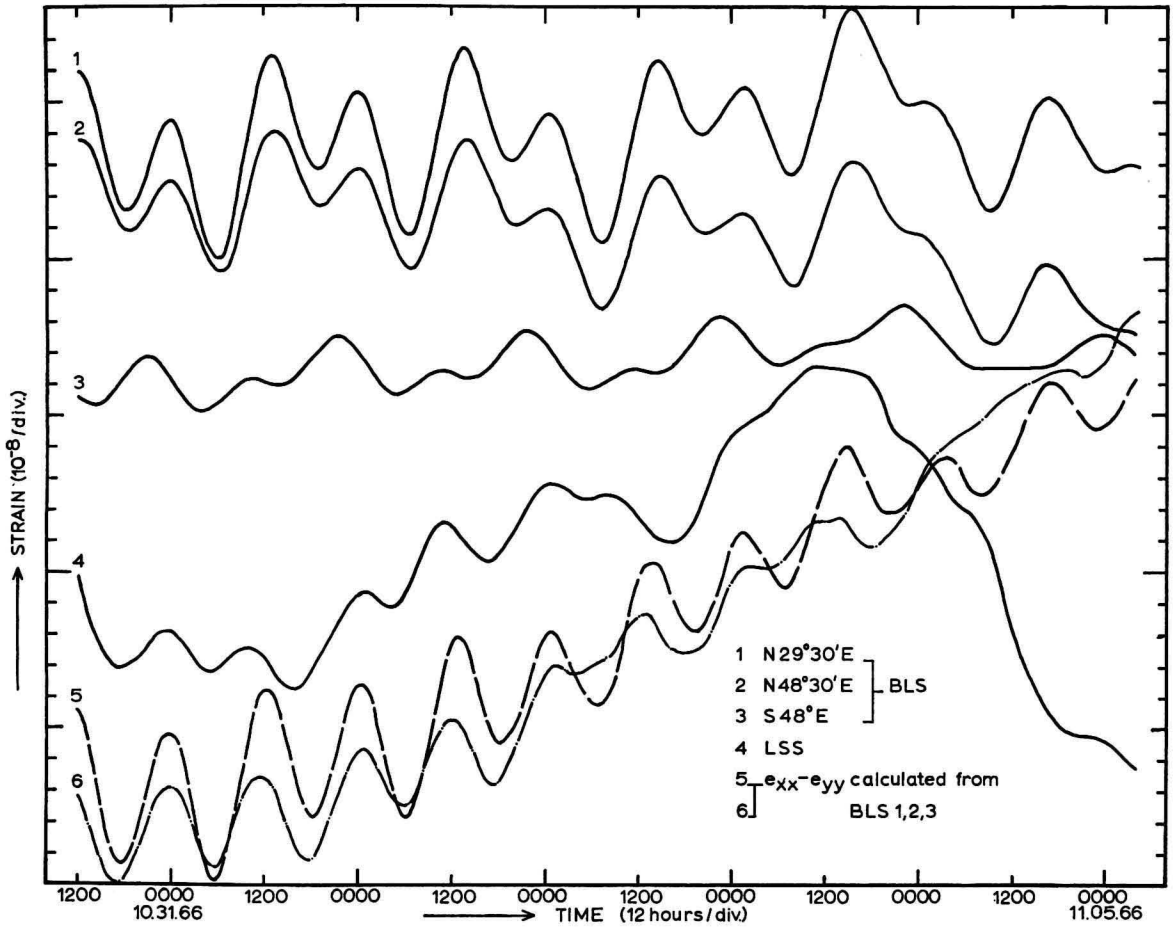

Fig. 4.2 Strains recorded in the period Oct 30-Nov 5, 1966. Curves 1, 2 and 3 are from the three horizontal Benioff linear strainmeters and curve 4 is the laser-recorded strain. With the records of the three horizontal components 1, 2 and 3, the laser response can also be calculated. This has been done for different calibration figures of the N 48° 30′ E instrument, resulting in the curves nr. 5 and 6.

TABLE 4.2

event	region	epicentral coordinates	date	origin-time (h m s)	depth (km)	distance from OGD (degrees)	azimuth from OGD (degrees)	Mag.
1	Aleutian Islands	50·6 N-171·3W	08·07·66	02·13·05	39	63	315	6·5
2	Gulf of California	31·8 N-114·5W	08·07·66	17·36·27	33	33	267	6·3
3	Southern Nevada	37·4 N-114·2W	08·16·66	18·02·36	33	31	276	6·1
4	off coast of Peru	10·7 S-78·7W	17·10·66	21·41·56	38	52	185	7·5

List of the four earthquakes of which laser strain seismograms are shown.

been calculated. The orientation of the instruments with respect to the earthquake epicenters is shown in Fig. 4.3, which also gives an indication of the relative sensitivities for longitudinal and transverse waves from the different events. These sensitivities are listed in table 4.3.

The polarity of the LSS signal depends on whether o.f. I (optical frequency of laser I) is larger or smaller than o.f. II. During the recording period covered in this chapter care was taken to keep the instrument tuned such that o.f. I > o.f. II. In this situation a relative elongation of cavity II ($N-S$ dilatation) causes the beatfrequency to increase. The signs in the top left diagram of Fig. 4.3 are given accordingly.

If a given epicentral azimuth is such that a particular instrument is near a node in its response pattern for a certain type of wave, not only will the expected amplitudes for this wave type be small, they will also vary rapidly with azimuth. For both reasons amplitude comparisons will be unreliable. An example e.g. is the Love wave response of BLS 2 and BLS 3 for the first event.

Because of their smaller amplitudes for shallow shocks, body phases are less suitable for amplitude comparisons than are surface waves, S waves moreover are complicated because on account of the presence of

TABLE 4.3

event / instrument	1		2		3		4	
	long	trans	long	trans	long	trans	long	trans
LSS	0·19	0·98	1·00	0·09	0·92	0·39	0·93	0·36
N 29°30′E	0·07	0·26	0·29	0·45	0·16	0·37	0·83	0·38
N 48°30′E	0·004	0·06	0·61	0·49	0·46	0·50	0·53	0·50
S 48°E	1·00	0·05	0·50	0·50	0·65	0·48	0·36	0·48

Relative response of the laser instrument and the three horizontal quartz tubes to longitudinal and transverse waves from the four earthquakes listed in table 4.2.

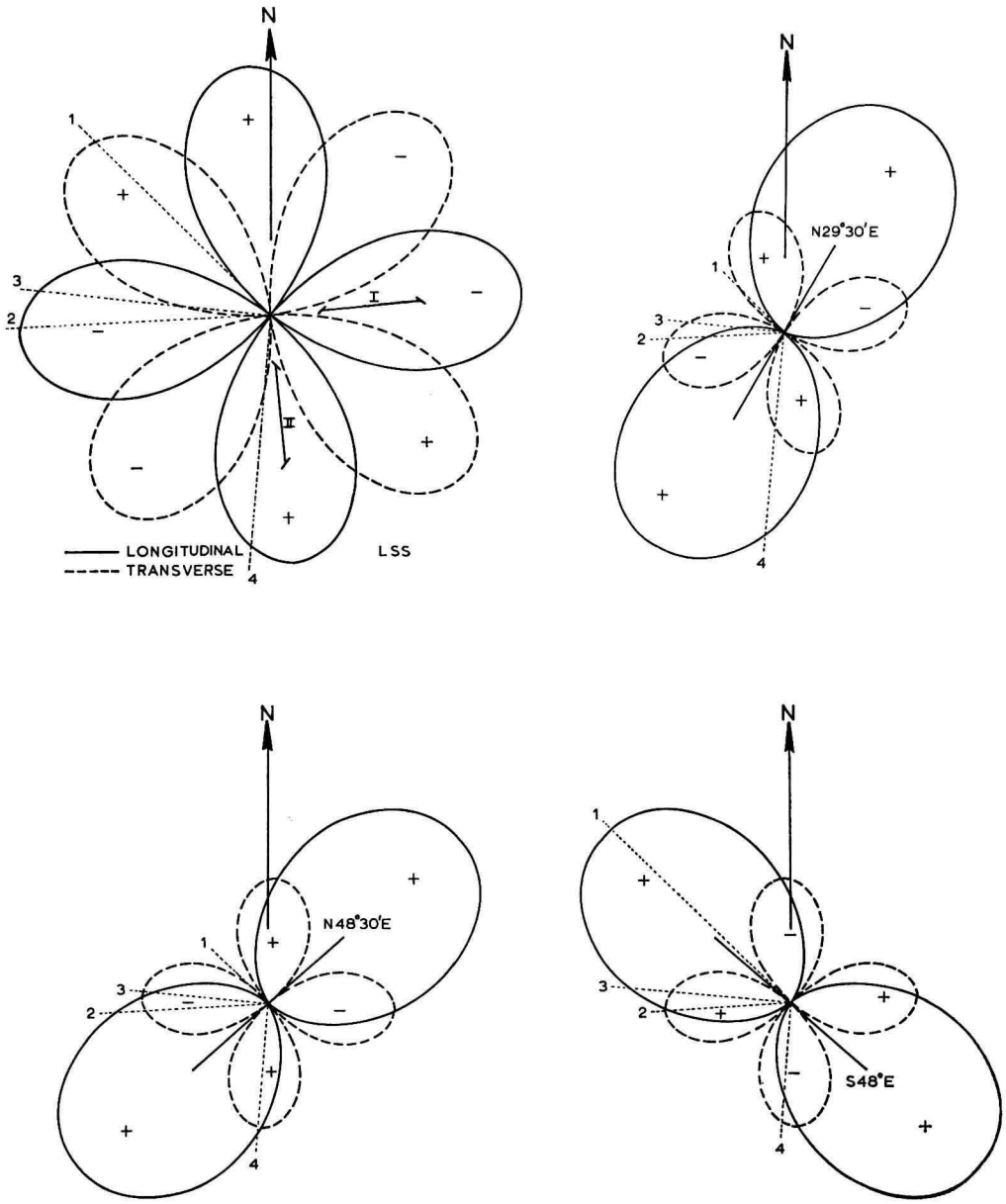

Fig. 4.3 Directional sensitivity patterns of the laser instrument and of the three horizontal quartz tube strainmeters for longitudinal and transverse waves. The directions towards the epicenters of the four earthquakes listed in table 4.2 are indicated and the relative sensitivities of the different instruments for seismic waves from these events are marked in a qualitative way.

SH and SV, both transverse and longitudinal motion is recorded, while in general the strain instrument will have different sensitivities for these types of motion. This also rules out most of the direct surface waves because of the mixture of Love- and Rayleigh motion. An exception are the first long period waves, which head the surface wavetrain, if these can be identified as Love waves. More useful for amplitude comparisons are the long period repetitions of Love- and Rayleigh waves which have circled the earth one or more times and which are well separated from each other owing to their different velocities. Only fairly large shocks, however, will generate these phases with sufficient amplitudes.

4.2.1. *Aleutian Islands Earthquake*

Records of the first event of table 4.2 are given in Figs. 4.4, 4.5 and 4.6. Fig. 4.4 shows the 4 inch/hour recordings of LSS and BLS 1, 2 and 3. Note that the sensitivities are all different. The BLS instruments also have an amplified and filtered output, which is recorded at 15 mm/min. The filter response which is shown in Fig. 4.7 is peaked at around $T = 600$

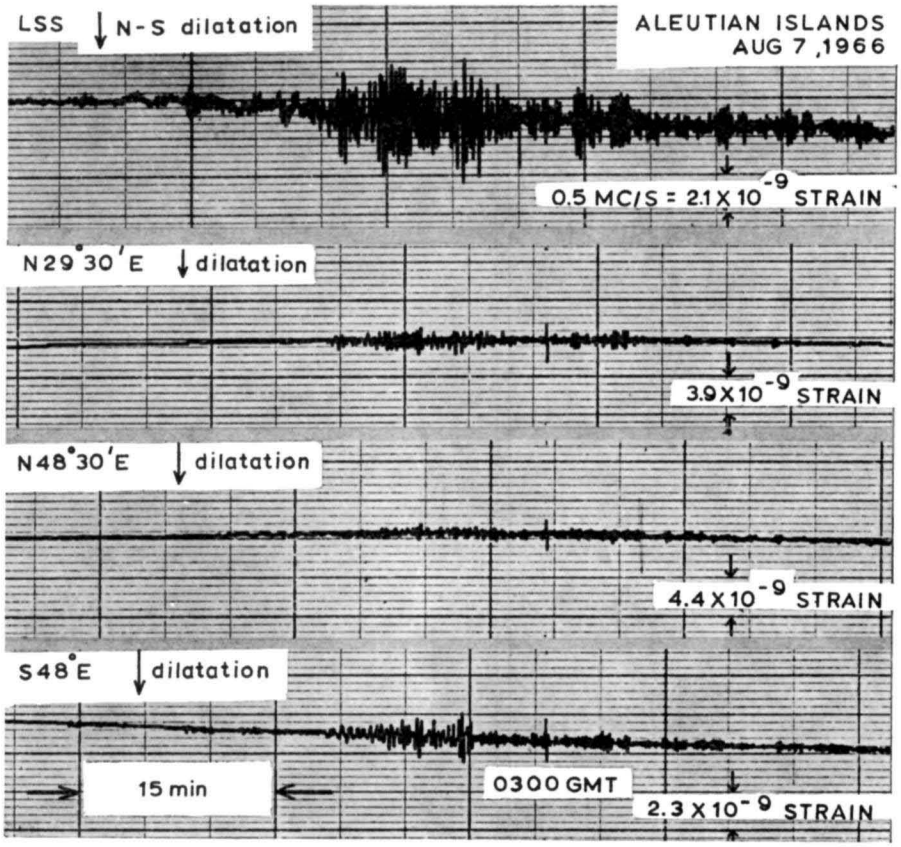

Fig. 4.4 LSS and three horizontal BLS strain records of event nr. 1, recorded at 4 inches per hour.

sec. and cuts off tides as well as most of the microseisms. This filtered output of BLS 1 is shown in Fig. 4.5. The top recording of Fig. 4.6 gives the LSS strain seismogram, now recorded at 6 mm/min. From table 4.3 it appears that the LSS is near its maximum response for Love waves, while of the three BLS instruments, only BLS 1 has a reasonable Love wave response. Consequently this event can be used to compare LSS with the N 29° 30′ E quartz tube strainmeter, results of which are given in table 4.4.

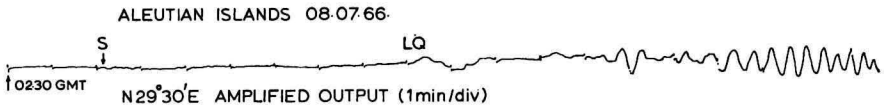

Fig. 4.5 Part of the second record of Fig. 4.4 after amplification and filtering.

4.2.2. *Gulf of California Earthquake*

Records of the Gulf of California earthquake, listed second in table 4.2 are shown in Figs. 4.6 and 4.8. At approximately three hours before the earthquake the discharge in one of the laser tubes had been off for roughly one minute; this disturbed the thermal equilibrium of the instrument as is evidenced by the 2 MHz/hour drift still existing at the time of the earthquake. The beat frequency at that time was some 28 MHz; since peak to peak surface wave deflections of some 10 MHz occurred, the signal repeatedly reached values that were above 30 MHz. Consequently, since at 1 MHz/cm sensitivity the recorder is set for registration of 0.00–9.99 MHz, it changed decades and part of the peaks at the bottom were cut off and written at the top of the paper. The 6 mm/min. recorder had sufficient paper speed and pen response for recovery of the original seismogram, which is shown in Fig. 4.6. The N 48° 30′ E recorder also

TABLE 4.4

instrument \ event	1	2	3	4
LSS	1·0 ± 0·2	-	-	1·0 ± 0·1
N29°30′E	1	1	1	1
N48°30′E	-	1·0 ± 0·2	0·7 ± 0·4	0·75 ± 0·1
S48°E	-	0·4 ± 0·2	0·5 ± 0·4	0·4 ± 0·1

The calibrations of the different strain instruments are compared with one another by studying corresponding earthquake phases on the recordings of events 1 to 4. It appears that amplitude readings on the laser instrument are consistent with those on the N 29° 30′ E instrument, while the N 48° 30′ E and S 48° E instruments give readings that are too low by a factor 0.8 and 0.4 respectively.

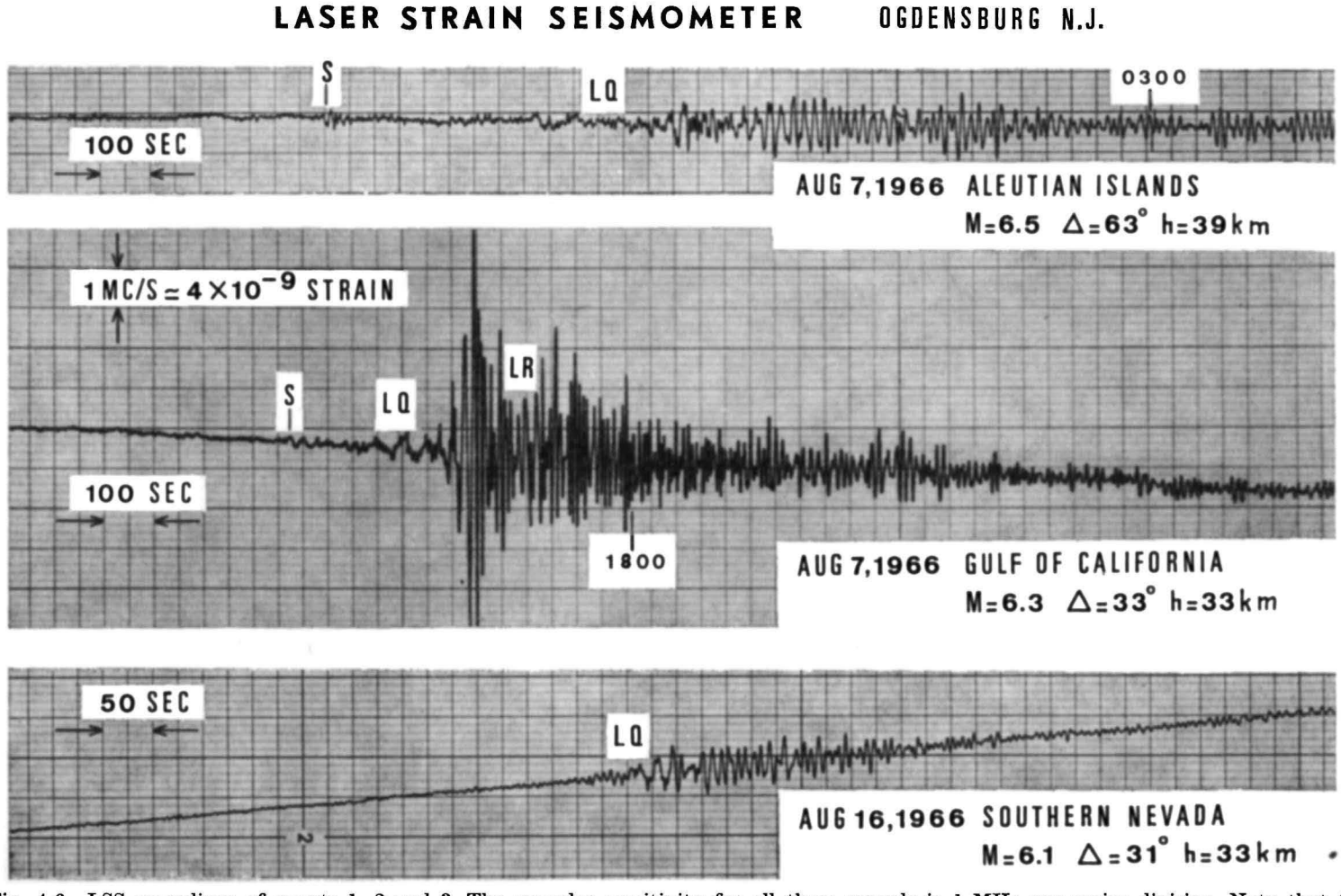

Fig. 4.6 LSS recordings of events 1, 2 and 3. The recorder sensitivity for all three records is 1 MHz per major division. Note that the third record has a two times higher paperspeed.

happened to be near one edge of the paper, since this was a regular analog output, part of the signal was lost (see Fig. 4.8). From table 4.3 it appears that this event is useful for comparing the three BLS instruments, since all have near maximum response for transverse waves. Apart from its time of arrival, the dispersed wavetrain marked LQ is identified as such by the fact that BLS 1 and 2 are in phase, while BLS 3 has opposite polarity. Rayleigh waves would have been in phase on all three components.

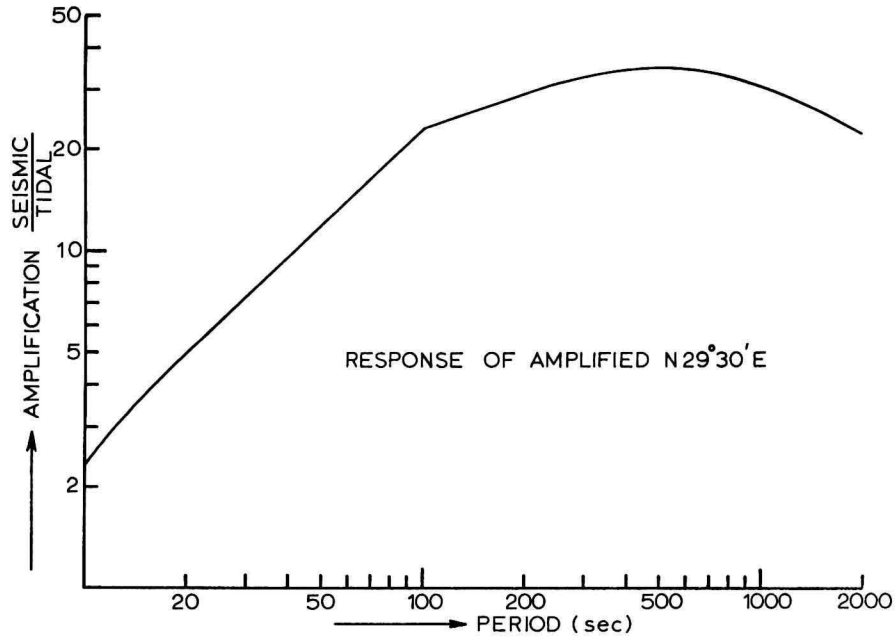

Fig. 4.7 Filter response of the N 29° 30' E "seismic" output. The filter is peaked around T = 600 sec; tides are removed and microseisms attenuated.

4.2.3. *Southern Nevada Earthquake*

Strain seismograms recorded at 4 inch/hour of an earthquake in Southern Nevada, number 3 in table 4.2, are given in Fig. 4.9. The 8 MHz/hour drift of the LSS signal was caused by a change in discharge current a few hours before the earthquake. The lower record in Fig. 4.6 is the LSS seismogram recorded at 12 mm/min. Events 2 and 3 are comparable in focal depth, distance and azimuth; judging from the difference in surface wave amplitudes on the Ogdensburg BLS and LSS strain records (compare Fig. 4.8 and 4.9) which is almost an order of magnitude, the assigned value of $M = 6.1$ for event 3 seems quite high as compared with $M = 6.3$ for event 2; this was confirmed by both Utah and Palisades which give $M = 5.5$ *). The first wiggle on the records of Fig. 4.9 is identified as

*) Private communication K. L. Cook, G. Boucher.

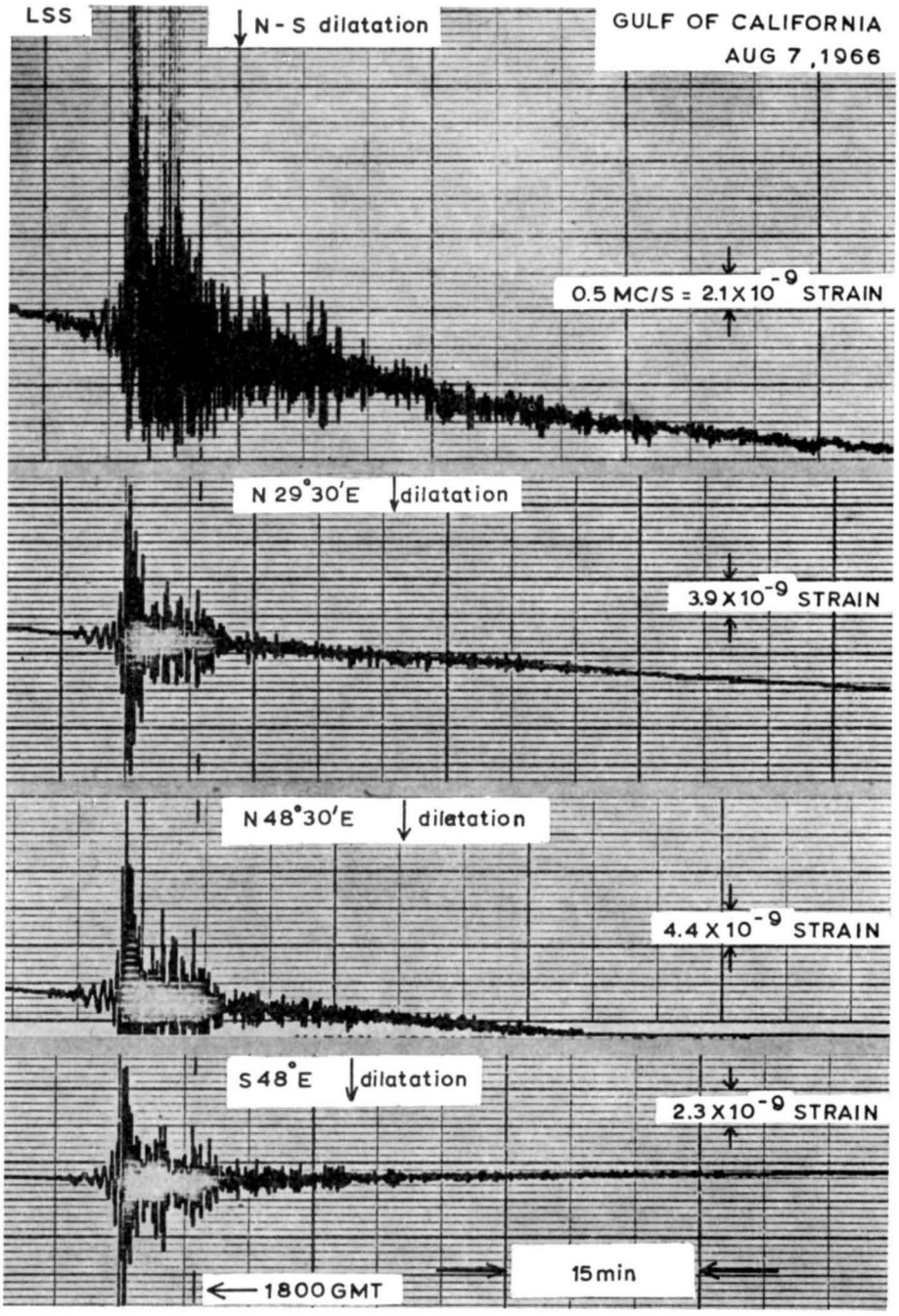

Fig. 4.8 LSS and three horizontal BLS strain records of event nr. 2.

transverse; a comparison of the different recordings is quite inaccurate, however, because of the small signal amplitudes.

4.2.4. *Off coast of Peru Earthquake*

The Magnitude $7\frac{1}{2}$ earthquake with epicenter off the coast of Peru (oct 17, 1966) produced a very nice set of strain seismograms on the Ogdensburg laser- and Benioff instruments, as can be seen in Fig. 4.10. The records cover a time span of some $4\frac{1}{2}$ hours after P. Even the vertical BLS, which at that time suffered from a very high noise level, produced

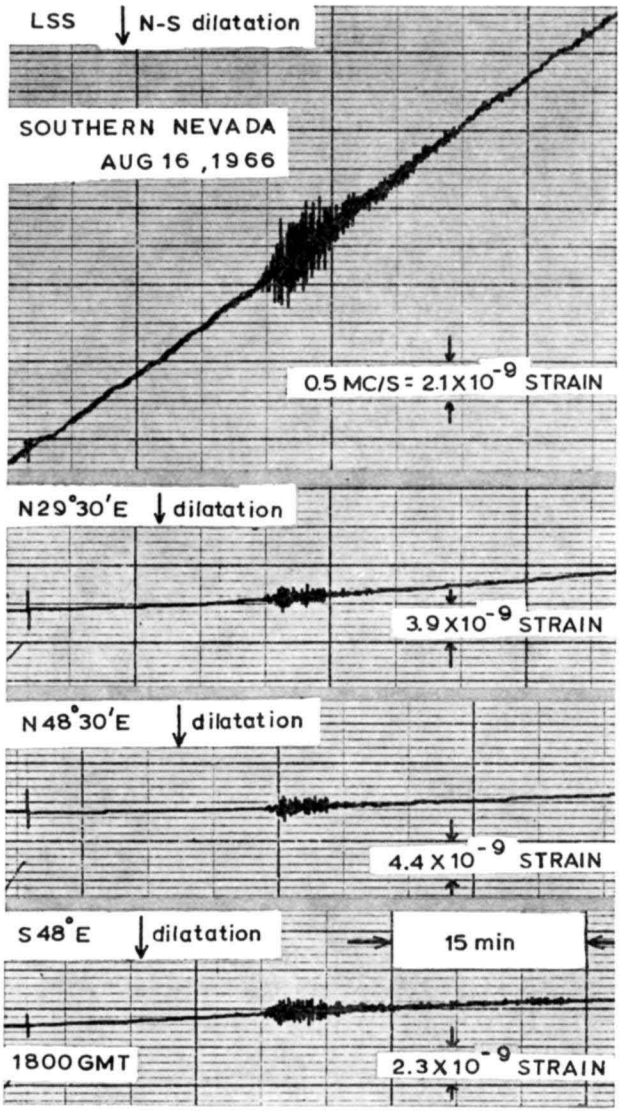

Fig. 4.9 LSS and three horizontal BLS strain records of event nr. 3. The drift of the laser signal shows that the instrument was still affected by a modification, that was made a few hours before the time of the earthquake.

a worthwhile recording. Besides the usual LSS recordings at 1 MHz/cm sensitivity and 12 mm/min. and 4 inch/hour paper speeds, another 4 inch/hour recorder was running at a ten times lower sensitivity: 10 MHz/cm (not shown). Since maximum peak to peak trace deflections of 19 MHz occurred, the signal repeatedly exceeded the full recorder span of 10 MHz. Consequently parts of the records were "cut off" and written at the opposite side of the paper, as was the case with event 2. The 12 mm/min. seismogram was later restored graphically by shifting back the displaced portions over a full decade. The LSS record with ten times lower sensitivity (i.e. 100 MHz full span) served as a check during this operation. The 12 mm/min. record, some five hours of which are shown in Fig. 4.11, was then digitized and plotted to have the same time scale as the 4 inch/hour BLS records in Fig. 4.10. This somewhat cumbersome procedure, during which no essential information was lost, however, may be circumvented by directly recording the counter output in digital form (see Fig. 2.8) and doing the plotting afterwards.

The different phases that can be recognised are indicated on the seismograms: the direct bodywaves P and S, the direct surface waves, a mixture of Love- and Rayleigh motion in which components with several hundreds seconds period are clearly visible. The first interesting phase after the direct arrivals is a group of waves with some 90 seconds period, coming in around 23.12 GMT. It is recorded by all strain-instruments, in phase on all horizontals and reversed in polarity on the vertical. This, together with the observed horizontal amplitudes, points to longitudinal linear particle motion. From the time of arrival, this phase was identified as a combination of multiple surface reflections: ${}_4SP_x$. The next phase, at approximately 23.53 GMT is recorded by all horizontal instruments. Note that LSS and BLS 3 are in phase, as are BLS 1 and 2, while the two pairs have opposite polarity. The absence of vertical motion plus this polarity behaviour points to transverse surface waves which, because of their time of arrival must have travelled by way of the antipodes: G_2.

Similarly, the wave group arriving around 0036 GMT has been identified as G_3: Love waves that pass the station for the second time after having completed one revolution around the earth. The LSS recording shows repetitions up to G_6. These G-waves correspond with the flat portion of the Love wave group velocity curve, which is almost a constant 4.4 km/sec for periods between 100 and 400 seconds. The wave trains arriving around 0020 GMT and 0112 GMT are recorded on all instruments and are in phase on all horizontals. When compared with the horizontals the signal on the vertical BLS, besides having opposite polarity, is also shifted in phase, which is characteristic for elliptical motion. These wave trains were identified as Rayleigh wave repetitions R_2 and R_3. In contrast to the G-waves, they appear as long drawn-out trains with a long- and short period branch which blend in an Airyphase minimum at $T = 225$ sec. The group velocities as determined from the LSS record of both R_2 and

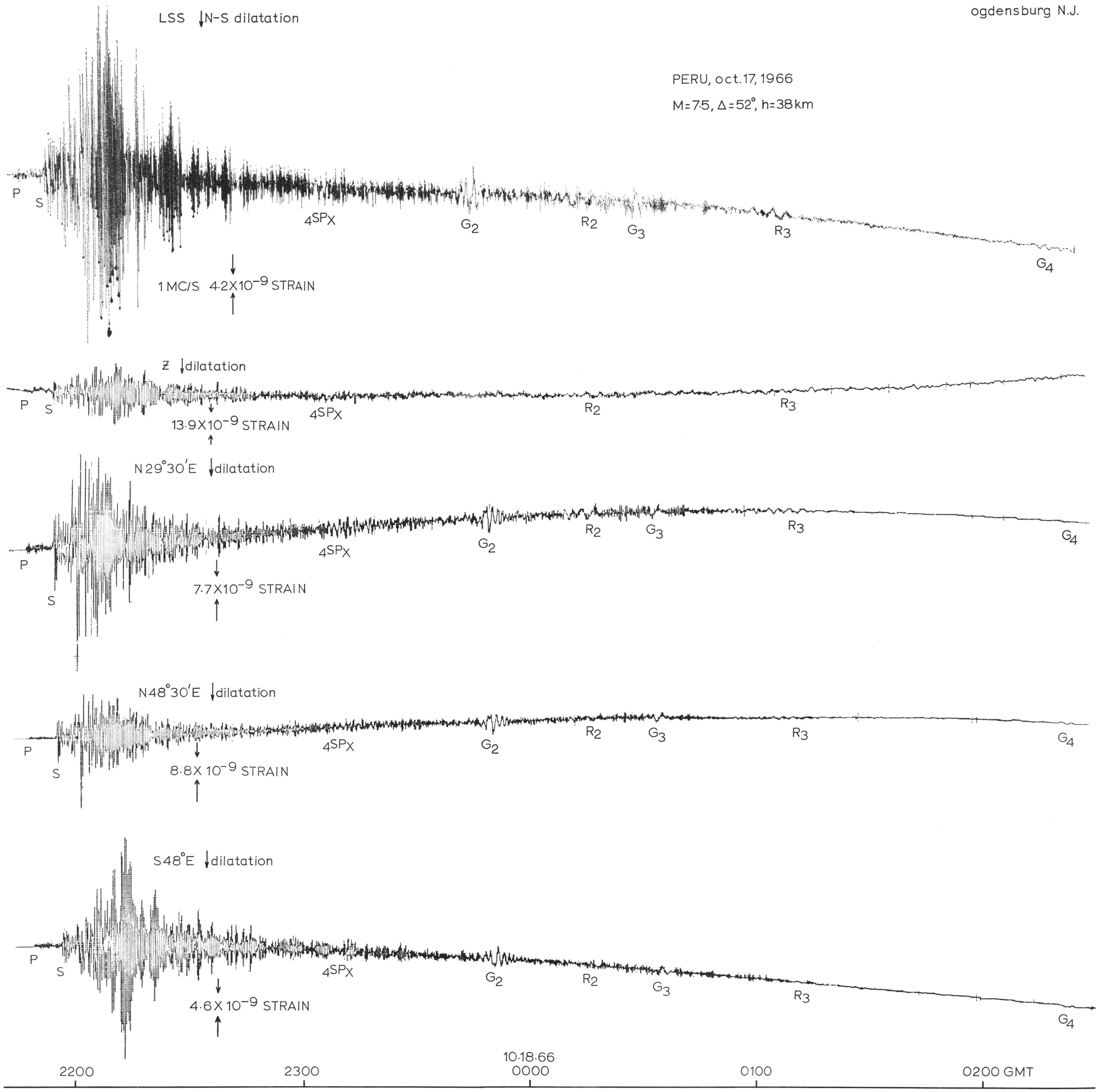

Fig. 4.10 Strain recordings of a Mag. 7½ earthquake off Peru (event nr. 4 of table 4.2) made by the laser instrument, the vertical quartztube strainmeter and the three horizontal quartztube strainmeters. Note that the sensitivities are all different.

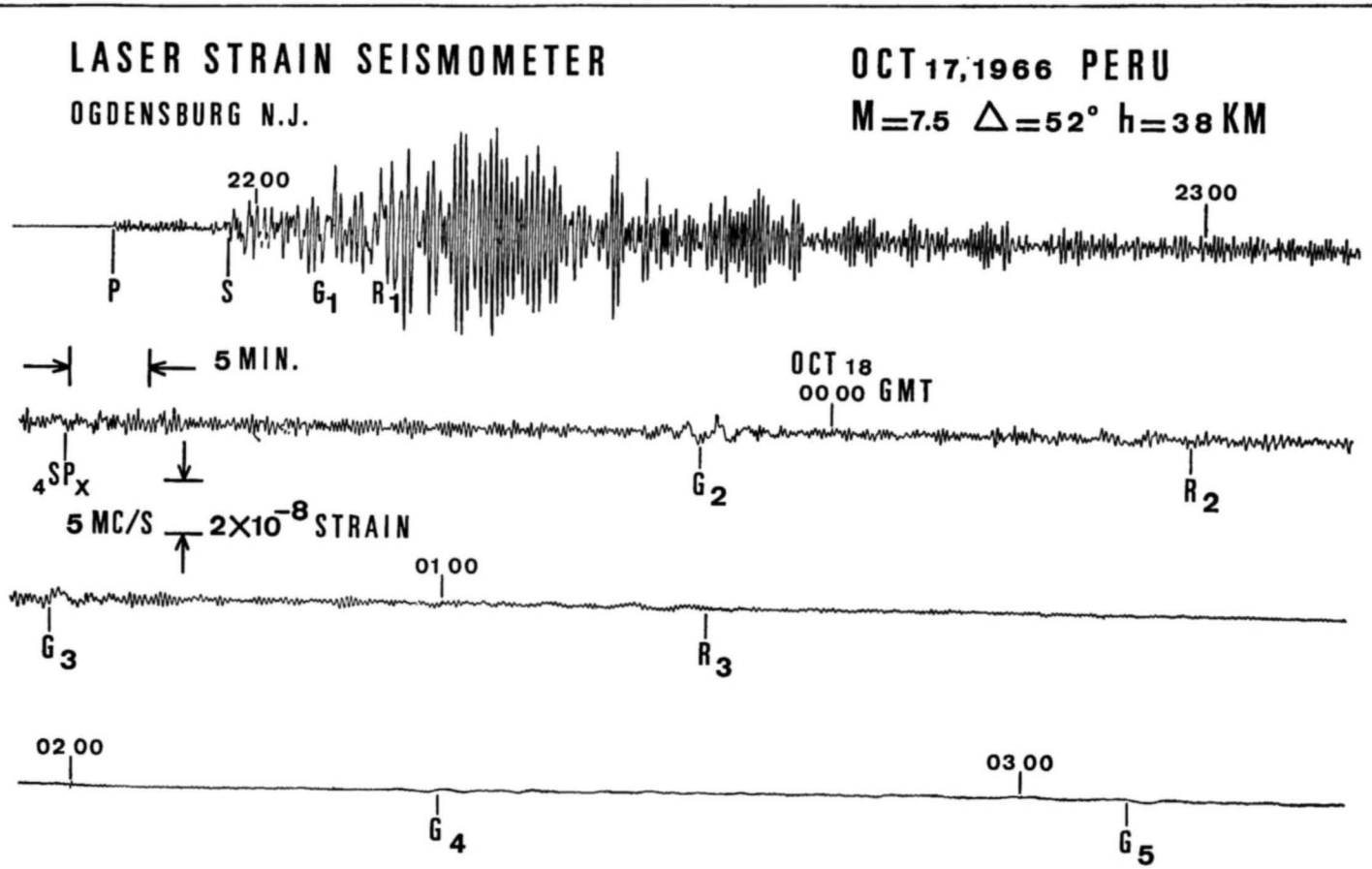

Fig. 4.11 Laser strain seismogram of the Peru-earthquake of Fig. 4.10, recorded at a 7 times higher paperspeed. The different recognisable phases, such as several surface wave repetitions have been marked.

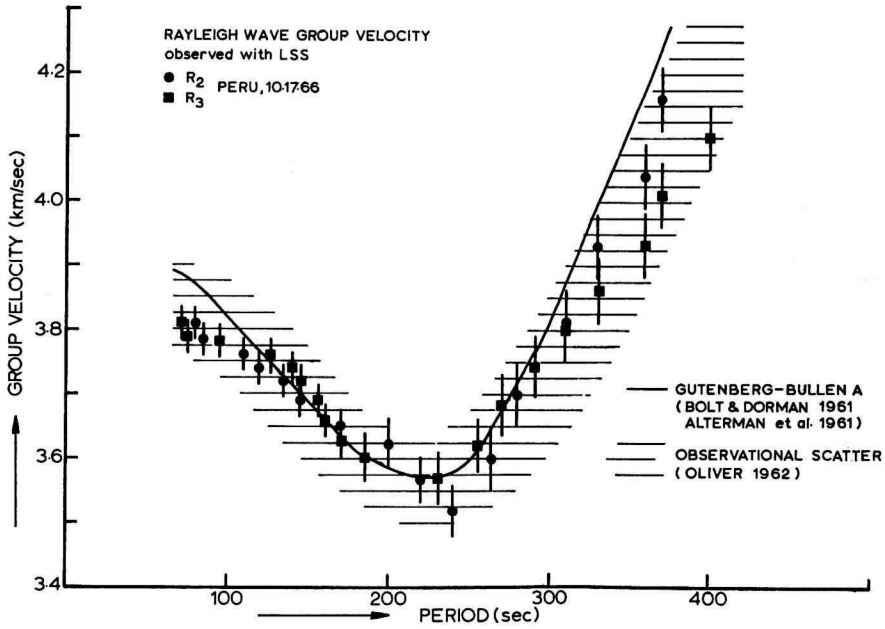

Fig. 4.12 Rayleigh wave group velocities, determined from the laser strain recording of the earthquake off Peru which took place on Oct 17, 1966.

R_3, are plotted in Fig. 4.12 and agree both in general trend and in scatter with other observational data (KOVACH, 1965).

Amplitudes of R_2, R_3, G_2 and G_3 on the LSS and horizontal BLS recordings were compared and the relative calibration figures listed in table 4.4. From these amplitude comparisons it is concluded that:

1. the LSS and N 29° 30′ E BLS calibrations are in mutual agreement.
2. the N 48° 30′ E instrument probably gives amplitude readings which are too low by a factor 0.8 ± 0.1.
3. the S 48° E gives readings which are too low by a factor 0.4 ± 0.1.

4.3. RESPONSE OF LSS TO FREE OSCILLATIONS

To evaluate the characteristic properties of the LSS more quantitatively, its response to the earth's free vibrations was considered. If the LSS makes an angle ψ with rectangular coordinate axes x and y, the strains e_I and e_{II} in the direction of the laser axes are, from eq. (4.1):

$$e_I = e_{xx} \cos^2 \psi + e_{yy} \sin^2 \psi + e_{xy} \sin \psi \cos \psi$$

$$e_{II} = e_{xx} \sin^2 \psi + e_{yy} \cos^2 \psi - e_{xy} \sin \psi \cos \psi$$

Consequently:

$$e_{LSS} = e_I - e_{II} = (e_{xx} - e_{yy}) \cos 2\psi + e_{xy} \sin 2\psi \qquad (4.4)$$

The horizontal strains can be written as

$$\begin{vmatrix} e_{xx} & e_{xy} \\ e_{xy} & e_{yy} \end{vmatrix} = \begin{vmatrix} \frac{1}{2}(e_{xx}-e_{yy}) & e_{xy} \\ e_{xy} & -\frac{1}{2}(e_{xx}-e_{yy}) \end{vmatrix} + \begin{vmatrix} \frac{1}{2}(e_{xx}+e_{yy}) & 0 \\ 0 & \frac{1}{2}(e_{xx}+e_{yy}) \end{vmatrix} \tag{4.5}$$

The first term on the right, a deformation without a change in area, is called pure shear, the second term is dilatational: areal strain without a change in shape. From (4.4) and (4.5) it is obvious that the LSS will be sensitive to pure shear only. The dilatational part of the surface deformation influences both lasers equally and therefore cancels out in the difference.

When only plane surface waves are considered, which travel in the direction of the x-axis for instance, the e_{yy} component of strain vanishes, as can be seen as follows: The horizontal displacements are

$$u_x = f_L\left(t - \frac{x}{v_L}\right) \qquad \text{for longitudinal motion}$$

$$u_y = f_T\left(t - \frac{x}{v_T}\right) \qquad \text{for transverse motion}$$

The horizontal strains are then

$$e_{xx} = \frac{\partial u_x}{\partial x} = -\frac{1}{v_L}\cdot\frac{df_L}{dt}$$

$$e_{yy} = \frac{\partial u_y}{\partial y} = 0$$

$$e_{xy} = \frac{\partial u_x}{\partial y} + \frac{\partial u_y}{\partial x} = -\frac{1}{v_T}\cdot\frac{df_T}{dt}.$$

Substitution in (4.4) yields:

$$e_{LSS} = -\frac{1}{v_L}\frac{df_L}{dt}\cdot\cos 2\psi - \frac{1}{v_T}\frac{df_T}{dt}\cdot\sin 2\psi. \tag{4.6}$$

Equation (4.6) is equivalent to (1.15) and (1.16) and is represented in Fig. 1.9 and 1.10. Since $e_{yy}=0$, no cancelling occurs in the difference measurement $(e_{xx}-e_{yy})$, and thus LSS and BLS have the same maximum response for longitudinal waves (see Fig. 1.7 and 1.9), while the LSS is a factor 2 more sensitive to transverse waves (Fig. 1.8 and 1.10).

If the plane wave assumption is invalid as happens with free vibrations, generally $e_{yy}\neq 0$. This will result in either higher or lower sensitivity of the LSS when compared with BLS, depending on whether e_{xx} and e_{yy} have opposite or equal sign. The horizontal strains associated with free spheroidal and toroidal oscillations are given by e.g. TAKEUCHI and ALSOP (1965); spherical coordinates r, θ and ϕ are used with the epicenter as

a pole; on the surface therefore θ and ϕ correspond with x and y respectively.

For toroidal oscillations the dilatation is zero at all times which means that $e_{\theta\theta} = -e_{\phi\phi}$ since also $e_{rr} = 0$. The deformations are pure shear and the LSS is well suited for recording them.

For spheroidal modes, the expressions for $e_{\theta\theta}$ and $e_{\phi\phi}$ have a common term representing strain caused by radial motion. Since it is known that some grave spheroidal modes have predominantly radial motion (ALTERMAN et al. 1959), it may be expected that the LSS will have limited sensitivity for those modes. For $m = 0$, m being the degree of the associated Legendre function, the expressions for the horizontal strains associated with spheroidal oscillations are:

$$\left.\begin{aligned} e_{\theta\theta} &= \frac{W(r)}{r} \cdot \frac{d^2 P_l}{d\theta^2} + \frac{U(r)}{r} \cdot P_l \\ e_{\phi\phi} &= \frac{W(r)}{r} \cdot \operatorname{cotg}\theta \cdot \frac{dP_l}{d\theta} + \frac{U(r)}{r} \cdot P_l \\ e_{\theta\phi} &= 0. \end{aligned}\right\} \tag{4.7}$$

where $P_l = P_l\ (\cos\theta)$ are Legendre polynomials of order l, and $W(r)$ and $U(r)$ are tangential and radial amplitude functions depending on the earth model. The relative sensitivities of LSS and BLS for spheroidal modes follow from a comparison of:

$$(e_{\theta\theta} - e_{\phi\phi}) \cdot \frac{r}{W(r)} \text{ for the } LSS \text{ and } e_{\theta\theta} \frac{r}{W(r)} \text{ for the } BLS.$$

These expressions take the form:

$$\frac{d^2 P_l}{d\theta^2} - \operatorname{cotg}\theta \cdot \frac{dP_l}{d\theta} \tag{4.8}$$

and

$$\frac{d^2 P_l}{d\theta^2} + \frac{U(r)}{W(r)} \cdot P_l \tag{4.9}$$

(4.8) and (4.9) have been computed up to order number $l = 20$ for epicentral distances $\theta = 5°, 10°, \ldots 90°$, the response for $90° < \theta < 180°$ following by symmetry. The values of $\frac{W(r)}{U(r)}$ that were used, are those tabulated by Takeuchi and Alsop (1965) (y_3 in their notation). The results are that ${}_0S_0$ and ${}_0S_1$ (notation MACDONALD and NESS, 1961) will not be detected by the LSS; this is immediately apparent for ${}_0S_0$ since this mode consists of purely radial motion without any surface shearing. From the other results, some of which is plotted in Fig. 4.13, it can be seen that the LSS has relatively low sensitivity for ${}_0S_2$ for all epicentral distances; also

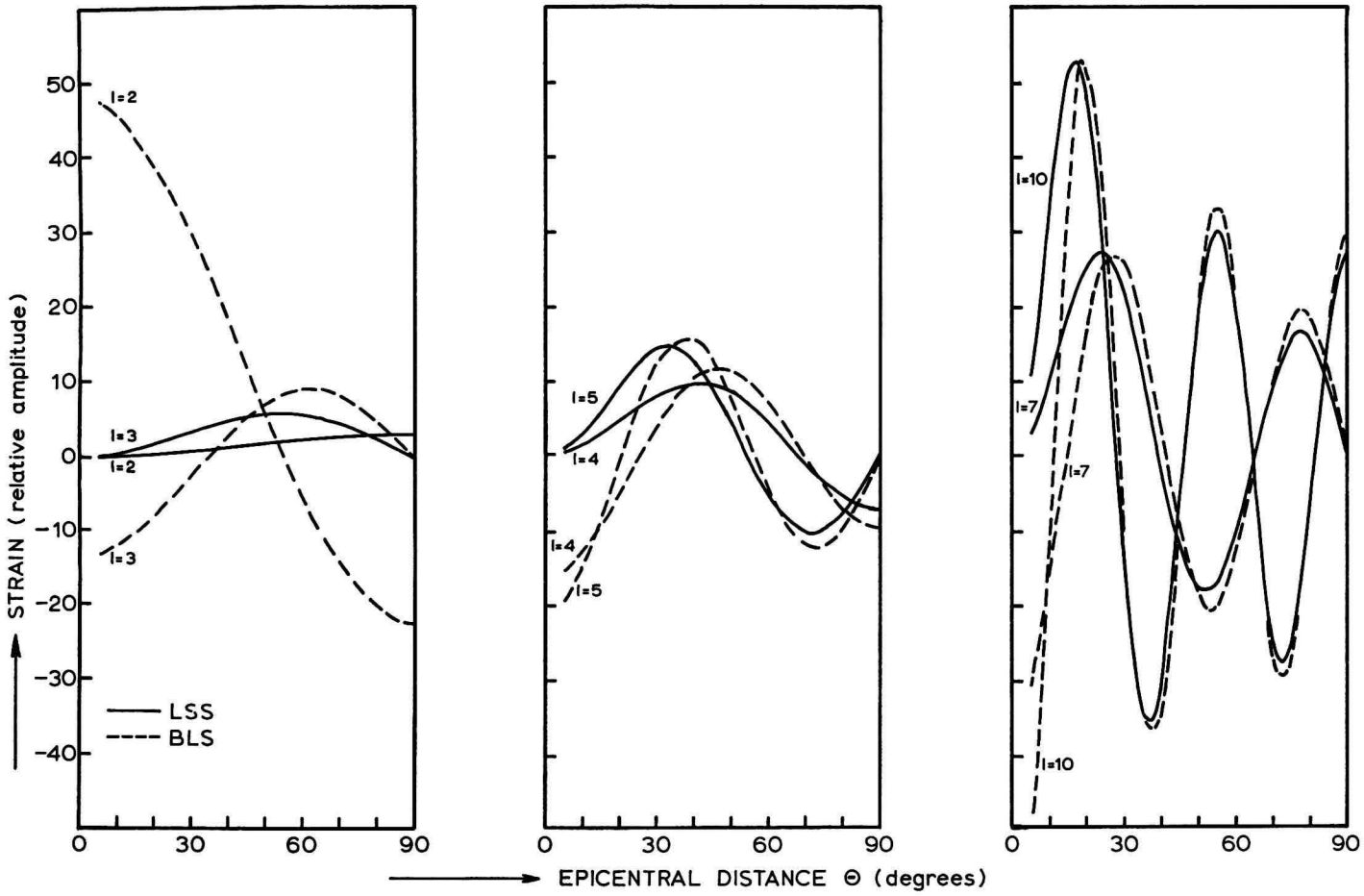

Fig. 4.13 Calculated relative response of laser instrument (solid curves) and quartz tube strainmeter (dashed curves) to free spheroidal oscillations of the earth with order number 2, 3, 4, 5, 7 and 10, as a function of epicentral distance.

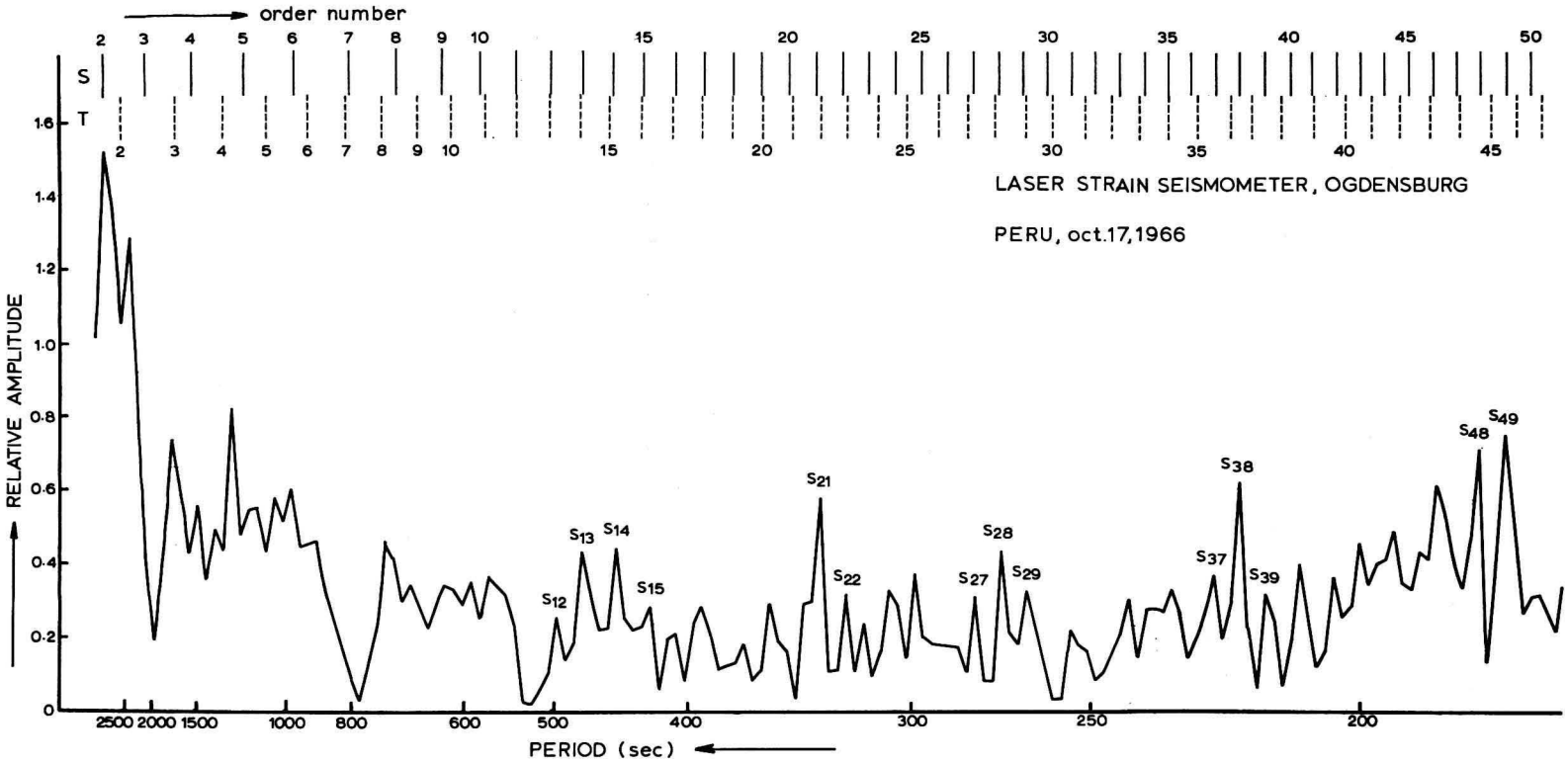

Fig. 4.14 Fourier spectrum of 8½ hours of laser recording following the earthquake off Peru on Oct 17, 1966. The fundamental spheroidal and toroidal free oscillation periods, given in the upper part of the figure, are theoretical values for a Gutenberg-Bullen A model earth from Alsop (1963) and Pekeris et al. (1961).

the LSS response for ${}_0S_3$ is generally lower than the BLS figure. For all higher order modes the responses of LSS and BLS are very similar for θ-values not to close to either 0° or 180°, their main difference being a slight shift of the nodal lines of response.

A Fourier analysis of the LSS strain seismogram of the Peru event was made, for which $8\frac{1}{2}$ hours of record were available; the resulting spectrum is shown in Fig. 4.14.

With this magnitude, one cannot expect grave oscillations to be sufficiently excited; therefore the effects on low order spheroidal modes described above cannot be illustrated here (see, however, S. W. SMITH, 1966).

In the spectrum, several peaks appear that are probably higher order modes. Because of the instrument's orientation, the LSS for this earthquake favors spheroidal modes and some of the more prominent peaks have been tentatively labeled as such. This is supported by a computation of the LSS response for spheroidal modes with order up to $l=50$ and epicentral distance $\theta=52°$. It appeared that all the prominent peaks on the spectrum of Fig. 4.14 fell at or near maxima of this computed response.

SUMMARY AND CONCLUSIONS

When the mirrors that form a gas laser cavity are fixed to the rock, strains of seismic or tidal origin will modulate the frequency of the laser radiation. By mixing the outputs of two such lasers mounted at right angles, a beatfrequency is obtained, which will be varied by changes in the horizontal strain. This laser strain seismometer is attractive for two reasons: its size is very much smaller than that of other types of strainmeters, while it should be capable of at least the same or even a ten times higher sensitivity.

In this thesis the construction of the instrument is described in detail. Furthermore the effects of several sources of noise both of 'seismic' and of 'tidal' periods, originating either from the environment or from the instrument itself, are investigated. For periods up to several minutes, the LSS has reached a stability of 1.6×10^{-10}. Its stability over periods of days is still considerably less: long-term drifts of 10^{-7} and 10^{-8} strain/day were observed, depending on whether or not large variations in barometric pressure took place. These long-term instabilities seemed to be caused mainly by slow changes in discharge current and in temperature and pressure. The discharge current stability can be improved at least by a factor 100 or more while the slow temperature changes may be eliminated by improving the air seals.

These and other measures should make it possible to reduce the long-term drifts to 10^{-9} or 10^{-10} per day. An improvement of the short-term stability (periods of 1 hour or less) of one and possibly two orders of magnitude is expected from a different mechanical design (section 3.3.3) and again: better current stabilisation.

It was shown that non linearities inherent to the gas-laser are insignificant if the lasers are adjusted near threshold of operation ($\eta \approx 1.04$).

Recordings of tides, earthquakes and microseisms were presented and whenever possible, compared with similar recordings made by the Benioff linear strainmeters, that were situated with the LSS in the same underground seismic station. When the differences in directional sensitivities were taken into account, the different recordings were found to be in good agreement. A comparison of the three BLS instruments suggests a modification of the calibration by a factor 0.8 and 0.4 for BLS 2 and BLS 3 respectively.

Strain seismograms of the earthquake with Magnitude $7\frac{1}{2}$, off Peru

(oct 17, 1966) were very useful in the above mentioned comparisons.

A Fourier analysis of the LSS recording of this earthquake showed several higher order spheroidal free vibrations.

The limited response of the LSS to the very low order ($l < 3$) spheroidal modes and its good response to toroidal modes was shown.

Monitoring several instrumental and environmental parameters simultaneously with the recording of the LSS signal, will facilitate in pointing out the relative importance of the different remaining sources of noise. This will be necessary to further increase the useful sensitivity of the laser strain seismometer, the initial development of which, was covered in this thesis.

BIBLIOGRAPHY

ALLEN, L. and D. G. C. JONES, Principles of gas lasers; ed. Butterworths London. (1967).

ALKEMADE, C. TH. J. en P. T. BOLWIJN, Ned. T. Natuurk. 32, 4, 114–137 (1966).

ALSOP, L. E., B.S.S.A., 53, 3, 483–501 (1963).

ALTEMOSE, V. O., J.A.P. 32, 1309 (1961).

ALTERMAN, Z., H. JAROSCH and C. L. PEKERIS, Proc. Roy. Soc. A, 252, 80 (1959).

ALTERMAN, Z., H. JAROSCH and C. L. PEKERIS, Geoph. J. of the Roy. Astron. Soc., 4, 219 (1961).

BALLIK, E. A., Ph. D. Thesis. Oxford University (1964).

BELLISIO, J. A., CH. FREED and H. HAUS, A.P.L. 4, 1, 5–6 (1964).

BENIOFF, H., B.S.S.A. 25, 4, 283–309 (1935).

BENIOFF, H., B.G.S.A. 70, 1019–1032 (1959).

BENNETT JR, W. R., A.O. Supplement on optical masers (1962).

BENNETT JR, W. R., A.O. Supplement 2 of chemical lasers, 3 (1965).

BIRNBAUM, G., Optical Masers; Academic Press, New York and London (1964).

BLAYNEY, J. L. and R. GILMAN, B.S.S.A., 55, 6, 955–970 (1965).

BOERSCH, H., G. HERZIGER and H. LINDNER, Zeitschrift für Physik, 199, 349 (1967).

BOLWIJN, P. T., Thesis, Rijksuniversiteit Utrecht (1967).

BORN, M. and E. WOLF, Principles of Optics; Pergamon Press Limited, Oxford. (1964).

BOYD, G. D. and J. P. GORDON, B.S.T.J., 40, 2, 489–508 (1961).

BOYD, G. D. and H. KOGELNIK, B.S.T.J., 41, 4, 1347–1369 (1962).

BRUNE, J. N., H. BENIOFF and M. EWING, J.G.R., 66, 9, 2895–2910 (1961).

FADDEYEVA, V. N. and N. M. TERENTEV, Mathematical Tables; Pergamon Press, Oxford. (1961).

FORRESTER, A. T., J.O.S.A., 51, 253 (1961).

FOX, A. G. and T. LI, B.S.T.J., 40, 2, 453–488 (1961).

FOX, A. G. and T. LI, Proc. I.E.E.E., 51, 80 (1963).

HOCHULI, U., P. HALDEMANN and D. HARDWICK, I.E.E.E. J. Quant. Electr. (1967).

JASEJA, T. S., A. JAVAN and C. H. TOWNES, Phys. Rev. Lett., 10, 165 (1963).

JASEJA, T. S., A. JAVAN, J. MURRAY and C. H. TOWNES, Phys. Rev., 133, 5A, 1221 (1964).

JAVAN, A., W. R. BENNETT JR. and D. R. HERRIOTT, Phys. Rev. Lett., 6, 3, 106–110 (1961).

KOGELNIK, H. and T. LI, A.O., 5, 10, 1550–1567 (1966).

KOVACH, R. L., Physics and Chemistry of the earth, 6, 252 (1965).

LAMB, JR., W. E., Phys. Rev., 134, 6A, A 1429–A 1450 (1964).

LENGYEL, B. A., Introduction to Laser Physics; John Wiley and Sons, Inc. New York, London, Sydney (1966).

LI, T., B.S.T.J., 44, 917–932 (1965).

MACDONALD, G. J. F. and N. F. NESS, J.G.R. 66, 6, 1865 (1961).

MAJOR, M. W., G. H. SUTTON, J. OLIVER and R. METSGER, B.S.S.A., 54, 1, 295–346 (1964).

MILNE, J., Trans. Seis. Soc. Japan, 12, 63 (1888).

MITCHELL, A. C. G. and M. W. ZEMANSKY, Resonance radiation and excited atoms. Cambridge Univ. Press (1961).

OLIVER, J., B.S.S.A., 52, 1, 81 (1962).

PEKERIS, C. L., Z. ALTERMAN and H. JAROSCH, Proc. Natl. Acad. Sci., U.S., 47, 91–98 (1961).

RIGROD, W. W., A.P.L., 51–53 (1963).

RIGROD, W. W., H. KOGELNIK, D. J. BRANGACCIO and D. HERRIOTT, J.A.P., 33, 743 (1962).

SCHAWLOW, A. L. and C. H. TOWNES, Phys. Rev., 112, 6, 1940–1949 (1958).

SINCLAIR, D. C., A.O., 3, 9, 1067–1071 (1964).

SMITH, S. W., J.G.R. 71, 4, 1183 (1966).

TAKEUCHI, H. and L. E. ALSOP, B.S.S.A., 55, 1, 153 (1965).

THORP, J. S., Masers and Lasers, MacMillan, London and St. Martin's Press, New York (1968).

TOWNES, C. H., Advances in Quantum Electronics, Columbia University Press, 3 (1961).

TURNER, R., K. M. BAIRD, M. J. TAYLOR and C. J. VAN DER HOEVEN, R.S.I., 35, 8, 996–1001 (1964).

VALI, V., R. S. KROGSTAD and R. W. MOSS, Rev. Sci. Instr. 36, 9, 1352 (1965).

VALI, V., IEEE Proc. Region Six Conference, 3C5, 1–6 (1968).

VAN VEEN, H. J., J. SAVINO and L. E. ALSOP, J.G.R. 71, 22, 5478 (1966).